Changes in chromatin accessibility by oncogenic YAP and its relevance for regulation of cell cycle gene expression and cell migration

Änderungen der Chromatinzugänglichkeit durch onkogene YAP und seine Relevanz für die Genexpression während des Zellzyklus und für die Zellmigration

Doctoral thesis for a doctoral degree
at the Graduate School of Life Sciences,
Julius-Maximilians-Universität Würzburg,
Section Biomedicine

submitted by

Maria Camila Fetiva Mora

from

Bogotá, Colombia

Würzburg, 2022

Submitted on:

……..……..

Office stamp

Members of the Thesis Committee

Chairperson: Prof. Dr. Manfred Gessler

Primary Supervisor: Prof. Dr. Stefan Gaubatz

Supervisor (Second): Prof. Dr. Svenja Meierjorhann

Supervisor (Third): Prof. Dr. Elmar Wolf

Substantial parts of this thesis were published in the following pre-print article:

Fetiva MC., Liss F., Gertzmann D., Thomas Julius., Gantert B., Vogl M., Sira N, Weinstock G., Kneitz S., Ade CP, Gaubatz S. (2022). **Oncogenic YAP mediates changes in chromatin accessibility and activity that drive cell cycle gene expression and cell migration.** BioRxiv. [**Preprint**]. September 08, 2022. Available from: https://doi.org/10.1101/2022.09.08.507127 (In revision in Nucleic Acids Research, 2022)

Summary

Various types of cancer involve aberrant cell cycle regulation. Among the pathways responsible for tumor growth, the YAP oncogene, a key downstream effector of the Hippo pathway, is responsible for oncogenic processes including cell proliferation, and metastasis by controlling the expression of cell cycle genes. In turn, the MMB multiprotein complex (which is formed when B-MYB binds to the MuvB core) is a master regulator of mitotic gene expression, which has also been associated with cancer. Previously, our laboratory identified a novel crosstalk between the MMB-complex and YAP. By binding to enhancers of MMB target genes and promoting B-MYB binding to promoters, YAP and MMB co-regulate a set of mitotic and cytokinetic target genes which promote cell proliferation. This doctoral thesis addresses the mechanisms of YAP and MMB mediated transcription, and it characterizes the role of YAP regulated enhancers in transcription of cell cycle genes.

The results reported in this thesis indicate that expression of constitutively active, oncogenic YAP5SA leads to widespread changes in chromatin accessibility in untransformed human MCF10A cells. ATAC-seq identified that newly accessible and active regions include YAP-bound enhancers, while the MMB-bound promoters were found to be already accessible and remain open during YAP induction. By means of CRISPR-interference (CRISPRi) and chromatin immuniprecipitation (ChIP), we identified a role of YAP-bound enhancers in recruitment of CDK7 to MMB-regulated promoters and in RNA Pol II driven transcriptional initiation and elongation of G2/M genes. Moreover, by interfering with the YAP-B-MYB protein interaction, we can show that binding of YAP to B-MYB is also critical for the initiation of transcription at MMB-regulated genes. Unexpectedly, overexpression of YAP5SA also leads to less accessible chromatin regions or chromatin closing. Motif analysis revealed that the newly closed regions contain binding motifs for the p53 family of transcription factors. Interestingly, chromatin closing by YAP is linked to the reduced expression and loss of chromatin-binding of the p53 family member ΔNp63. Furthermore, I demonstrate that downregulation of ΔNp63 following expression of YAP is a key step in driving cellular migration.

Together, the findings of this thesis provide insights into the role of YAP in the chromatin changes that contribute to the oncogenic activities of YAP. The overexpression of YAP5SA not only leads to the opening of chromatin at YAP-bound enhancers which together with the MMB complex stimulate the expression of G2/M genes, but also promotes the closing of chromatin at ΔNp63 -bound regions in order to lead to cell migration.

Zusammenfassung

Ein Kennzeichen vieler Tumoren ist die fehlerhafte Aktivierung von zellzyklusregulierenden Signalwegen. Ein für das Tumorwachstum wichtiger Signalwege ist der Hippo-Signalweg und das durch ihn regulierte Onkogen YAP, ein transkriptioneller Koaktivator. Durch die Regulierung von Zellzyklusgenen ist YAP verantwortlich für onkogene Prozesse wie Zellproliferation und Metastasierung. Der MMB-Multiproteinkomplex wiederum – er entsteht, wenn B-MYB an das MuvB-Kernmodul bindet – ist ein wichtiger Regulator der mitotischen Genexpression, welche ebenso mit der Tumorentstehung in Verbindung gebracht wurde. Unser Labor hat zuvor einen neuen Mechanismus der Regulation mitotischer Gene durch den MMB-Komplex und YAP identifiziert: Durch die Bindung an Enhancer der MMB-Zielgene und die Förderung der B-MYB-Bindung an Promotoren reguliert YAP eine Reihe von mitotischen und zytokinetischen Zielgenen, welche die Zellproliferation fördern. Diese Doktorarbeit befasst sich mit den Mechanismen der YAP- und MMB-vermittelten Transkription und charakterisiert die Rolle der YAP regulierten Enhancer während der Transkription von Zellzyklusgenen.

Die in dieser Dissertation dargelegten Ergebnisse zeigen, dass die Expression von konstitutiv aktivem, onkogenem YAP5SA zu weitreichenden Veränderungen in der Chromatinzugänglichkeit nicht-transformierter humaner MCF10A Zellen führt. ATAC-seq zeigte, dass ein grosse Anzahl YAP-gebundene Enhancer zugänglich und aktiviert werden. Gleichzeitig konnte festgestellt werden, dass die MMB-gebundenen Promotoren bereits vor der Expression von YAP zugänglich sind und während der YAP-Induktion offen bleiben. Mittels CRISP-Interferenz (CRISPRi) und Chromatin-Immunpräzipitationen (ChIP) konnten wir zeigen, dass YAP-gebundene Enhancer die Rekrutierung von CDK7 an MMB-regulierten Promotoren sowie die Initiation und Elongation der Transkription von G2/M Genen fördert. Durch die experimentelle Blockade der YAP-B-MYB Proteininteraktion konnten wir darüber hinaus belegen, dass auch die Bindung von YAP an B-MYB für die Initiation der Transkription an MMB-regulierten Genen entscheidend ist. Unerwarteterweise führte die Überexpression von YAP5SA auch dazu, dass bestimmte Regionen im Genom weniger zugänglich werden. Motivanalysen ergaben, dass diese neu geschlossenen Regionen Bindungsmotive für die p53-Familie von Transkriptionsfaktoren enthalten. Die Chromatinschließung durch YAP ist an eine reduzierte Expression und an den Verlust der Chromatinbindung des p53-Familienmitglieds ΔNp63 gekoppelt. Schließlich konnte gezeigt werden, dass die Inhibition von ΔNp63 durch YAP ein wichtiger Schritt in der YAP-abhängigen Förderung der Zellmigration ist.

Zusammenfassend liefern die Ergebnisse dieser Dissertation Einblicke in die Rolle von YAP bei Chromatinveränderungen welche zu den onkogenen Aktivitäten von YAP beitragen. Die

Überexpression von YAP führt dabei einerseits zur Öffnung des Chromatins an YAP-gebundenen Enhancern, die zusammen mit dem MMB-Komplex die Expression von G2/M Genen stimulieren. Andererseits fördert YAP auch das Schließen von Chromatin an ΔNp63-gebundenen Regionen, was wiederum Zellmigration nach sich zieht.

1. Introduction

1.1 Mammalian cell cycle

1.1.1 Overview of the cell cycle

This thesis deals with transcriptional control of cell cycle genes. Therefore, I first give an overview of cell cycle regulation. The cell cycle is a coordinated and controlled process that is determined by duplication and division. First, the entire genomic DNA is replicated and distributed into the two genetically identical formed daughter cells. The cell cycle has four stages: In G1 the cells increase in size, followed by a stage of DNA synthesis during S phase, next in G2 the cells prepare for the entrance into the M (mitosis) phase where the cells divide (Figure 1). G1 and G2 are the gaps stages where the cells grow and transcribe the necessary proteins for either DNA replication or mitosis. Additionally, these phases provide time to monitor the external and internal environment and signals. Within the first gap stage, in G1 phase the cells respond to external conditions and extracellular signals in order to decide to either undergo to the next phase of DNA replication or to delay the progress through G1 and may exit from the cell cycle and enter in a specialized resting stage known as quiescent or G0. The cells can remain in G0 for undetermined time, even years. When there are signals to grow and divide, cells in early G1 or G0 progress through a restriction point, and after reaching this step cells are committed to performing DNA replication. During the second gap stage, in G2 phase, cells grow and perform synthesis of the proteins necessary for division. The G1, S, and G2 phases together compose the interphase and the chromosome segregation and cell division occur during M phase (Alberts et al., 2015; Ding et al., 2020; Morgan, 2016; Otto & Sicinski, 2017; Weinberg, 2014). Mitosis can be subdivided in four phases known as prophase, metaphase, anaphase and telophase. In prophase, the nuclear envelope breaks down and the duplicated DNA is packaged and condensate into chromosomes conformed of a pair of identical sister chromatids, that are sustained by the microtubules of the mitotic spindle. Metaphase is a pause phase where the chromosomes are aligned at the equator of the mitotic spindle. In anaphase, the sister chromatids separate, and the chromosomes are pulled and move to opposite poles of the spindle. Through telophase, nuclear division is achieved, and the chromosomes decondense and reform intact nuclei. The process ends by the cytoplasmic division called cytokinesis (Alberts et al., 2015; Ding et al., 2020; Malumbres & Barbacid, 2001;

Morgan, 2016; Otto & Sicinski, 2017; Weinberg, 2014). Within cell cycle progression exist numerous checkpoints to ensure that cells will not progress into the next phases before completing properly and successfully the current phase. The three major checkpoint controls are discussed in section 1.1.4 below.

1.1.2 Cell cycle regulation

The cell cycle transition is mainly regulated by different cyclins and cyclin-dependent kinases (CDKs) which are serine/threonine kinases. CDKs form complexes with cyclins that are regulatory subunits that stimulate their catalytic activity to control cell cycle via phosphorylation of a set of downstream protein targets in order to lead cells throughout the cell cycle phases (**Figure 1**) (Morgan, 2016; Weinberg, 2014).

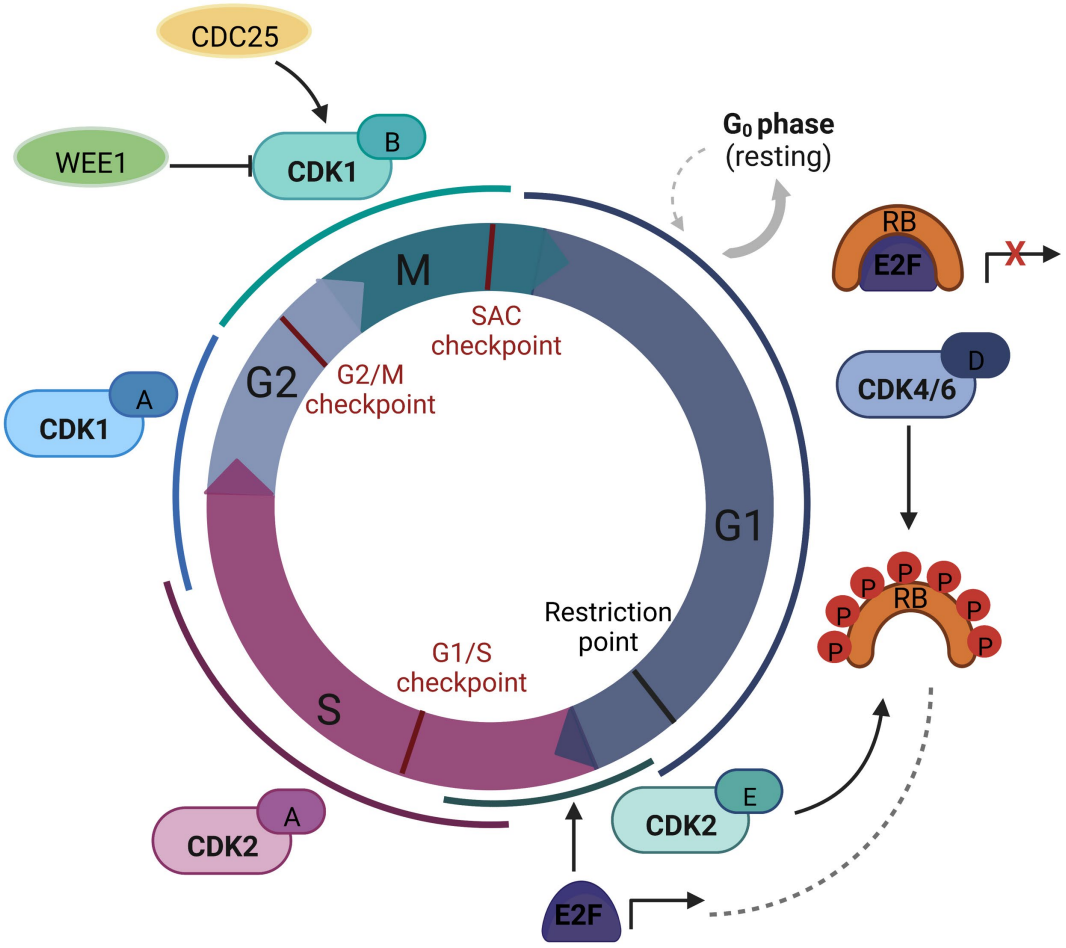

Figure 1. Progression mammalian cell cycle and its regulation
The mammalian cell cycle consists of four major phases. Cell cycle is regulated by the association of cyclins (Cyclin D, E, A, B) with CDKs. First in G1 phase cells could enter a reversible state of quiescence

(G0), after some stimulatory signals cells enter into the cell cycle. In S phase cells perform DNA synthesis and drive to G2 phase to prepare for the next phase, mitosis (M). In early G1 at the restriction point cyclin D-CDK4/6 hypophosphorylates the retinoblastoma protein RB. At the end of G1 cyclin E-CDK2 leads hyperphosphorylation of RB to release E2F transcription factors to lead progression from G1 to S phase. Additional check point controls occur at G1/S, G2M and late mitosis (SAC checkpoint). Adapted from (Otto & Sicinski, 2017; Weinberg, 2014). Created with BioRender.com.

During cell cycle transitions, different cyclin-CDK complexes are formed, and the concentration of CDK proteins is largely constant while the levels of most cyclins vary across the cell cycle. Activation of cyclin-CDKs is controlled by mitogenic signals and inhibited by cyclin-dependent kinase inhibitors (CKIs). To drive cell-cycle progression from G0 or G1 to S phase CDK4 and CDK6 are associated with the D-type cyclins (cyclin D1, cyclin D2, and cyclin D3). The activity of CDK4/6 is inhibited by binding to CDK inhibitors of the INK4 family ($p16^{INK4A}$, $p15^{INKB}$, $p18^{INK4C}$, and $p19^{INK4D}$) (Malumbres & Barbacid, 2001; Weinberg, 2014). During late G1 phase the cyclins E1 and E2 are activated thus binding and activating CDK2 that was previously sequestered and inhibited by $p21^{CIP}$ and $p27^{KIP1}$ which lead to ubiquitin-mediated proteolysis. The cell division cyclin 25A (CDC25A) activates also CDK2 to lead cell cycle transition. Then the activated CDK4/6 and CDK2 mediate the cell cycle progression towards S phase. In late S phase cyclin E is replaced by cyclin A to form the complex cyclin A/CDK2 which leads to the ending of S phase (**Figure 1**) (Ding et al., 2020; Malumbres & Barbacid, 2001; Watanabe et al., 1995; Weinberg, 2014). By mid-S phase, CDK1 is activated by Cyclins A binding until late G2 phase. Then cyclins A are replaced by Cyclins B which binds to CDK1 at the end of G2 phase, to activate M phase regulating the expression of genes required for mitosis. CDK1 is essential for cell cycle progression, it guarantees the exactitude of the sequence of events during mitosis and ensures cellular replication with high fidelity (**Figure 1**). The activity of CDK1 is controlled by WEE1 and MYT1 which phosphorylates CDK1 to inhibit it, and is activated by CDC25A phosphorylation (Santamaria et al., 2007; Weinberg, 2014).

1.1.3 E2F-RB-complexes regulate gene expression at the R-point

The family of pocket proteins including the retinoblastoma protein (pRB) and its paralogs p107 and p130 is the major substrate of the CDKs mediating cell cycle regulation in the G1 phase. In particular, the pRB is a tumor suppressor that recruits and suppresses E2F transcription factors

E2Fs (E2F1, E2F2 and E2F3a) to inhibit G1/S transition by recruiting histone deacetylases (HDACs) to E2F regulated promoters. In a series of events cyclin D-CDK4/6 hypophosphorylate pRB, promoting the overexpression of Cyclin E. Previous to the R-point Cyclin E/CDK2 are inhibited by $p21^{Cip1}$ and $p27^{Kip}$ (Frolov & Dyson, 2004; Otto & Sicinski, 2017; Weinberg, 2014). Then CDC25 activates CDK2, and Cyclin E together with CDK2 hyperphosphorylate pRB to inactivate it and to override the restriction point of the G1/S phase leading cells into cell cycle progression from G1 to S phase (**Figure 1**). Consequently, the derepression of E2Fs triggers gene expression by attracting other proteins as histone acetylases to remodel chromatin and induce transcription initiation by the RNA polymerase at promoters of G1/S target genes such as cyclin E (CCNE), CCNA, and CCNB. This mechanism of regulation by pRB represents a positive feedback loop, resulting in cell commitment to enter the cell cycle (Bertoli et al., 2013; Ding et al., 2020; Weinberg, 2014).

The E2F proteins are DNA-binding transcription factors composed by eight different proteins (E2F1–E2F8). Particularly E2F1–E2F6 require binding to dimerization partner 1 or 2 (DP1/2) for DNA binding. As mentioned before E2F is involved in progression from G1 phase and in DNA replication (Bracken et al., 2004; Classon & Dyson, 2001; Frolov & Dyson, 2004). E2F mediates recruitment of pocket proteins, in quiescent G0 cells E2F4 and E2F5 are associated with p130/p107 to repress gene expression at promoters of E2F target genes. Functionally E2F family is subdivided into repressors (E2F4, E2F5, E2F6, and E2F3b) and activators (E2F1, E2F2, and E2F3)(Humbert et al., 2000) and the atypical subgroup (E2Fs, E2F7 and E2F8) which comprise two DNA binding domains and execute gene repression independent of DP1/2 (Bertoli et al., 2013; Bracken et al., 2004; Kent & Leone, 2019).

1.1.4 Checkpoint controls

Sustained genomic integrity is critical for cell division. DNA damage can occur as a result of errors in DNA replication and exogenous or endogenous stressors stimuli that can cause DNA breaks. The DNA damage response (DDR) is driven by the protein kinases ataxia-telangiectasia-mutated (ATM) and ataxia telangiectasia and Rad-related (ATR) (**Figure 2**). Specifically, ATM responds to double-strand breaks and acts via CHK2, while ATR acts via CHK1 and responds to single-strand damages developed at stalled replication forks commonly generated as a result

of chemotherapeutic drugs and UV radiation (Alberts et al., 2015; Neizer-Ashun & Bhattacharya, 2021; Weinberg, 2014). The kinases CHK1 and CHK2 block the cell cycle transition inhibiting CDC25 phosphatases and as described before CDC25 activity is necessary for entry into mitosis. Phosphorylation of CDC25A by CHK1 mediates the inhibition of CDK1/2 activity and consequently leads to cycle arrest at the intra-S and G2/M checkpoints (**Figure 2**) (Alberts et al., 2015; Wang et al., 2002; Zhao et al., 2002). CHK1 also phosphorylates CDC25B to inhibit activation of centrosomal CDK1, and CDC25C to suppress cyclin B-CDK1 in the G2/M checkpoint (Kramer et al., 2004; Neizer-Ashun & Bhattacharya, 2021; Peng et al., 1997; Schmitt et al., 2006). In addition, regulation by CHK1 also negatively regulates the serine/threonine-protein kinase PLK1, the main regulator of the spindle assembly checkpoint (SAC). The SAC checkpoint guarantees that all chromosomes are properly organized into the mitotic spindle, thus preventing chromosome misalignment and premature segregation during anaphase (Fang et al., 1998; Morgan, 2016; Weinberg, 2014). On the other hand, CHK2 is phosphorylated by ATM as a response to DSBs, mediating principally the G1 arrest point through p53 to allow time for DNA repair, and has auxiliary roles in intra-S and G2/M checkpoints by inhibiting CDC25A (**Figure 2**) (Alberts et al., 2015; Matsuoka et al., 2000; Smith et al., 2010).

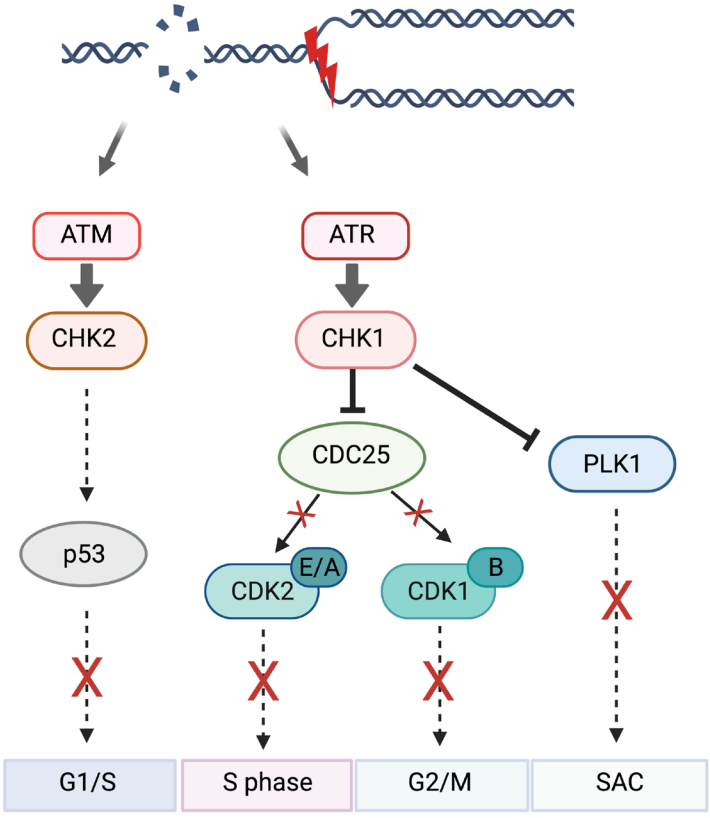

Figure 2. Checkpoint controls of the mammalian cell cycle.

DNA damage response is led by ATM and ATR kinases. ATM responds to DSBs and activates CHK2 to facilitate the G1/S checkpoint through p53. ATR responds to replication stress and activates CHK1 which through CDC25 inhibition leads to the regulation of the checkpoints at intra-S and G2/M phases. CHK1 also inhibits PLK1 to mediate the spindle assembly checkpoint SAC. Adapted from (Neizer-Ashun & Bhattacharya, 2021). Created with BioRender.com.

1.1.5 The Roles of CDKs in Transcription

In mammals, the CDKs not only have roles in the regulation of cell cycle progression but also in transcription mediated by the RNA polymerase II (RNA pol II) (Malumbres, 2014). Transcription is catalyzed by RNA pol II and subdivided into four discrete phases: initiation, pausing, elongation and termination (**Figure 3**). A vital component of the RNA pol II is the C-terminal domain (CTD), which is evolutionary conserved and has a role in the coordination of RNA transcription and chromatin organization by changes in its phosphorylation level (Jeronimo et al., 2013; Suh et al., 2013; Whittaker et al., 2017). The kinase CDK8 has roles as either a repressor or an activator of transcription at different genes, in response to stimuli (Fant & Taatjes, 2019; Galbraith et al., 2010); CDK8 or 19 associate with Cyclin C and induce the pre-initiation complex (PIC) at promoters. The pre-initiation of transcription is a complex process where the RNA pol II interacts with multi-subunit mediator complex and transcription factors to recognize promoters forming PIC. For initiation of transcription at promoters the DNA is unwound by the helicase activity of the TFIIH to form a single-strand DNA, then the CTD-RNA Pol II is phosphorylated at Ser5 and Ser7 by CDK7, which is a component of the initiation factor TFIIH. CDK7-dependent phosphorylation at RNA pol II at Ser5 promotes co-transcriptional 5′-end-capping of the nascent transcript (**Figure 3**) (Bird et al., 2004; Compe et al., 2019; Ebmeier et al., 2017; Fisher, 2012; Kanin et al., 2007). Once the transcription initiates levels of Ser5 phosphorylation decrease and is required for the Positive transcription elongation factor b (P-TEFb) recruitment in the next steps (Viladevall et al., 2009). During pause release, CDK9 phosphorylates the negative elongation factor (NELF) to release the stalling of the elongation complex and the RNA pol II is phosphorylated at Ser2 to engage its RNA polymerizing activity (Larochelle et al., 2012; Peterlin & Price, 2006). CDK9 binds to cyclins T conforming the P-TEFb leading promoter to release from proximal arrest and to stimulate elongation. Finally, CyclinL/CDK11 are involved in the regulation of RNA splicing, promoting transcription termination via dephosphorylation of Ser5 of CTD-RNAPII (**Figure 3**), and CDK12/13 promote

phosphorylated CTD ser2 to induce cleavage, polyadenylation of the nascent pre-mRNA(Lim & Kaldis, 2013; Parua & Fisher, 2020; Whittaker et al., 2017).

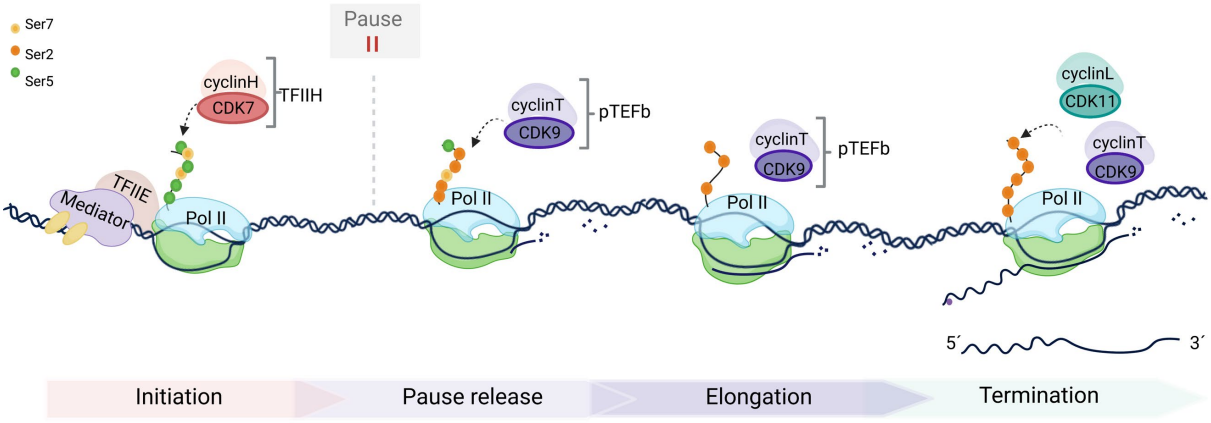

Figure 3. CDKs in transcription regulation
Regulation of transcription by cyclin/CDKs is subdivided into initiation, pause release, elongation and termination. Initiation of transcription begins by the formation of PIC and the phosphorylation of the RNA pol II at Ser5 by CDK7 followed by a pause release driven by CDK9 phosphorylation of RNA pol II at Ser2 and to NELF leading to elongation of transcription. CDK11,12 and 13 are involved in the coordination of transcription termination, mRNA splicing, and polyadenylation. Adapted from (Lim & Kaldis, 2013; Parua & Fisher, 2020). Created with BioRender.com.

1.2 MMB complex

1.2.1 MuvB complexes

MuvB complexes can either form a transcription repressor complex known as the DREAM complex or together with B-MYB and FOXM1 form the Myb-MuvB (MMB) complex that activates expression of cell cycle genes to lead progression through G2/M phases (Fischer & Muller, 2017). MuvB complexes share a common protein core the MuvB core which was first genetically identified in *C. elegans* (Sadasivam & DeCaprio, 2013). In mammals, the MuvB core is composed of LIN9, LIN37, LIN52, LIN54 and RBBP4. The MuvB core interacts with different proteins during the cell cycle progression and these interactions define its function from transcription repressor during G0-G1 to a transcription activator at S, G2 and M phases. During G0 and early G1, the repressor complex DREAM (dimerization partner (DP), RB-like, E2F and MuvB) is formed by the interaction of the MuvB core with E2F4/5, DP1/2 and p130/p107 to repress G1/S and G2/M (**Figure 4**) (Litovchick et al., 2007; Pilkinton et al., 2007; Sadasivam et al., 2012; Schmit et al., 2007). In late G1, E2F4/5, DP1/2 and p130/p107 dissociate from the

MuvB core, which then binds to B-MYB in S phase forming the MMB complex (Myb-MuvB) (Figure 4), the MMB complex activates the expression of G2/M genes required for the cell cycle progression. In G2 FOXM1 binds to MMB complex to stimulate gene expression peak during G2 and M phases (Down et al., 2012; Fischer & Muller, 2017; Litovchick et al., 2007; Osterloh et al., 2007; Sadasivam et al., 2012; Schmit et al., 2007).

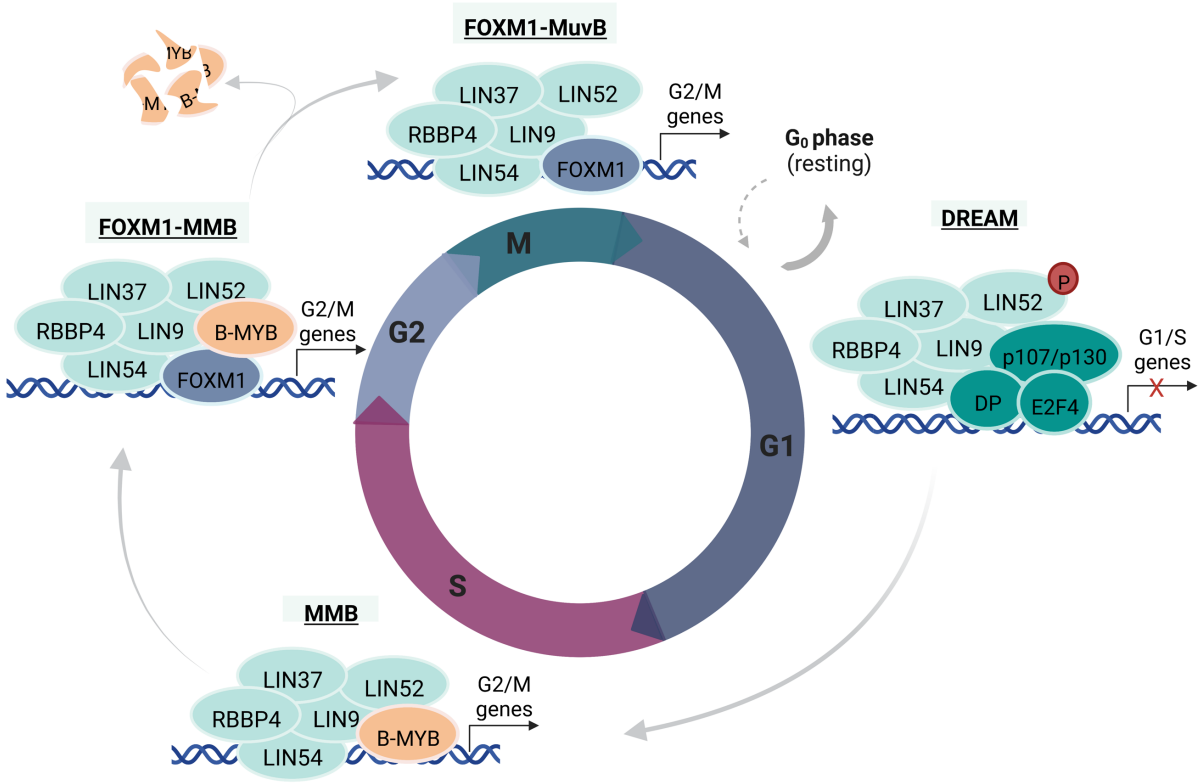

Figure 4. Cell cycle regulation by MuvB complexes
MuvB core consists of LIN9, LIN54, LIN37, LIN52 and RBBP4. It binds to p107/p130, E2F4/5, and DP1/2 to conform the DREAM complex, which during G0/G1 arrest represses the expression of G1/S and G2/M genes. In late G1 the MuvB core dissociates from p107/p130, E2F4/5, and DP1/2 and during S phase B-MYB binds to MuvB to form the MMB complex. At the early G2 phase, FOXM1 Binds to the MMB complex and fully activates G2/M gene expression. In mid-G2 B-MYB is dissociated from the MuvB core and its proteasome is degraded. FOXM1 stays with the MuvB core and activates late mitotic genes. Adapted from (Fischer & Muller, 2017; Sadasivam & DeCaprio, 2013). Created with BioRender.com.

LIN52 is involved in the switch between the repressor DREAM and the activator MMB complexes: LIN52 is phosphorylated by DYRK1A at S28 which allows p130 to bind the MuvB core (Guiley et al., 2015; Litovchick et al., 2011). LIN9 binds to LIN52, B-MYB and FOXM1 (Schmit et al., 2007) and it is a central component of the MuvB core for the formation of both repressor

and activator MuvB complexes. LIN9 depletion has been described to result in reduced expression of mitotic genes and mitotic defects and a delayed cell cycle progression (Eckerdt et al., 2014; Esterlechner et al., 2013; Knight et al., 2009; Osterloh et al., 2007; Pilkinton et al., 2007; Reichert et al., 2010; Schmit et al., 2007; Wiseman et al., 2015). DNA binding of the MMB complex is mediated by LIN54 which binds to CHR elements in promoters of late cell cycle genes (Marceau et al., 2016; Matsuo et al., 2012; Schmit et al., 2009), whereas RBBP4 binds to histones H3 and H4 and recruits chromatin-bound proteins, such as histone deacetylases (HDAC) (Murzina et al., 2008; Nicolas et al., 2001; Saade et al., 2009; Zhang et al., 2013). The subunit LIN37 has been described to be only essential for the DREAM complex function and is one of the least studied components of the MuvB core (Knight et al., 2009; Schmit et al., 2007). B-MYB and FOXM1 are transcription factors that promote the expression of genes needed for G2/M progression, which cannot bind and activate G2/M genes independently from the MuvB core (Musa et al., 2017; Sala, 2005; Wang et al., 2005; Zhu et al., 2004). B-MYB binds to the MuvB core through its interaction with LIN52 and LIN9 (Guiley et al., 2018; Osterloh et al., 2007), and its interaction is essential for FOXM1 recruitment (Chen et al., 2013; Down et al., 2012; Sadasivam et al., 2012). Recently it was shown that B-MYB binds to the transcriptional co-activator YAP, the downstream effector of the Hippo pathway, to activate a set of genes relevant for G2/M phase (Grundl et al., 2020; Pattschull et al., 2019; Wei et al., 2019). In late G2 B-MYB is ubiquitinated and degraded by the proteasome while the FOXM1 interaction with the MuvB core remains and FOXM1-MuvB bound to CHR promoters to fully activate G2/M genes (Down et al., 2012; Fischer & Muller, 2017; Johnson et al., 1999; Sadasivam & DeCaprio, 2013; Sadasivam et al., 2012). In late mitosis, FOXM1 is ubiquitinated and is degraded by the proteasome (Park et al., 2008). Loss of B-MYB or FOXM1 is lethal during embryonic development in mice (Krupczak-Hollis et al., 2004; Tanaka et al., 1999), and has been found to lead to mitotic defects in various cell lines (Knight et al., 2009; Laoukili et al., 2005; Tarasov et al., 2008).

1.2.2 MMB complex in cancer

Given the role of the MMB complex in promoting cell cycle progression, its components have been associated with cancer. For instance, FOXM1 is overexpressed in different cancer types

and its gene amplification has been found in several testicular germ cell tumors, high-grade serous ovarian cancer, and basal breast cancer (Barger et al., 2019; Gartel, 2017). Similarly, overexpression of B-MYB promotes the progression of cancer and is correlated with poor prognosis in many cancers including breast, liver, and ovarian cancer (Calvisi et al., 2011; Cicirò & Sala, 2021; Tanner et al., 2000; Thorner et al., 2009). The amplification and overexpression of *MYBL2* (B-MYB gene) seems to be sufficient to disrupt DREAM complex and lead to the activation of DREAM target genes (Iness et al., 2019; Iness et al., 2021). In high-grade serous ovarian cancer (HGSOC) B-MYB is highly expressed and associated with deregulation of DREAM/MMB-mediated cell cycle and is suggested as a prognostic target gene in ovarian cancer (Iness et al., 2021). Overexpression of LIN9 has been related to breast cancer development (Roberts et al., 2020; Sahni et al., 2017), esophageal adenocarcinoma (Wiseman et al., 2015) and hepatocellular carcinoma (Calvisi et al., 2011) and low overall survival (Roberts et al., 2020; Sahni et al., 2017). In HCC tumor-derived tissues high of LIN9–B-Myb (MMB) and low formation DREAM were associated with shorter survival (Calvisi et al., 2011). Depletion of B-MYB or LIN9 inhibits tumor formation in a mouse model of lung adenocarcinoma (Fischer & Muller, 2017; Iltzsche et al., 2017). Specifically, conditional deletion of *B-Myb* or *Lin9* in a K-Ras^{G12D};$p53^{null}$ mouse model of lung cancer showed a requirement for the MMB complex in lung tumorigenesis (Iltzsche et al., 2017) and demonstrated that the MMB target gene *KIF23* is required for lung tumor formation (Hanselmann et al., 2018; Iltzsche et al., 2017). In the breast cancer cell line MDA-MB-231, inhibition of the MMB target genes, KIF23 and PRC1 reduced significantly cell proliferation. Other MMB target genes as the Aurora kinase A (*AURKA)* and the DNA topoisomerase 2α (*TOP2A*) are frequently highly expressed in human tumors (Sadasivam & DeCaprio, 2013). Some MMB target genes as *NUSAP1* and *PRC1* are part of cancer test profiles as MammaPrint (Agendia) profile, which is a diagnostic tool to predict breast cancer metastasis (Tian et al., 2010). Moreover, *MYBL2* is included in the 21-gene panel Oncotype Dx (Genomic Health) test, which is used to evaluate the risk of recurrence in estrogen receptor-α positive, lymph node-negative breast cancer (Paik et al., 2004).Similarly, a subset of MMB target genes is part of Oncotype Dx as *CCNB1*, *AURKA* and *BIRC5* (O'Connell et al., 2010). High expression of MMB target genes is associated with poor survival being suggested as a prognostic signature or therapeutic targets (Sadasivam & DeCaprio, 2013; Wolter et al., 2017).

1.3 The hippo pathway

1.3.1 Signaling cascade

Part of this thesis deals with the crosstalk between B-MYB and YAP, the protein effector of the hippo pathway, in the regulation of G2/M target genes expression and cell cycle progression. Therefore, I give a general overview of the hippo pathway signaling cascade. The hippo pathway is an evolutionarily conserved regulator of growth, organ size control and tissue homeostasis that is often altered in human cancers due (Ehmer & Sage, 2016; Harvey et al., 2013). This pathway was discovered in flies and many functions are conserved between flies and mammals (Badouel et al., 2009). The Hippo pathway is a kinase cascade signaling pathway, that controls the activity of the downstream protein effectors YAP and TAZ. The core of this pathway consists of the upstream kinases MST1 and MST2 which work together with the two adaptor proteins SAV1/WW45. It has been described that Sav1 works as a bridge to bring MST1/2 and Lats1/2 together (Callus et al., 2006; Tapon et al., 2002). When the pathway is active MST1/MST2 and SAV1/WW45 phosphorylate and activate LATS1 and LATS2. Then, the activated LATS1/2 kinases together with MOB1 phosphorylate the downstream effectors Yes-associated protein (YAP) and transcriptional co-activator with PDZ-binding motif (TAZ). The kinases LATS1/2 recognize the substrate consensus sequence HXRXXS, and all the five HXRXXS sites on YAP are phosphorylated by LATS1/2 (Zhao et al., 2010; Zhao et al., 2007). Afterward, the phosphorylation of YAP/TAZ leads to 14-3-3 mediated cytoplasmic accumulation and ultimately to its ubiquitination and proteasomal degradation. Therefore, the active Hippo pathway inhibits YAP/TAZ through its cytoplasmic retention and degradation (**Figure 5**)(Kanai et al., 2000; Zhao et al., 2007). Nevertheless, not all cytoplasmic YAP/TAZ is degraded, where other pathways as WNT or TGF-β signaling can associate with the cytoplasmic and phosphorylated YAP and TAZ to modify signaling through alternate pathways (Azzolin et al., 2014; Varelas et al., 2010). When the Hippo pathway is inactive (OFF), unphosphorylated YAP/TAZ translocates to the nucleus where they act as transcriptional co-factors and interact with different transcription factors to activate gene expression (**Figure 5**) (Ehmer & Sage, 2016; Meng et al., 2016; Yu et al., 2015). YAP/TAZ do not have a DNA-binding domain, but they activate transcription of cell proliferation and survival genes mainly by its binding to its major transcriptional binding partners the TEAD/TEF transcription factor family (TEAD1-4)(Yu & Guan, 2013; Zhao et al., 2008). Genome-

wide assays have revealed that YAP and TEAD not only bind to proximal promoters of target genes but also to distal enhancers suggesting YAP/TAZ mediated transcription regulation via multiple mechanisms including recruitment of transcription factors, modification of epigenetic markers and chromatin remodeling (Lian et al., 2010; Stein et al., 2015; Zanconato et al., 2015). In addition to YAP/TAZ role as co-activators of transcription, it has been stated that they can also act as repressors of the expression of certain genes. For example, YAP/TAZ interact with the nucleosome remodeling and histone deacetylase (NuRD) complex to mediate transcriptional repression (Kim et al., 2015). YAP/TAZ can be either regulated directly by LATS1/2 or independently of LATS1/2 (Low et al., 2014), both types of regulation are triggered by extracellular signals, intracellular cell machineries or non-cellular mechanisms (Boopathy & Hong, 2019; Ehmer & Sage, 2016; Yu et al., 2015).

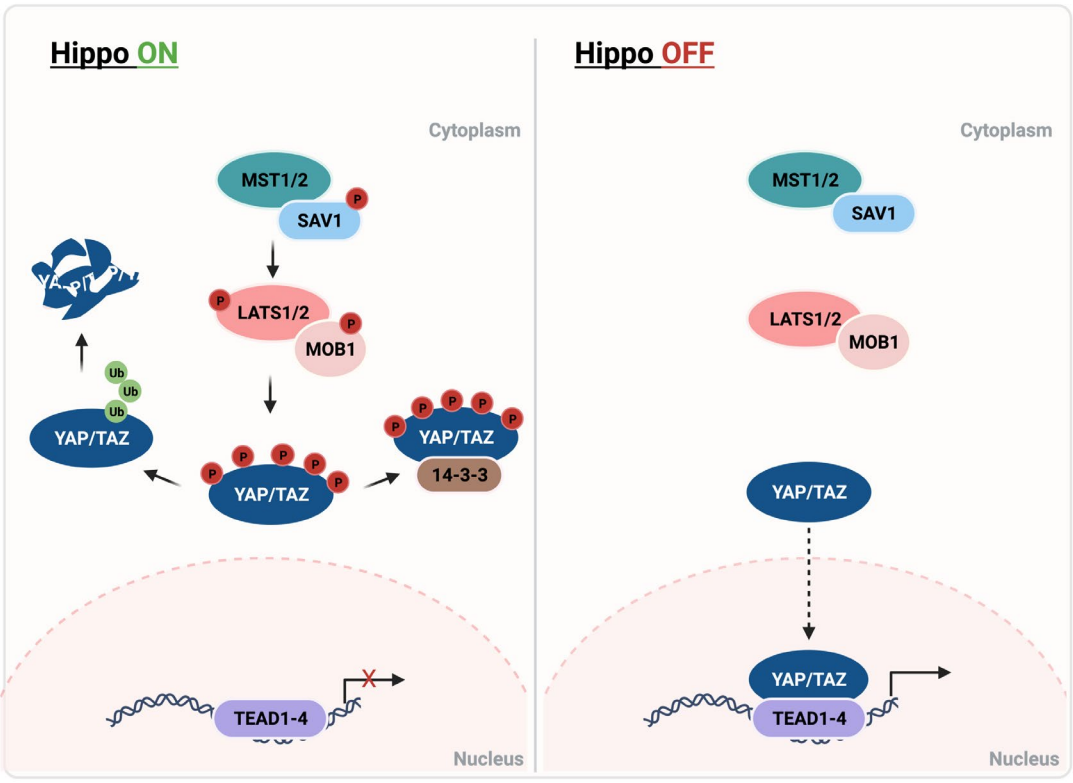

Figure 5. The Hippo pathway cascade.
When the hippo pathway is ON (left), the kinases MST1/2 together with the activated SAV1 phosphorylate LATS1/2 and MOB1. The activated LATS1/2-MOB1 phosphorylate the protein effector of the Hippo pathway, YAP and its paralog TAZ. The phosphorylation of YAP/TAZ leads to either its cytoplasmic retention through the 14-3-3 protein and to its proteasomal degradation. Contrary, when the Hippo pathway is OFF (right), the cascade is inactive thus YAP/TAZ are unphosphorylated and are translocated into the nucleus, and together with their transcriptional partners TEAD1-4, activate gene expression of pro-proliferative genes. Adapted from (Yu et al., 2015). Created with BioRender.com.

1.3.2 Cell Cycle regulation by YAP/TAZ

The kinases LATS1/2 are phosphorylated in a cell cycle-dependent manner and are considered regulators of G1/S, G2/M and of the mitosis checkpoint (Tao et al., 1999). It has been reported that failures in cytokinesis activate LATS2 which then stabilizes p53 and inactivates YAP/TAZ by phosphorylation (Ganem et al., 2014). Additional to LATS1/2 function to inhibit YAP/TAZ by preventing their translocation to the nucleus and therefore inhibit gene expression of YAP-regulated cell cycle genes, LATS1/2 also stimulates the assembly of the repressor complex DREAM which blocks the expression of G1/S genes (Litovchick et al., 2011; Tschop et al., 2011). Numerous reports have demonstrated that YAP/TAZ regulate expression of cell cycle genes that are required for the G1/S transition. A set of YAP-regulated genes are also E2F target genes, which are important for programming cell cycle control, such as *BIRC5* (Survivin)(Jiang et al., 2004) and *c-MYC* (Dong et al., 2007; Neto-Silva et al., 2010; Thalmeier et al., 1989). More recently it has been found that YAP also regulates genes that are required for mitosis and cytokinesis (Bai et al., 2012; Kapoor et al., 2014; Lange et al., 2015; Pattschull et al., 2019; Shen & Stanger, 2015; Tremblay et al., 2014; Zanconato et al., 2015). Although YAP was first found to bind to promoters of its target genes, in recent reports it has been reported that YAP mainly regulates gene expression by binding to distal enhancers of its target genes (Galli et al., 2015; Kapoor et al., 2014; Pattschull et al., 2019; Stein et al., 2015; Zanconato et al., 2015). Recently, it was described that YAP directly interacts with B-MYB a component of the activator complex MMB (1.2.1), and through its binding to distal enhancers, YAP induces B-MYB promoters binding and expression of a subset of common G2/M target genes (Grundl et al., 2020; Pattschull et al., 2019).

1.3.3 YAP regulates enhancers

Enhancers or super-enhancers are key gene transcription elements that regulate distant target genes; their activity can determine levels of gene expression and they also play a role in cancer biology. Enhancers can be located at any region within the genome and they interact with promoter regions by loop formation (Hnisz et al., 2013; Shlyueva et al., 2014). Recent studies have shown that YAP regulates gene transcription through binding to distal enhancer regions which are marked by histone posttranslational modifications such as H3K27ac and H3K4me1,

typical chromatin marks for active enhancers (Cebola et al., 2015; Galli et al., 2015; Lopez-Hernandez et al., 2021; Pattschull et al., 2019; Zanconato et al., 2015). At enhancers, YAP/TAZ stimulates the recruitment of the mediator complex to establish enhancers-promoters contacts through chromatin looping and of the chromatin reader BRD4, a member of the bromodomain and extra terminal domain (BET) family and its paralogues. This triggers the elongation of transcription by phosphorylation of the initiating/stalled RNA Pol II on Ser2 at the CTD domain (Galli et al., 2015; Zanconato et al., 2018). As mentioned above (1.3.2), YAP and the MMB complex interact via promoter-enhancer loops to stimulate the expression of G2/M target genes (Pattschull et al., 2019). It has been suggested that YAP/TAZ also could be involved in chromatin remodeling at enhancers regions, based on the fact that AP-1 a major partner of YAP, remodels nucleosome-occluded enhancers by recruiting the chromatin-remodeling SWI/SNF complex (Vierbuchen et al., 2017). YAP-regulated enhancers have also been implicated in development. For example, during pancreatic development, YAP regulates a subset of temporarily controlled enhancers together with other TFs such as HNF1B, ONECUT, PDX1, FOXA1, and GATA6 (Cebola et al., 2015). In cardiomyocytes, YAP leads to loss of nucleosomes and the opening of chromatin mediating reprogramming into fetal-like progenitors (Monroe et al., 2019). The newly opened regions correspond mainly to developmental cardiac enhancers which drive the expression of cell cycle genes needed for embryonic development (Tanner et al., 2000). Enhancers regulation by YAP/TAZ is also relevant for cancer: For instance, chromatin remodeling of the regions enriched by TEAD are associated with an invasive phenotype of melanomas, whereas the knockdown of TEAD was found to reduce dramatically these invasive properties, suggesting a pivotal role of YAP/TAZ in chromatin rearrange in melanoma (Verfaillie et al., 2015). In cancer cells a large fraction of super-enhancers may explain the transcriptional addiction executed by YAP/TAZ overexpression (Galli et al., 2015; Zanconato et al., 2018). However, a comprehensive view of the role of YAP-regulated enhancers in cell cycle regulation remained largely unknown.

1.3.4 Role of YAP/TAZ in cancer

Dysregulation of YAP/TAZ has been related to many human cancers (Halder & Camargo, 2013; Hong & Guan, 2012; Moroishi et al., 2015; Pan, 2010). YAP-mediated oncogenic activities are diverse from cell survival proliferation, migration, invasiveness, metastasis, immunoresistance

and chemo-resistance. In regard to cell proliferation, YAP/TAZ coordinate the expression of cell cycle genes, activating a core of transcription factors such as MYC, E2F, AP-1, and B-MYB in normal and transformed cells (Croci et al., 2017; Ehmer & Sage, 2016; Pattschull et al., 2019; Zanconato et al., 2015). YAP overexpression is related to metastasis in melanomas while silencing some of its target genes as AXL, THBS1, and CYR61 reduced metastasis formation (Zhang et al., 2020). In addition, YAP can regulate Epithelial–mesenchymal transition (EMT) by regulating the expression of EMT genes and by activating other transcription factors creating a regulatory network. For instance, ZEB1 is a transcriptional repressor required for EMT, and YAP and ZEB1 share a subset of regulated genes in breast cancer suggesting a collaborative network that mediates malignant cancer progression and therapy resistance, stimulating cancer aggressiveness. In particular, in the claudin-low subtype of aggressive breast cancer ZEB1 together with YAP seems to regulate a canonical sunset of target genes responsible of malignant cell programming mediating cell migration, cytoskeletal reorganization and focal adhesion (Feldker et al., 2020; Lehmann et al., 2016). Moreover, YAP/TAZ is also related to migration and invasion which are associated with EMT and cytoskeletal remodeling. YAP expression boosts migration and invasion in prostate-ductal adenocarcinomas (PDAC) and it was found that YAP metastatic activity depends on the upregulation of the LPA receptor 3 (LPAR3)(Yang et al., 2015). Interestingly in breast and lung epithelial cells, the p63 isoform ΔNp63 is downregulated by TAZ overexpression where the suppression of ΔNp63 by TAZ/TEAD seems to reduce cell–cell adhesion leading to increased cell migration (Valencia-Sama et al., 2015).

Accordingly, inhibition of YAP/TAZ to prevent its oncogenic functions that are mainly associated with metastasis and tumor development represent promising approaches in cancer treatment of tumors where malignancy activities are programmed by overexpression of YAP/TAZ (Ehmer & Sage, 2016; Lopez-Hernandez et al., 2021).

1.4 p53 family

1.4.1 Overview of p53 family of proteins

The family of p53 proteins are transcription factors, comprised of p53, p63 and p73, and each protein has recognized isoforms. p53 is a tumor suppressor that sensors cellular stress, and

activates the mechanism of DNA repair or apoptosis, to prevent accumulation of malignant mutations and the development of cancer (Wei et al., 2012; Zawacka-Pankau, 2022). The three proteins have similar domains structures comprised of transactivation domain (TAD), DNA-binding domain (DBD) and oligomerization domain (OD); in addition, p63 and p73 have the Sterile Alpha Motif domain (SAM) (Melino et al., 2003). There are several transcriptional variants, which are mainly classified as TA and ΔN, the TA variants contain a N-terminal transactivation domain TAD while the ΔN isoforms lack the TAD (Vilgelm et al., 2010; Yang & McKeon, 2000). In addition, via alternative splicing different splice variants have been identified as for p63 and p53 (*α*, *β*, *γ*), and for p73 (*α*, *β*, *γ*, *δ*, *ε*, *ϑ*, *ζ*, *η*, and *η*1). Functionally, all the protein members have the ability to induce apoptosis after UV-induced DNA damage (Belyi et al., 2010). p53, TAp63, and TAp73 can induce cell cycle arrest, apoptosis, or senescence and the three proteins have similar targets however the apoptotic potential can vary depending on the isoform (Dohn et al., 2001). p53 is a well-described transcription factor that transactivates several genes involved in cell cycle arrest and apoptosis. In normal cells p53 is expressed in low levels and constantly degraded by protein ligase MDM2 (Haupt et al., 1997; Honda et al., 1997; Kubbutat et al., 1997). In human cancers, *TP53* is the most frequently mutated gene, and the inactivation of p53 is associated with aggressive cancers and poor outcomes (de Andrade et al., 2021). Even though p53, p63 and p73 seem to have in general similar roles, not all the functions are entirely redundant and the different isoforms and variants could have unique functions that are tissue-specific by acting not only as tumor suppressors but also as oncogenes (Bourdon, 2007; Zawacka-Pankau, 2022).

1.4.2 p63 isoforms

The human *p63* is expressed in 3 isoforms (α, β, γ) which are generated by alternatively splicing in C-terminal. As mentioned above the TAp63 contains an extra N-terminal domain in contrast with the ΔNp63 isoform. There are 6 different p63 isoforms: TAp63α, TAp63β, TAp63γ, ΔNp63α, ΔNp63β, and ΔNp63γ (Bourdon, 2007; Helton et al., 2006). Mutations in p63 gene are extremely rare in human cancers (Hagiwara et al., 1999; Park et al., 2000; Sunahara et al., 1999). ΔNp63 has been reported as an oncogene: In Rat-1A cells ectopic expression of ΔNp63 promotes soft agar colony formation (Hibi et al., 2000). Moreover, it was found that ΔNp63 cooperates with Ras in order to induce tumor-initiating stem-like proliferation (Keyes et al.,

2011). The predominant isoform in epithelial cells is ΔNp63 and its overexpression correlates with poor outcomes and has been found in several cancers such as nasopharyngeal, head and neck, urinary tract, lung, and ovarian tumors (Compérat et al., 2007; Crook et al., 2000; Marchini et al., 2008; Massion et al., 2003; Yamaguchi et al., 2000). For instance, in a subset of breast and head and neck tumors, ΔNp63 was related to increased chemoresistance (Leong et al., 2007; Rocco et al., 2006), and to reduce transcriptional activities of the tumor suppressors p53, TAp63 and TAp73 (Flores, 2007). However, ΔNp63 plays a dual role in cancer biology by promoting tumor development and also suppressing metastasis (Adorno et al., 2009; Truong et al., 2006). Conversely, in response to DNA damage TAp63 isoform resembles full-length p53 promoting cell cycle arrest and apoptosis (Flores et al., 2002). As p63 was also reported to suppress the TGF*β*-dependent cell migration, invasion, and metastasis, analysis of the role of p63 in tumorigenesis arises conflicting results probably due to contradictory phenotypes between TAp63 and ΔNp63 transgenic mice (Koster et al., 2004; Romano et al., 2009).

In regard to YAP, it was previously demonstrated that YAP interacts with ΔNp63 mediating maintenance and self-renewal of lung basal stem cells in order to keep epithelial size (Zhao et al., 2014). In lung cancer cells YAP was found to repress ΔNp63 through the regulation of ZEB2 expression, to inhibit the squamous cell differentiation (Gao et al., 2015). In squamous carcinoma, p63 interacts with the chromatin remodeling factor ACTL6A mediating the activation of YAP signaling to induce tumorigenesis (Saladi et al., 2017). In conclusion, it is suggested that ΔNp63 determines the outcome of the Hippo pathway activation either by it is direct interaction with YAP or by promoting the translocation of YAP to the nucleus (Raj & Bam, 2019).

1.5 Aim of the thesis

YAP was previously found to not only regulate S phase genes but also together with the MMB complex it promotes the expression of relevant genes for G2/M progression (Pattschull et al., 2019; Zanconato et al., 2015). In addition, YAP binds to enhancers and through chromatin loop promotes B-MYB chromatin binding (Pattschull et al., 2019; Zanconato et al., 2018). Even though YAP is considered an oncogene, the specific mechanisms by which YAP activates G2/M target genes to stimulate cell cycle transition remain unexplored. The main major object of this

thesis was to explore YAP-leaded transcription of G2/M genes by evaluating the global changes in the chromatin accessibility induced by YAP overexpression, which can contribute to the induced transcription of G2/M genes and the YAP-mediated downregulation of p63. In addition, this thesis aimed to determine the role and importance of YAP-regulated enhancers in the transcription of G2/M genes through approaches as CRISPR-dCas9, combined with qPCR and ChIP-qPCR.

2. Material and Methods

2.1 Material

2.1.1 Chemical stocks and reagents

Unless otherwise stated, all chemicals were purchased from AppliChem, Roth, Invitrogen, Merck or Sigma Aldrich.

Table 1. Chemical stocks and reagents

Chemical	Stock concentration
4-Hydroxytamoxifen (4-OHT)	25 µM in ethanol
Acetic acid (CH3COOH)	N/A
Agarose	N/A
Ammonium persulfate (APS)	10% in ddH2O
AMPure XP Beads (Beckman Coulter)	N/A
β-Glycerol phosphate	1M in ddH2O
Bovine serum albumin (BSA)	N/A
Bromophenol blue	N/A
Crystal violet	1% in ddH2O
Diethyl pyrocarbonate (DEPC)	ready-to-use
Dimethyl sulfoxide (DMSO)	ready-to-use
Digitonin	1% in ddH2O
Dithiothreitol (DTT)	1 M in ddH2O
dNTPs	2 mM in ddH2O
Edu	10 µM
Ethanol	N/A
Ethidium bromide	ready-to-use (10 mg/ml)
Formaldehyde, 37%	N/A
Glycine	1 M in dH2O
Glycogen (Roche)	ready-to-use (20 mg/ml)
Hoechst 33258	10 mg/ml in ddH2O
ImmuMount (ThermoFisher)	ready-to-use
Isopropanol	N/A
Luminol	250 mM in DMSO
NP-40	ready-to-use
p-Coumaric acid	90 mM in DMSO
peqGOLD TriFast (Trizol; Peqlab)	ready-to-use
Phenylmethylsulfonyl fluoride (PMSF)	100 mM in isopropanol
Ponceau S solution	0.1% Ponceau S in 5% acetic acid

Protease inhibitor cocktail (PIC; Sigma)	ready-to-use
Protein G Dynabeads (Thermo Fisher)	ready-to-use
Protein A/G Magnetic beads	ready-to-use
Proteinase K	10 mg/ml in 50 mM Tris pH 8.0, 1 mM CaCl2
ProtoGel (30%; Acrylamide)(National Diagnostics)	ready-to-use
PSP	3% paraformaldehyde, 2% sucrose in ddH2O
Random primer (Roche)	500 µg/ml in ddH2O
RNase A	10 mg/ml in 10 mM Tris pH 7.4, 150 mM NaCl
Sodium dodecyl sulfate (SDS)	20% in ddH2O
SYBR Green (Sigma)	1:10 in DMSO for storage
Tetramethylethylenediamine (TEMED)	ready-to-use
Thiazolyl Blue Tetrazolium Bromide	5 mg/ml in 1xPBS
Triton-X-100	ready-to-use
Tween-20	ready-to-use
Xylene	ready-to-use

2.1.2 Antibiotics

Table 2. Antibiotics used for the selection of bacteria and mammalian cells

Antibiotics	Stock concentration	Final Concentration	Application
Ampicillin	100 mg/ml	100 µg/ml	Selection of DH5α bacteria
	100 mg/ml	50 µg/ml	Selection of BL21 (DE3) bacteria
Blasticidin	10 mg/ml	10 µg/ml	Selection of MCF10A and MDA-MB231 cells
Kanamycin	50 mg/ml	50 µg/ml	Selection of DH5α bacteria
Neomycin	200 mg/ml	300-800 µg/ml	Selection of MCF10A and MDA-MB231 cells
Puromycin	10 mg/ml	1 µg/ml	Maintenance of MCF10A/YAP2SA and MCF10A/YAP2SA/MYCOMP cells

2.1.3 Enzymes

Table 3. Enzymes

Enzyme	Company
5x RT reaction buffer (for Reverse Transcriptase)	Thermo Fisher
HisTaq16 DNA Polymerase [5 U/µl]	provided by AG Gessler
Phusion Hot Start II DNA Polymerase [2 U/µl]	Thermo Fisher
Restriction endonucleases (10 U/µl)	Thermo Fisher & New England Biolabs
RevertAid Reverse Transcriptase (RT) [200 U/µl]	Thermo Fisher
RiboLock RNase Inhibitor (RI) [40 U/µl]	Thermo Fisher
SYBR Select Master Mix	Thermo Fisher
T4 DNA Ligase	NEB

2.1.4 Kits and protein/DNA markers

Table 4. Commercial kits used for molecular and cellular biology

Kit	Company
(DNF-471) Fragment Analyzer RNA Kit	Agilent
(DNF-474) HS NGS Fragment Kit (1-6000bp)	Agilent
Duolink® In Situ Detection Reagents Red (DUO92008)	Sigma Aldrich
Gibson assembly	NEB
Golden Gate assembly	NEB
NEBNext Multiplex Oligos for Illumina (Dual Index Primers Set 1)	New England Biolabs
NEBNext Ultra II DNA library Prep Kit for Illumina	New England Biolabs
Nextera Transposase and buffers	Illumina
NextSeq. 500/550 High Output Kit v2 (75 cycles)	Illumina
PureLinkTM HiPure Plasmid Midiprep or Maxiprep Kit	Thermo Fisher
QIAquick PCR Purification Kit	Qiagen
Quant-iT PicoGreen dsDNA Assay Kit	Thermo Fisher

2.1.5 Protein/DNA markers

Table 5. Protein and DNA markers

Marker	Company
100 bp DNA ladder	Thermo Fisher
GeneRuler 1 kb DNA Ladder	Thermo Fisher
PageRulerTM Prestained Protein Ladder, 10 to 180 kDa	Thermo Fisher

2.1.6 Buffers and solutions

2.1.6.1 General buffers

Table 6. General buffers

Buffer	Ingredients
0.5 M EDTA, pH 8.0	0.5 M EDTA in ddH2O adjust pH to 8.0 with NaOH pellets
10x TE	100 mM Tris-HCl, pH 7.5 10 mM EDTA (pH 8.0)
1x TE	buffer 10x TE diluted 1:10 in ddH2O and autoclaved
Phosphate buffered saline (1xPBS)	137 mM NaCl 2.68 mM KCl 10.14 mM Na2HPO4 1.75 mM KH2PO4 pH is adjusted to 7.4 with HCl

2.1.6.2 Cell biological buffers

Table 7. Cell biological buffers

Buffer	Ingredients
33% Acetic acid	33% (v/v) Acetic acid in ddH2O
0.1 % Crystal violet staining solution	1% Crystal violet dissolved in ddH2O is diluted 1:10 in 20% Ethanol
50 mM Tris-HCl pH 7.4	in ddH2O, autoclaved
4 M NaCl	in ddH2O, autoclaved
50 mM Tris-HCl pH 7.4	in ddH2O, autoclaved
PBS-T (for Immunofluorescence)	0.1% Triton X-100 in PBS
PSP (3% paraformaldehyde, 2% sucrose in PBS)	15 g paraformaldehyde 10 g sucrose ad 500 ml 1x PBS
Edu-Reaction cocktail	1 X TBS, 100mM $CuSO_4$, AF488-Azide, 100 mM Na-Ascorbate

2.1.6.3 Buffers for molecular biology

Table 8. Buffers for molecular biology

Buffer	Ingredients
5x DNA loading buffer	15% (v/v) Ficoll 0.05% (w/v) Bromophenol blue 0.05% (w/v) Xylene cyanol 0.05 M EDTA in 1xTAE buffer
10x ReproFast buffer	100 mM (NH4)2SO4 100 mM KCl 20 mM MgSO4 200 mM Tris/HCl, pH 8.8 1% (w/v) BSA 1% (v/v) Triton X-100
1x TAE	40 mM Tris/HCl 5 mM acetic acid 10 mM EDTA (pH 8.0)
Base buffer	25 mM NaOH 0.2 mM EDTA adjust to pH 12 with NaOH
DEPC-ddH2O	0.1% (v/v) DEPC is stirred overnight and then autoclaved
LB Medium	40 g/l LB powder, autoclaved
S1 buffer	25 mM Tris/HCl, pH 8.0 10 mM EDTA
S2 buffer	200 mM NaOH 1% SDS
S3 buffer	0.6 M KCH3COO 20% (v/v) acetic acid

2.1.6.4 Buffers for protein biochemistry

Table 9. Buffers used for whole cell lysates and nuclear extracts

Buffer	Ingredients
20 mM HEPES, pH 7.4	in ddH2O

Bradford solution	Bradford solution TNN lysis buffer 50 mg Comassie Brilliant Blue G250 23.75 ml Ethanol 50 ml 85% (v/v) phosphoric acid ad 500 ml ddH2O / filter twice
Buffer A (for nuclear extracts)	10 mM HEPES, pH 7.4 10 mM NaCl 3 mM MgCl2
Nuclei lysis buffer (for nuclear extracts)	20 mM HEPES, pH 7.4 400 mM NaCl 1.5 mM MgCl2 0.1 mM EDTA 15% Glycerol
TNN buffer, pH 7.5	50 mM TrisHCl, pH 7.5 120 mM NaCl 5 mM EDTA 0.5% NP-40 4°C 10 mM Na4P2O7 2 mM Na3VO4 100 mM NaF adjust pH with 37% HCl to 7.5

Table 10. Buffers for SDS-PAGE and immunoblotting

Buffer	Ingredients
0.5 M Tris, pH 6.8	0.5 M Tris base in ddH2O adjust pH with 37% HCl to 6.8
1.5 M Tris, pH 8.8	1.5 M Tris base in ddH2O adjust pH with 37% HCl to 8.8
1x Blotting buffer	125 mM Tris 75 mM Glycine 15% (v/v) Methanol
1x SDS running buffer	192 mM Glycine, 25 mM Tris, 3.5 mM SDS
3x ESB buffer	300 mM Tris/HCl, pH 6.8 15 mM EDTA 150 mM DTT 12% (w/v) SDS 0.03% (w/v) Bromophenol blue
Blocking solution	5% (w/v) milk or BSA in TBS-T
Chemiluminescence solution	10 ml 100 mM Tris-HCl pH 8.5 50 µl 250 mM Luminol 22 µl 90 mM p-Coumaric acid 3 µl 30% H2O2

Ponceau S solution	0.1% Ponceau S 5% CH3COOH
TBS-T	50 mM Tris/HCl, pH 7.4 150 mM NaCl 0.1% (v/v) Tween-20

Table 11. Buffers for Proximity ligation assay (PLA)

Buffer	Ingredients
Wash buffer A	10 mM Tris/HCl, pH 7.4 150 mM NaCl 0.05% Tween
Wash buffer B	200 mM Tris/HCl, pH 7.5 100 mM NaCl

Table 12. Buffers for Chromatin immunoprecipitation (ChIP)

Buffer	Ingredients
5 M NaCl	in ddH2O
3 M C2H3NaO2 (sodium acetate)	in ddH2O
Lysis buffer I	5 mM PIPES, pH 8.0 85 mM KCl 0.5% NP-40
Lysis buffer II (RIPA buffer)	50 mM HEPES, pH 7.9 140 mM NaCl 1 mM EDTA 1% Triton X-100 0.1% C24H39NaO4 0.1% SDS
Wash buffer I	20 mM Tris-HCl, pH 8.1 150 mM NaCl 2 mM EDTA 0.1% SDS 1% Triton X-100
Wash buffer II	20 mM Tris-HCl, pH 8.1 500 mM NaCl 2 mM EDTA 0.1% SDS 1% Triton X-100
Wash buffer III	10 mM Tris-HCl, pH 8.1 250 mM LiCl 1 mM EDTA 1% NP-40 1% C24H39NaO4
Elution Buffer (freshly prepared)	1% SDS 0.1 M NaHCO3

Table 13. Buffers for ATAC-seq

Buffer	Ingredients
ATAC lysis buffer	10mM Tris pH 7.4, 10mM NaCl, 3 mM MgCl2, 0.1% Tween 20
Transposition reaction mix	25 µl 2X TD buffer 2.5 µl TDE1 Nextera transposase (Illumina) 16.5 µl PBS, 0.5 µl 1% digitonin, 0.5 µl 10% Tween-20, and 5µl of nuclease free water

2.1.7 Antibodies

Table 14. Primary antibodies

Name	Internal number	Origin	Company	Application and dilution	Cat number
ß-ACTIN (C4)	196	Mouse	Santa Cruz	WB 1:5000	sc-47778
B-MYB (LX015.1)	149	Mouse	gift from Watson lab (Hybridoma)	WB 1:3 – 1:5	Tavner et al. (2007)
B-MYB (N-19)	79	Rabbit	Santa Cruz	ChIP-qPCR 3 µg	sc-724
BrdU (Bu20a)	319	Mouse	Cell Signaling	IF 1:1000,	5292
CDK7	356	mouse	Cell Signaling	PLA 1:100	#2916
CDK7	357	rabbit	Bethyl	PLA 1:100. ChIP-qPCR 3 µg	A300-405A
HA.11	92	Mouse	Covance	WB 1:1000 ChIP-seq 9 µg	MMS-101P
Histone H4ac	334	Rabbit	Merck Millipore	ChIP-qPCR 3 µg	Merck Millipore
Histone H3K27ac	309	Rabbit	Merck Millipore	ChIP-qPCR 3 µg	06-598
Histone H2A.Z	341	Rabbit	Abcam	ChIP-qPCR 3 µg	ab232908
IgG	104	Rabbit	Sigma- Aldrich	IP 2 µg ChIP-qPCR 3 µg ChIP-seq 9 µg	I5006
LIN9	292	Rabbit	Biomol (Bethyl)	IP 1µg PLA 1:150	A300-BL2981
Phospho-Chk1 (Ser345)	339	Rabbit	Cell Signaling	WB: 1:1000	2341

Phospho H3 (Ser10)	290	Rabbit	Santa Cruz	IF 1:100 – 1:200	sc-8656-R
p63 a (D2K8X)	323	Rabbit	Cell Signaling	WB: 1:1000 ChIP-seq 9 µg	#13109
RNA Pol II (8WG16)	328	mouse	Santa Cruz	ChIP-seq 9 µg	sc-56767
RNA Pol II (phospho S2)	252	Rabbit	Abcam	ChIP-qPCR 3 µg ChIP-seq 9 µg	ab5095
RNA Pol II (phospho S5)	253	Rabbit	Abcam	ChIP-qPCR 3 µg ChIP-seq 9 µg	ab5131
RNA Pol II CTD4H8 (Ser5)	351	Mouse	Santa Cruz	ChIP-qPCR 3 µg ChIP-seq 9 µg	sc-47701
YAP	297	Mouse	Santa Cruz	WB: 1:1000 PLA: 1:200 IF: 1:200	Sc-101199
XPD	--	Rabbit	Cell Signaling	IP: 1:1000	AB_2797781

Table 15. Secondary antibodies

Name	Application and dilution	Company	Cat number
anti-mouse HRP conjugated	WB 1:5000	GE healthcare	NXA931
anti-mouse IgG (H+L) Alexa Fluor 488	IF 1:500	Thermo Fisher	A11029
anti-mouse IgG (H+L) Alexa Fluor 594	IF 1:500	Thermo Fisher	A-11032
anti-rabbit IgG (H+L) Alexa Fluor 488	IF 1:500	Thermo Fisher	A-21206
anti-rabbit IgG (H+L) Alexa Fluor 594	IF 1:500	Thermo Fisher	A-11037
Duolink In Situ PLA Probe Anti-Mouse PLUS	PLA 1:5	Sigma-Aldrich	DUO92001
Duolink In Situ PLA Probe Anti-Rabbit MINUS	PLA 1:5	Sigma-Aldrich	DUO92005
HRP Protein A	WB 1:5000	BD Biosciences	610438

2.1.8 Plasmids

Table 16. Plasmids for transient expression and lentivirus production in mammalian cells

Name	Internal number	Description
pBABE_H2B-GFP	746	GFP expression vector, used to determine transfection efficiency

pINDUCER-B-MYB-RNAi-resistant	1716	Lentiviral construct with doxycycline inducible expression of WT B-MYB
ΔNP63alpha	1826	Expression vector used to clone WT ΔNP63. Addgene: 26979
pInd20/ΔNP63	1828	Lentiviral construct with doxycycline inducible expression of ΔNP63. Backbone of ΔNP63 from Addgene plasmid #26979,
pCRIS-PITCH/B-MYB.N-Ter-FKBP12(F36V)	1767	PITCh dTAG donor vector for BSD-P2A-2xHA-FKBP_F36V knock-in into the N-terminus of the human B-MYB locus.
pCRISPR-Cas9/B-MYB.N-Ter	1766	PITCh sgRNA, N-terminal B-MYB sgRNA, and Cas9 expressing plasmid for use with the dTAG knock-in system
pCRIS-PITChv2-BSD-dTAG (BRD4)	1685	Vector with an N-terminal dTAG cassette for endogenous protein degradation, replaced the EGFP cassette in the original pCRIS-PITChv2 plasmid- Addgene plasmid #91792
px330A-1x2	1682	Vector to express Cas9 nuclease and gRNA. Addgene plasmid #58766
px330S-2-PITCh	1683	Vector to expresses Cas9 nuclease and the PITCh-gRNA. Addgene plasmid #63670

2.1.9 Primers

Table 17. Primers for cloning

Gene	Internal #	Sequence (5’ to 3’)	Directionality
B-MYB N-Ter_CRISPR_ oligo	2806	CACCGGGGCCGGGGGGATGTCTCGG	Top
	2807	AAACCCGAGACATCCCCCCGGCCCC	Botton
	2810	gttacatagcatcgtacgcgtacgtgtttggTCCGGGCC GGGGGGATGTCTatggccaagcctttgtctcaag	Forward

dTAG_B-MYB(N-Ter) Gibson	2811	gttacatagcatcgtacgcgtacgtgtttggTCTCGGACCCTCATCTTGTCtggtggcggtggctcg	Reverse

Table 18. Primers for knock-in confirmation of human cells

Gene	Internal number	Sequence (5' to 3')	Directionality
FKBP12/B-MYB-N-Ter	2870	GGGATGCTTGAAGATGGAAA	Forward
	2871	GGGGAGGGGTGAGTTAAAGG	Reverse
B-MYB 5' and N-Ter	2900	GGCGGGAGATAGAAAAGTGC	Forward
	2871	GGGGAGGGGTGAGTTAAAGG	Reverse
pCRIS-PITCh	2814	TCGCCCTTAATTGTGAGCGGA	sequencing primer forward
pCRIS-PITCh	2815	GAAAGGACAGTGGGAGTGGCA	sequencing primer reverse
p63 (internal)	2952	CAGCAAGTTTCGGACAGTACAAG	sequencing primer forward

Table 19. Primers for qPCR of human cDNA

Gene	Internal no.	Sequence (5' to 3')	Directionality
AMOTL2	2391	AGGCTGCAGAGAGACAATGAG	Forward
	2392	CTCAGAGAGCCGCTGGATT	Reverse
AURKA	2548	GCAGATTTTGGGTGGTCAGT	Forward
	2549	TCCGACCTTCAATCATTTCA	Reverse
BIRC5	568	GCCCAGTGTTTCTTCTGCTT	Forward
	569	CCGGACGAATGCTTTTTATG	Reverse
CCNA2	572	GGTACTGAAGTCCGGGAACC	Forward
	573	GAAGATCCTTAAGGGGTGCAA	Reverse
CDC20	2273	CTGTCTGAGTGCCGTGGAT	Forward
	2274	TCCTTGTAATGGGGAGACCA	Reverse
CTGF	2295	CAAGGGCCTCTTCTGTGACT	Forward
	2296	ACGTGCACTGGTACTTGCAG	Reverse
CYR61	2389	CAACCCTTTACAAGGCCAGA	Forward
	2390	TGGTCTTGCTGCATTTCTTG	Reverse
ΔN-p63	2944	GAAAACAATGCCCAGACTCAA	Forward
	2945	TGCGCGTGGTCTGTGTTA	Reverse

DLG5	3074	ACCAGAAGGAGATCGGTGAC	Forward
	3075	ATCTCGGATGACCCGTTGT	Reverse
GAPDH	645	GCCCAATACGACCAAATCC	Forward
	646	AGCCACATCGCTCAGACAC	Reverse
IRF6	3058	TTTGTCTGGAAACATTCCTTAGC	Forward
	3059	CCCCAAAGCATAAGTAGATCTCAA	Reverse
KIF23	1862	CCTAACGTCCCGCAGTCTT	Forward
	1863	AGGTTTCCGGGGTGTCTTAG	Reverse
LAPTM5	3096	GCCCGCCTACCTCAAGTT	Forward
	3097	CAGCTGCAGCGTCATCAG	Reverse
MINK1	3127	AGAAGCGGGGTGAGAAAGA	Forward
	3128	CGTTCATGATGGAGCTTGG	Reverse
MYBL2	630	TCCACACTGCCCAAGTCTCT	Forward
	631	AGCAAGCTGTTGTCTTCTTTGA	Reverse
NCAPH	2995	ACCTCAAACCAGGCACCA	Forward
	2996	TCTTCATAATGCTCAGTCTCTACCC	Reverse
P53	771	AGGCCTTGGAACTCAAGGAT	Forward
	772	CCCTTTTTGGACTTCAGGTG	Reverse
SYNPO	3094	AGGGAGGACCTAGCAGACG	Forward
	3095	GTCAGCTGGGCTGCAATC	Reverse
TOP2A	2421	TCTGGTCCTGAAGATGATGCT	Forward
	2422	TTAGTTAACCATTCCTTTCGATCA	Reverse
YAP	2277	GACATCTTCTGGTCAGAGATACTTCTT	Forward
	2278	GGGGCTGTGACGTTCATC	Reverse

Table 20. Primers for qPCR of human ChIP-DNA

Gene	Internal no.	Sequence (5' to 3')	Directionally
CDC20 -428	2837	GGCTCTCCTTCCCCTTCTAG	Forward
	2838	TCCGAGAACCTGCAGAAGTT	Reverse
CDC20 -41	2556	GGTTGCGACGGTTGGATTTT	Forward
	2557	CTTTAACACGCCTGGCTTACG	Reverse
CDC20 +120	2969	GGTGGCCCTGATTTTGTGG	Forward
	2970	CTGGAGGAAAGGAGGCGAC	Reverse
CDC20 +1827	3042	TCCACCACCATGATGTTCGG	Forward
	3043	TCCACCACCATGATGTTCGG	Reverse
CDC20 +4020	3034	GAGTCTGACCATGAGCCCAG	Forward
	3035	CTCAGGGTCTCATCTGCTGC	Reverse
CDC20 +4113	3036	ATGGCGCTGTTTTGAGTTGG	Forward
	3037	ACTGAGGTGATGGGTTGGTC	Reverse

CDC20 TES	3038	ACCTTTGGCCCAGAAGCTAC	Forward
	3039	CAAAGGGTCTCGTGGCCTT	Reverse
CDC20 enhancer 1	2598	CCTGCAGAGTGAGCCATGTG	Forward
	2599	GAGCTGGCTGTGTCCTTTGA	Reverse
CDC20 enhancer 1-peak1	2981	AATCCCAGCAGTTTCCCTTT	Forward
	2982	AAGCCATGACTCGCTCTGTT	Reverse
CDC20 enhancer 2-peak2	2975	AAATACTCTTGGCCACGCAC	Forward
	2976	AGTCTCACCATGCTGCCTAG	Reverse
DLG5 enhancer	3092	TGAGTGCTCCTGAGGAAGTG	Forward
	3093	TCTACTTCCTTACCGCCTGC	Reverse
GAPDHS Promoter	540	GGCAGCAAGAGTCACTCCA	Forward
	541	TGTCTCTTGAAGCACACAGGTT	Reverse
IRF6 enhancer	2987	TCCTTGACCCTGATTGAGCC	Forward
	2988	TCCAGACATTGACGCAGGTA	Reverse
KIF23 Promoter	1894	CCTAACGTCCCGCAGTCTT	Forward
	1895	GCCTCGTACTCACGCTGAC	Reverse
NCAPH Promoter	3150	CTGCCTCACACTCCTCAGTT	Forward
	3151	CAACGGTAACCACATCGCTT	Reverse
MINK1 enhancer	2989	TCACACATCCCTCTGGCATA	Forward
	2990	AGAAGGAAGGCGAAGAAACC	Reverse
TOP2A Promoter	2342	GGTGCCTTTTGAAGCCTCTC	Forward
	2343	TCCACCTATGAACGGCTGAG	Reverse
SYNPO enhancer	3131	CACGAGTCCCGTGTACCTG	Forward
	3132	AGCCTGTGCTACACACAGCA	Reverse

Table 21. Oligos used for ATAC-seq

Name	Internal no.	Sequence (5' to 3')
Ad1_noMX	2682	AATGATACGGCGACCACCGAGATCTACACTCGTCGGCAGCGTCAGATGT*G
Ad2.1	2683	CAAGCAGAAGACGGCATACGAGATTCGCCTTAGTCTCGTGGGCTCGGAGATG*T
Ad2.2	2684	CAAGCAGAAGACGGCATACGAGATCTAGTACGGTCTCGTGGGCTCGGAGATG*T
Ad2.3	2685	CAAGCAGAAGACGGCATACGAGATTTCTGCCTGTCTCGTGGGCTCGGAGATG*T
Ad2.4	2686	CAAGCAGAAGACGGCATACGAGATGCTCAGGAGTCTCGTGGGCTCGGAGATG*T

*phosphorothioate modification

2.1.10siRNAs

The siRNAS used were purchased from Eurofins Genomics or Dharmacon and dissolved to a stock concentration of 75 µM.

Table 22. siRNAs

Target gene	Name	Species	Internal number	Sequence (5'to 3')	Supplier
Non-targeting	siCtrl	/	S53	UAGCGACUAAACACAUCAA	Eurofins Genomics
p63	siP63	human	S77	CAAUGCCCAGACUCAAUUUTT	Eurofins Genomics
YAP	siYAP	human	S73	UCUCUGACCAGAAGAUGUC	ThermoFischer
TAZ	siTAZ	human	S72	ACGUUGACUUAGGAACUUU	Thermo Fisher Scientific

2.1.11 Cell lines

Table 23. Mammalian cell lines

Cell line	Organism	Description	Reference
HEK293T	*homo sapiens*	human embryonic kidney cells with constitutive expression of SV40 large T antigen and neomycin resistance gene; used to produce lentivirus cell lines	SBI Cat.-no.: LV900A-1
MCF10A	*homo sapiens*	non-tumorigenic, breast epithelial cells	ATCCL® CRL-10317tm
MCF10A-YAP5SA	*homo sapiens*	non-tumorigenic, breast epithelial cells stably transduced with pInducer21-Strep-YAP5SA	Eyss et al, 2015
MCF10A-ER-YAP2SA	*homo sapiens*	Non-tumorigenic, breast epithelial cells stably transduced with pLEGO -ER-YAP2SA which allows fast activation of YAP by 4-OHT	Gründl et al, 2020

MCF10A-ER-YAP2SA-MY-COMP	*homo sapiens*	non-tumorigenic, breast epithelial cells stably transduced with pLEGO -ER-YAP2SA and pInd20/MY-COMP (for B-MYB-YAP competition) which allows activation of YAP by 4-OHT and expression of MY-COMP (for B-MYB-YAP competition) by induction with Doxycycline.	Gründl et al, 2020
MCF10A YAP5SA-ΔNp63	*homo sapiens*	Non-tumorigenic, epithelial mam- mary breast cells stably transduced with pInducer21-Strep-YAP5SA and pInd20/ΔNP63	This Study
MCF10A-ER-YAP2SA-ΔNp63	*homo sapiens*	Non-tumorigenic, breast epithelial cells stably transduced with pLEGO -ER-YAP2SA and pInd20/ΔNP63, which allows activation of YAP by 4-OHT and overexpression of ΔNP63 by induction with Doxycycline.	This Study
MCF10A-dCas9-KRAB/sgRNA-CDC20 Enhancers	*homo sapiens*	Non-tumorigenic, breast epithelial cells stably transduced with the doxycycline inducible lenti_sgCDC20-enhancer1+2-multiplex-blast (ME)+ Cas9-KRAB	generated in lab
MCF10A-dCas9-KRAB/sgRNA-ctrl	*homo sapiens*	Non-tumorigenic, breast epithelial cells stably transduced with the doxycycline inducible lenti_sgRNA-blast (ctrl)-multiplex-blast (ME)+ Cas9-KRAB	generated in lab
MCF10A-YAP5SA-dCas9-KRAB/sgRNA-CDC20 Enhancers	*homo sapiens*	Non-tumorigenic, breast epithelial cells stablytransduced with pInducer21-Strep-YAP5SA and with the doxycycline inducible lenti_sgCDC20-enhancer1+2-multiplex-blast (ME)+ Cas9-KRAB	generated in lab
MCF10A YAP5SA_ dCas9-KRAB/sgRNA-ctrl	*homo sapiens*	Non-tumorigenic, breast epithelial cells stablytransduced with pInducer21-Strep-YAP5SA and with the doxycycline inducible lenti_sgRNA-blast (ctrl) -multiplex-blast (ME)+ Cas9-KRAB	generated in lab
MDA-MB-231	*homo sapiens*	Mammary gland/breast; derived from metastatic site: pleural effusion	ATCC; CRL-12532

MDA-MB231-B-MYBdTAG	*homo sapiens*	Mammary gland/breast; derived from metastatic site: pleural effusion. stably transfected with pCRIS-PITCHv2/B-MYB-N-Ter-FKBP12(F36V) (BSD) and pX330A-nB-MYB-CRISPR-Cas9 N-Ter to induce endogenous degradation of B-MYB.	This Study

2.1.12 cell culture reagents, media and additives

Table 24. Cell culture reagents and additives

Reagents	Supplier
1xPBS	see Table 6
Cholera Toxin	Sigma-Aldrich
DMEM (1X) + GlutaMAX	Thermo Fisher
FBS	Thermo Fisher
Horse serum	Thermo Fischer Scientific & PAN Biotech
Human EGF	Sigma-Aldrich
Hydrocortisone	Sigma-Aldrich
Insulin solution human	Sigma-Aldrich
Penicillin-Streptomycin (10,000 U/ml)	Thermo Fisher
Trypsin-EDTA (0.05%), phenol red	Thermo Fisher

Table 25. Composition of cell culture medium

Media	Cell line	Composition
DMEM	MDA-MB-231, MDA-MB231-B-MYBdTAG, HEK293TN	DMEM 10% FBS 1% pen-strep
MCF10A medium	MCF10A YAP5SA, MCF10A-ER-YAP2SA, MCF10A-ER-YAP2SA-MY-COMP	DMEM/F-12 (1:1) 5% horse serum 1% pen-strep 20 ng/ml hEGF 100 ng/ml cholera toxin 10 µg/ml insulin 500 ng/ml hydrocortisone

Starving Medium	MCF10A, MCF10A YAP5SA	DMEM/F-12 (1:1) 0,25% horse serum 1% pen-strep 20 ng/ml hEGF 100 ng/ml cholera toxin 10 µg/ml insulin 500 ng/ml hydrocortisone
MCF10A cells, freezing medium	MCF10A, MCF10A YAP5SA, MCF10A-ER-YAP2SA, MCF10A-ER-YAP2SA-MY-COMP	25% F-12 25% DMEM 40% horse serum 10% DMSO
MDA-MB231 cells, freezing medium	MDA-MB-231, MDA-MB231-B-MYBdTAG	50% DMEM 40% FBS 10% DMSO
Mammosphere medium	MCF10A YAP5SA	DMEM/F-12 (1:1) 1% pen-strep B27 supplement (1x) BPE (52 µg/ml) Insulin (5 µg/ml) Hydrocortisone (0.5 µg/ml) EGF (10 ng/ml)

Table 26. Reagents used for the treatment of mammalian cells

Reagent	Dissolved in	Stock concentration	Final concentration	Supplier
4- Hydroxytamoxifen (4-OHT)	100% Ethanol	25 µM	10 nM	Sigma-Aldrich
Verteporfin	DMSO	2 mg/ml (2.78 mM)	7.5 µM	Sigma-Aldrich
Prexasertib	DMSO	10 mM	100 nM	Biozol
Doxycycline (hyclate) (dox)	ddH2O	1 mg/ml	0.5 µg/ml	Sigma-Aldrich
THZ1	DMSO	10 mM	500nM	Sigma-Aldrich

DRB (5,6-dichloro-1-beta-D-ribofuranosyl-1H-benzimidazole)	DMSO	10 mM	50 µM	Biomol
BI-1347	DMSO	10 mM	50 nM	MedChem Express
dTAG13	DMSO	2,5 mM	500nM	Sigma-Aldrich
Blasticidin	--	10 mg/ml	10 µg/ml	InvivoGen

2.1.13 Transfection reagents

Table 27. Reagents used for transfections

Transfection reagent	Supplier
2.5 M CaCl2	sterile filtered
2x HBS pH 7.05	8.2 g NaCl 5.95 g HEPES free acid 0.105 g Na2PO4 ddH_2O to a final volume of 500 ml pH 7.05 sterile filtered
Lipofectamine 3000 RNAiMax	Thermo fisher
RNAiMax	Thermo fisher
Opti-MEM (1x) + GlutaMAX	Thermo fisher

2.1.14 Bacterial strains

Table 28. Bacterial strains

Bacterial strain	Genotype	Application
BL21 (DE3)	F-ompT hsdSB (rB-, mB-) galdcmrne131 (DE3)	expression of recombinant protein
DH5α	F– Φ80lacZΔM15 Δ(lacZYA-argF) U169 recA1 endA1 hsdR17 (rK–, mK+) phoA supE44 λ– thi-1 gyrA96 relA1	cloning

2.1.15 Devices

Table 29. Devices

Device	Supplier
Agarose gel electrophoresis system	Peqlab
Cytomics FC 500 flow cytometer	Beckman Coulter
DynaMag-2 Magnet	Thermo fisher
DynaMag-96 Side Magnet	Thermo fisher
Electrophoresis Power Supply E835	Consort
Electrophoresis Power Supply EV231	Consort
Fragment Analyzer Automated CE System	Advanced Analytical
ImageQuant 800	AMERSHAM
Infinite M200 plate reader	Tecan
Leica DFC350 FX digital camera	Leica Microsystems
Leica DMI 6000B inverted microscope	Leica Microsystems
Lumen 200 fluorescence light source	Leica Microsystems
Min-PROTEAN 3 Cell System	Bio-Rad
Mini Trans-Blot Cell System	Bio-Rad
Multiskan Ascent plate reader	Labsystems
qTOWER^{3G}	Analytikjena
NanoDrop 2000 spectral photometer	Peqlab
NextSeq 500	Illumina
qTower3 6	Analytikjena
Sonifier W-250 D	Branson
T1 Thermocycler	Biometra
Ultrospec 2100 pro spectrophotometer	mersham Biosciences
DMI 6000B	Leica
Operetta® CLS™	PerkinElmer

2.1.16Software

Table 30. Software used for data analysis

Software	Reference
Adobe Illustrator CC 2020	Adobe Inc.
BEDTools v2.26.0	Quinlan and Hall, 2010
Bowtie v2.3.2	Langmead and Salzberg, 2012
CXP Acquisition and Analysis (Cytomics FC 500)	Beckman Coulter
DeepTools 2	Ramírez et al, 2016
FASTQ Generation Software v1.0.0	Illumina
FeatureCounts	Liao et al, 2014

Fiji	Schindelin et al, 2012
Galaxy Web-based platform	Afgan et al, 2018
Genrich	John M. Gaspar
GSEA (Broad Institute)	Subramanian et al, 2005
Integrative Genomics Viewer (IGV)	Ramirez et al, 2016
Leica Application Suite (LAS) 3.7	Leica Microsystems
MACS v.2.1.1	Zhang et al, 2008
NucleoATAC	Schep et al, 2015
Prism 9	GraphPad Software, Inc
Tecan i-control	Tecan

2.2 Methods

2.2.1 Mammalian cell culture

2.2.1.1 Cell lines and culturing conditions

All cell lines used in this thesis were cultured at 37°C and 5% CO_2 at sterile conditions. MDA-MB231 cells were maintained in GIBCO® Dulbecco's Modified Eagle Medium (DMEM) supplemented with 10% (v/v) fetal bovine serum (FBS) and 1% (v/v) penicillin-streptomycin. MCF10A cells were cultures in a 1:1 mixture of F12/DMEM supplemented with 5% horse serum, 1% penicillin-streptomycin, 20 ng/ml human EGF, 100 ng/ml cholera toxin, 10 µg/ml insulin, and 500 ng/ml hydrocortisone.

2.2.1.2 Passaging and seeding cells

Cells were subcultured every three to four days by removing old medium and washing once with 1X PBS followed by 3-15 min incubation with 0,05% Trypsin/EDTA at 37°C. Detached cells were resuspended in medium and seeded onto a new cell culture dish according to demanded cell concentration (Table 31).

Table 31.MCF10A cells number for subconfluent conditions

Aplication	MCF10A cell lines
RNA isolation	150,000 cells/6 cm dish
Whole cell lysates	1.5 x 10^6/15 cm dish

ChIP	1.7 x 10^6/15 cm dish
PLA	35,000 cell/ibidi plate wells
IF	70,000 cells/6 wells plate

2.2.1.3 Counting cells

A Neubauer chamber was used to determine cell number in a suspension. After trypsinization cells were resuspended in medium as described in (2.2.1.1). 10 µl of the cell suspension were placed into a Neubauer chamber. Cells were counted under a light microscope. Cells were counted under a light microscope. The average number of cells of four quadrants was multiplied per 10,000 to estimate the number of cells per milliliter.

2.2.1.4 Freezing cells

For freezing, cells were trypsinized and resuspended in medium followed by a centrifugation step for 5 minutes at 300 xg at room temperature (RT). The resulting pellet was resuspended in corresponding freezing medium (Table 25). Aliquots of 1 ml were transferred into cryotubes and placed at -80°C. For long term storage, cells were transferred into liquid nitrogen.

2.2.1.5 Thawing cells

Cryotubes were thawed in a 37°C water bath. Cells were immediately transferred to a 15 ml falcon tube which contains 9ml of prewarmed medium. After cells were centrifuged for 5 minutes at 300 g at RT. The supernatant was discarded, and the cell pellet was resuspended in new medium. Then, cells were transferred onto a 10 cm cell culture plate.

2.2.1.6 Cells treatments

4-hydrotamoxifen (4-OHT)

To induce the nuclear translocation of the fusion protein YAP2SA/Estrogen receptor (ER), MCF10A-ER-YAP2SA and MCF10A-ER-YAP2SA-MY-COMP cells were treated with 1 µM 4-OHT for the indicated times. YAP2SA is a mutant version of YAP whith two serine to alanine substitutions which has a similar inhibitory effect on the degradation of YAP as YAP5SA (Zhao et al., 2007).

Doxycycline

MCF10A/YAP5SA cells were treated with 0.5 µg/ml doxycycline (dox) to induce the expression of YAP5SA for the indicated time. MCF10A YAP5SA-ΔNp63 were treated with 0.01 µg/ml of doxycycline to overexpress YAP5SA and ΔNp63 simultaneously. MCF10A-ER-YAP2SA-MY-COMP cells were treated with 0.01 µg/ml of doxycycline to overexpress ΔNp63 independently of YAP induction. The MCF10A cell lines to silence enhancers of CDC20 (Table 23) cells were treated with 0.5 µg/ml doxycycline to induce the activation of the dCas9/KRAB system. MDA-MB231-B-MYB/dTAG cells were treated 0.01 µg/ml to induce B-MYB WT and infected with Pindu20-B-MYB WT.

Verteporfin

To inhibit the interaction between YAP and TEAD, cells were treated with 7.5 µM verteporfin for the indicated times.

Prexasertib

To inhibit the checkpoint kinase 1, for survival curves cells were treated with different concentrations of prexasertib 0-10,000 nM during 42h for MTT assays. For standard treatments, cells were treated with 100nM of prexasertib.

Thymidine

To synchronize cells in G1/S phase single or double treatments with 2mM of thymidine were performed at the indicated times.

dTAG13

In order to degrade endogenous B-MYB, MDA-MB231-B-MYBdTAG cells were treated with 500nM of dTAG13 at the indicated times. dTAG13 works as a bridge between B-MYB and an E3 ubiquitin ligase (cereblon; CRBN), which leads to proteasome degradation of B-MYB.

THZ1 (CDK7i)

In order to inhibit CDK7 a component of CAK and TFIIH complexes, cells were treated with 500nM of THZ1 (Sigma).

2.2.1.7 Plasmid transfection using calcium phosphate

Cells were seeded onto 10 cm cell culture dishes, 50 µL of 2.5 M CaCl2 were mixed with up to 18 µg of plasmid DNA and filled up with 500 µl of sterile ddH_2O. Additionally, 500 µl 2xHBS buffer were bubbled in a 15 ml falcon tube by using a pipette aid and a Pasteur-pipette. Next, the DNA CaCl2 mixture was pipetted dropwise into the HBS solution, and incubated for 20 minutes at room temperature. The final solution was then added dropwise to the cells. Cells were incubated for 24 hours and fed with fresh medium.

2.2.1.8 Plasmid transfection using Lipofectamine 3000

To produce a cell line in which endogenous B-MYB was fused to the degradation domain FKBP12. $3*10^5$ MDA-MB-231 cells were seeded in a 6-well plate with a free antibiotic medium. Next day, cells were co-transfected with vector1: pCRISPR-Cas9/B-MYB.N-Ter and vector 2: pCRIS-PITCH/B-MYB.N-Ter- FKBP12(F36V) using lipofectamine 3000 reagents according to (Table 32). The DNA mix was added to the lipofectamine and mixed by pipetting, followed by a 15 minutes incubation at RT. Afterwards, the mix was added to the cells dropwise, and the plate was mixed by rocking. In parallel, a transfection control was performed using a 1.4 µg GFP vector (#746) in order to evaluate transfection effectiveness.

The next day, transfection efficacy was tested in the microscope, and cells were fed with complete DMEM medium. Three days after transfection, cells were trypsinized and transferred to 15 cm cell culture dishes. Subsequently, cells were selected by adding medium containing 10 µg/ml Blasticidin every 3 days, including GFP vector-transfected cells. Single clones were isolated in 96-well plates until cells were confluent and transferred to 24-well plates. Genomic DNA was isolated as described in (2.2.2.14), knock-in was confirm through PCR reactions and sequencing as described in (2.2.2.15).

Table 32. Plasmid transfection with lipofectamine

Mix	Lipofectamine	P3000	DNA	Opti-MEM
Lipofectamine Mix	10 µl	-	-	125 µl
DNA/P3000 Mix	-	5 µl	1.8 µg (1,2µg vector 1 +0.6µg vector2)	125 µl

2.2.1.9 Plasmid transfection with PEI

To produce a cell line in which endogenous B-MYB was fused to the degradation domain FKBP12. $3*10^5$ MCF10A-Y5SA cells were seeded in a 6 well plate with free antibiotic medium. Next day, cells were co-transfected with vector1: CRISPR-Cas9/B-MYB.N-Ter and vector 2: CRIS-PITCH/B-MYB.N-Ter using polyethylenimine (PEI) according to table 4. Each mix was vortexed and incubated at RT during 5 minutes. The PEI mix was added to the DNA mix, mixed by vortex followed by a 15 minutes incubation at RT. Medium was changed and the transfection mix was added to the cells dropwisely, and the plate was mixed by rocking. In parallel, a transfection control was performed using a 1.8 µg GFP vector (#746) in order to evaluate transfection effectiveness. The next day, transfection efficacy was tested in the microscope and cells were fed with complete DMEM medium. Three days after transfection, cells were trypsinized and transferred to 15 cm cell culture dish. Subsequently, cells were selected by adding a medium containing 10 µg/ml Blasticidin every 3 days, including GFP vector transfected cells. Single clones were isolated in 96-well plates until cells were confluent and transferred to 24-well plates.

Table 33. Plasmid transfection with PEI

Mix	DNA	DMEM	PEI
DNA/DMEM Mix	2.0 µg (1,3 µg vector 1+0.7 µgvectpr2)	100 µl	-
PEI/DMEM Mix	6 µl	100 µl	125

2.2.1.10 siRNA transfection

The double-stranded siRNAs were transfected in a final concentration of 75 µM and silencer select siRNAs were transfected in a final concentration of 10µM using RNAiMAX (Thermo Fisher Scientific) according to the manufacturer's protocol. siRNAs are listed in Table 22.

2.2.1.11 Lentivirus production using HEK293T cells

HEK293T cells were used to produce lentiviral vectors. $5.0*10^6$ HEK293T cells were seeded onto a 10 cm dish. On the next day 3 hours before the transfection, medium was removed and 8ml of antibiotic-free DMEM supplemented with 10% FBS medium was added 3 hours before the

transfection. Calcium phosphate was used to transfect HEK293T cells (2.2.1.7)with the following amounts of DNA plasmid:

- 9 µg (10 cm) lentiviral vector
- 6 µg (10 cm) psPAX2
- µg (10 cm) pCMV-VSV-G

Next morning, old medium was changed to 8ml of fresh DMEM (10% FBS, 1% pen-strep) medium. Approximately 40h after transfection, lentivirus supernatant was collected and stored at 4°C and 8ml of fresh DMEM medium was added to the dish. 20h later lentiviral supernatant was collected for the second time and mixed with 40-h supernatant and stored at 4°C. The mixed lentiviral supernatant was centrifuged at 1000 rpm for 5 min (RT) ad filtered using a 0,45µm pyrogen filter and either directed used for lentiviral infection or stored at -80°c.

2.2.1.12 Generation of stable cell lines using lentiviruses

To generate stable cell lines, 240,000 target cells (MCF10A-YAP5SA, MCF10A-ER-YAP2SA or MDA-MB-231-B-MYBdTAG) were seeded on a 6-well plate. On the next day to infect the cells, a 2ml of the mixture of lentiviral supernatant and target cell culture medium in a 1:1 ratio was added to the cells. Polybrene was added to a final concentration of 8 µg/ml, cells were incubated overnight. Next day, medium was changed and cells were incubated one day more and then split and selected with 600 µg/ml neomycin. Uninfected cells were used as a control. Cells were selected for 8-10 days until control cells were dead. The levels of neomycin were reduced to 300 µg/ml to keep cells on culture.

2.2.1.13 Flow cytometric analysis of cell cycle with propidium iodide DNA staining

For flow cytometry analysis (FCA) 450,000 cells were seeded per 6 cm dish. Corresponding treatments were performed and incubated for the necessary time. Then, the medium was aspired and collected into a 15ml falcon tube to include death cells in the analysis. Attached cells were harvest by trypsinization and transferred into the same 15ml polystyrol falcons. Cells were then centrifuged at 1.200 rpm for 5 minutes at 4°C and washed with ice-cold PBS and centrifuged once more. Cell pellet was fixed by adding 1 ml of 80% ethanol dropwise under constant and slowly vortexing. Cells were stored at 4°C for at least 1 day. Fixed cells were

centrifuged (1,200 rpm for 5 minutes at 4°C) and washed once with 5ml of cold PBS. The resulting pellet was resuspended in 500 µl ice-cold 38mM Na-citrate buffer. RNA was digested by adding 25 µl RNase A (10mg/ml) for 30 minutes at 37°C. Next, DNA was stained by the addition of 15 µl propidium iodide (1mg/ml). Cell cycle profiles were analyzed using a FC 500 flow cytometer (Beckman Coulter).

2.2.1.14 Crystal violet staining

To stain cells attached to the cell culture plates, 10,000 MDA-MB 231 dTAG and (cl6-3) cells were seeded in a 24 well-plate. dTAG13 positive treated cells, were 24 hours before pretreated with dTAG13 500nM. On the next day cells were treated with prexasertib in different concentrations (100nM, 250nM, 500nM). 72 hours after prexasertib treatment, medium was removed from the wells and cells were fixed with 100% cold methanol for 20 minutes. Next, methanol was removed and cells were stained with 0,1% crystal violet in 20% ethanol for 30 minutes rocking at room temperature. Finally, stained plates were rinsed with tap water and air dried, and pictures were taken. For quantification, crystal violet was solubilized by adding 200 µl of 33% acetic acid during 20 minutes of rocking at room temperature. Absorbance at 595nm of 100 µl extracted dye was measured in a 96-well plate by using the Multiscan Ascent microtiter plate reader (Labsystems). Three replicates per condition were measured and the average values were calculated.

2.2.1.15 MTT Assay for cell Viability and proliferation

To measure cell viability in MDA-MB231-dTAG-B-MYB cells after prexasertib treatment, 4500 cells per well were seeded on 96-well plate, by using a multistep pipette. On the next day, 10 different concentrations of prexasertib (0,1-10000 nM) were tested in triplicates. An initial dilution was performed in DMEM medium 1:100 (100000 nM) and subsequent serial dilutions of prexasertib were prepared in DMEM medium, in 1.5 ml tubes.

Table 34. Serial dilutions of prexasertib

Final concentration nM	Volume (µl)	Sample	µl medium	Final volume µl
10000	100	1:100 dilution (100000 nM)	900	900
1000	100	10000 nM	900	500

500	500	1000 nM	500	500
250	500	500 nM	500	600
100	400	250 nM	600	500
50	500	100 nM	500	800
10	200	50 nM	800	900
1	100	10 nM	900	500
0,5	500	1 nM	500	800
0,1	200	0.5 nM	800	1000
0	0	0	1000	1000

Once the serial dilutions were prepared, medium was removed from each well, and 100 µl of corresponding dilution were added, cells were incubated for 72 hours. At the 5 fifth day, Thiazolyl Blue Tetrazolium Bromide (MTT) solution (5mg/ml) was thawed in the water bath for 5 minutes, next 20 µl were added to the cells followed by 2h incubation at 37°C. Next, the medium was removed without disturbing the cells, 100 µl of DMSO were added as a solvent. The plate was covered with tin foil and incubated for 20 minutes on slowly shaking. The plate was measured in a microplate reader at 590nm.

The absorbance was normalized with the negative control without cells, and the cell viability was calculated relative to DMSO control. Cell survival graphics were generated plotting cell viability % on Y-Axis and Prexasertib concentration in nM on X-Axis.

2.2.1.16 Immunofluorescence

Cells were seeded in 6 well plates with a glass coverslip at the bottom. All next steps were carried out at room temperature. On the harvesting day, cells were washed once with 1xPBS and fixed using PSP (3% paraformaldehyde, 2% sucrose in PBS) for 10 minutes. Cells were then washed again two times with 1xPBS for a few seconds and one more time for 5 minutes. For permeabilization, cells were incubated 5 minutes with 1xPBS with 0.2% Triton X-100 and then rinsed twice for 5 minutes with 1xPBS with 0.1% Triton-X100 (PBS-T). To reduce unspecific binding sites, fixed cells were incubated 30 minutes with 3% BSA in PBS-T, followed by three washes for three minutes in PBS-T. Primary antibody was diluted to the desired concentration in blocking solution and incubated in a humid chamber for 1h, followed by three washes in PBS-T for 3 minutes each. The secondary antibody and Hoechst were diluted 1:500 in blocking solution, then cells on coverslips were incubated with the secondary antibody for 30 minutes

in a humidified chamber. Cells were washed four times with PBS-T for 5 mean each. Coverslips were then mounted on glass slides using ImmuMount, dried for 1 hour, and sealed with colorless nail polish. Samples were stored at 4°C in the dark until they were analyzed using an inverted Leica DMI 6000B microscope equipped with a Prior Lumen 200 fluorescence light source and a Leica DFC350 FX digital camera. Leica Application Suite (LAS) 3.7 and Fiji (Schindelin et al. 2012) were used for the analysis as well.

For EdU staining, 3000 cells were seeded per well in a 96 well plate. Multichannel pipettes were used for all the steps. First, cells were labeled for 30 minutes with 10 µM 5-EdU (Jena Bioscience) at 37°C and 5% CO_2. Then, cells were washed, fixed and permeabilized as described before (volume 100 µl). Then cells were washed with PBS 1X three times and blocked in 3% BSA for 30 min at room temperature, followed by 3 washed steps with PBS. For detection of incorporated EdU by click chemistry, the EdU mix was prepared fresh, and each component was added as indicated (1 X TBS, 100mM $CuSO_4$, AF488-Azide (Jena Bioscience), 100 mM Na-Ascorbate), EdU mix was vortexed and added to the cells during 30 minutes at RT. After three washing steps with PBS-T, Hoechst 33258 (Sigma) was diluted 1:500 in 3% BSA in PBS-T and incubated with the coverslips for 60 minutes at room temperature. Finally, cells were washed three times with PBS-T and mounted with Immu-Mount™ (Thermo Fisher Scientific). Pictures were taken with an inverted Leica DMI 6000B microscope equipped with a Prior Lumen 200 fluorescence light source and a Leica DFC350 FX digital camera.

2.2.1.17 Double thymidine block

450,000 cells/dish were seeded in 6 cm plates, per condition. Next day cells were synchronized with 2mM thymidine for 19 hours, then cells were released in the cell cycle with complete medium at desired times. For double thymidine block, cells were 1^{st} released in the cell cycle during 9 hours, followed by a second thymidine block during 14 hours. Cells were released for 2^{nd} time in the cell cycle with complete medium at desired times.

2.2.1.18 Mammosphere assay

Cells were trypsinized and resuspended in mammosphere medium, followed by 5 minutes centrifugation at 300xg at room temperature. Cell pellet was resuspended in 6 ml of mammosphere medium, by 10 times pipetting up and down. A single cells suspension was done

by resuspending cells 8 times using a 10 ml syringe (25G needle). Using trypan blue the cells were counted and 1ml of cell suspension 5 x 10^4 cells/ml was prepared. Finally, 2000 cells/well in 24-well plates were seeded with mammosphere medium. Cells were incubated for 7 days, taking care of not moving or disturbing the plates during this time. Mammospheres were counted and analyzed with a light microscope.

2.2.1.19 Transwell migration assay

In order to evaluate cell migration 100.000 MDA-MB231 and MCF10A cells were plated in 6 well plates. The next day, cells were treated with starvation medium (MDA-MB231cells medium supplemented with 0.5% FBS; MCF10A cells medium supplemented with 0.25% horse serum). On the third day, the membrane well inlets (OMNILAB) were equilibrated for 30 minutes by the addition of 250μl on top and 660μl on the bottom of the starvation medium. In parallel, the starved MDA-MB231 and MCF10A cells were trypsinized, resuspended, and diluted (50,000 cells/24 wells plate; 20,000 cells/24 wells plate). The top medium was removed and 500 μl cells were added to the top layer, cells were incubated. 14 hours after the bottom medium was changed to a complete medium. MDA-MB231 cells migrated for 6 hours and MCF10A cells for 38 hours. After cell migration, the top layer of the membrane was scrapped with a cotton tip. Next, the bottom layer was washed once with 1x PBS. Migrated cells were fixed for 10 minutes in ice-cold Methanol. In order to stain the migrated cells were incubated for 20 minutes with Crystal violet 2% in Methanol, proceeded by three washing steps with PBS 1X. Finally, the membrane was cut out of the inlet and placed in a glass slide with immuMount, covered with a cover slide dried for 1 hour, and sealed with colorless nail polish. Migrated cells were photographed by an inverted Leica DMI 6000B microscope and quantified by crystal violet measurement as in 2.2.1.14.

2.2.2 Molecular Biology

2.2.2.1 Transformation of chemically competent bacteria with plasmid DNA

The DNA plasmids were transformed in chemically competent DH5α or BL21(DE3) *E.coli* bacteria. 50 μl or 100 μl of bacteria were thawed on ice and 1 μg of plasmid DNA was slowly added and gently mixed by flicking the tube. The plasmid-bacteria mix was incubated for 30

minutes on ice. Heat shock was performed by incubating the tubes for 45 seconds at 42°C. Directly afterwards, samples were placed onto ice for 2 minutes and 300 µl of pre-warmed LB medium without any antibiotics was added. Tubes were incubated for 30-60 minutes at 37°C in a thermomixer with constant shaking at 600 rpm. Next, bacteria were pelleted by centrifuging for 1 min at full speed and resuspended in 100µl of fresh LB medium. The bacteria were then spread onto pre-warmed LB agar plates containing appropriate antibiotics. Plates were incubated upside down overnight at 37°C.

2.2.2.2 Mini preparation of plasmid DNA from bacteria

To verify positive clones, mini preparation of plasmid DNA was performed. After transformation, a single bacterial colony was inoculated into a 3ml LB-medium containing proper antibiotics and incubated overnight at 37°C at 160 rpm shaking. On the next day, 1.5 ml of the culture was transferred onto a 1.5 ml Eppendorf tube followed by centrifugation for 2 minutes at full speed. The supernatant was discarded and the bacterial pellet was resuspended in 150 µl S1 buffer supplemented with RNAse A. Bacteria were lysed by adding 150 µl S2 buffer, followed by inverting up and down the tubes several times. Samples were incubated at room temperature for 5 minutes, followed by the addition of 150 µl S3 buffer, and the tube was inverted several times in order to mix the samples. Next, samples were centrifuged for 5 minutes at 14,000 rpm and 4°C. The supernatant that contains the plasmid DNA was transferred to a new Eppendorf tube. In order to precipitate the plasmid DNA, 800 µl of 100% cold ethanol were added to the samples, tubes were centrifuged for 15 minutes at 14,000 rpm and 4°C. The supernatant was discarded, and pellet was washed with 500 µl of 50% ethanol, and centrifuged 10 minutes at 14,000 rpm and 4°C. The pellet was air-dried for approximately 5 minutes. Finally, the dried pellet was resuspended in 50 µl TE buffer and used for the next cloning steps.

2.2.2.3 Midi and Maxi preparation of plasmid DNA from bacteria

A single colony was inoculated into 3 ml LB-medium supplemented with appropriate antibiotics and cultured for 6-8 hours at 37°C and 160 rpm. For further grown the clone was diluted in 200 ml (Midi) or 250 ml (Maxi) of LB medium supplemented with appropriate antibiotics and cultured overnight at 37°C and 160 rpm. On the next day, the plasmid DNA was purified using

the PureLinkTM HiPure Plasmid Midi/MaxiPrep Kit according to the manufacturer´s instructions.

2.2.2.4 Polymerase chain reaction (PCR) for standard cloning

For polymerase chain reaction (PCR), the enzyme phusion™ High-Fidelity DNA Polymerase (Thermo Fisher) was used according to Table 35 and Table 36. The annealing temperature for primers was defined using the T_m calculator of Thermo Fisher.

Table 35. PCR pipetting scheme for standard cloning

Reagents	Volume (µl)
DNA template (50ng/µl)	1 µl
5XHF buffer	10 µl
dNTPs (2mM)	5 µl
Primer forward (10 µM)	2.5 µl
Primer reverse (10 µM)	2.5 µl
DMSO (final 10%)	5 µl
Phusion	1 µl
ddH_2O	23 µl
Total volume	50 µl

Table 36. PCR temperature for standard cloning

Temperature	Time	Cycles
98°C	30 s	1
98°C Annealing °C 72°C	10 s 30 s 30 s/kb	30
72°C	300 s	1
4°C	∞	1

2.2.2.5 Agarose gel electrophoresis

PCR products were separated and analyzed through agarose gel electrophoresis. The appropriate amount of agarose was weighed and boiled in 50 ml (small gel tray) or 100 ml (large gel tray) of 1X TAE. The agarose solution was cooled down and ethidium bromide was added to a final concentration of 0.4 µg/ml, this mixture was then poured into a gel tray with inserted well comb. Once the agarose gel was solidified, it was placed into the gel box and filled up with

1x TAE. The DNA samples were mixed with 5x loading buffer, and loaded onto the gel. 1kb or 100 bp DNA ladder from Thermo Fisher was used as a size marker. The gel ran at 100 V for 45-70 minutes. DNA bands were visualized and photographed using a UV transilluminator. For DNA fragments extraction, the band was sliced out, weighed, and saved in a 1.5 ml Eppendorf tube.

2.2.2.6 Extraction of DNA fragments from agarose gels

After agarose gel electrophoresis, DNA bands of fragments from PCR or digested vectors were extracted by the use of the GeneJet PCR Purification kit from Thermo Fisher following the manufacturer´s protocol.

2.2.2.7 Restriction digestion using DNA endonucleases

For the digestion of vector backbones or PCR products, DNA endonucleases from New England Biolabs and Thermo were used following the manufacturer´s instructions. For cloning, 1 µg of the plasmid DNA and half of the extracted PCR were digested in a reaction volume of 50 µl. When necessary double digestion was performed according to the DoubleDigest Calculator from Thermo fisher. Agarose gel electrophoresis was performed to confirm correct digestion (2.2.2.5).

2.2.2.8 Ligation

Ligation reaction of digested plasmid DNA and PCR product was performed using the T4 DNA Ligase enzyme from New England Biolabs according to the manufacturer´s instructions. Digested vector backbone and PCR product were ligated in a ratio 1:2 (plasmid: PCR) to a final volume of 10 µl and were incubated for 45 minutes at room temperature. Afterwards, the whole ligation reaction was transformed into DH5α *E.coli* as described in 2.2.2.1. As ligation negative control a not digested PCR product was used.

2.2.2.9 Standard cloning procedure

In order to clone specific DNA inserts into an appropriate vector, the DNA to insert was amplified by PCR as it was described in 2.2.2.4. The correct size of the insert was verified and purified according to 2.2.2.5 and 2.2.2.6. Afterward, the vector DNA and the PCR product were digested with the appropriate DNA endonucleases and separated in an agarose gel electrophoresis. The digested backbone vector and DNA insert were purified 2.2.2.6, ligated

2.2.2.8, and transformed 2.2.2.1. The obtained single bacterial clones were cultured and plasmid DNA purification was performed. The correct cloning was checked first by restriction digestion and also by corresponding sanger sequencing.

2.2.2.10 Recombinational cloning

The PCR product ligated in a pENTR3C vector and was then used for gateway cloning and mixed as described in Table 37.

Table 37: Gateway cloning of PCR fragments into pInducer20 backbone

Compound	Time
PCR product in a pENTR3C vector	1.5 µl
pInducer20 (#1343)	1.5 µl
TE 1X	1 µl
Clonase II Mix	1 µl
TOTAL	5 µl

After mixing by pipetting, the mix was incubated for 18 hours at 25°C. On the next day, 1 µl of the proteinase K was pipetted in and incubated at 37°C for 10 min. The cloning product was stored at -20°C or directly transformed into competent bacteria 2.2.2.1.

2.2.2.11 Gibson assembly cloning

In order to generate the vector pCRIS-PITCH/B-MYB.N-Ter- FKBP12(F36V) (Table 16) which contains the B-MYB N-ter microhomologies, the degradation domain FKBP12(F36V), and the cassette of blasticidin resistance. A previous PCR was performed to generate the microhomologies cassette by the use of the primers: SG2812-SG2813 and the template pCRIS-PITChv2-BSD-dTAG (BRD4) (1685); the purified PCR product was used for the next steps. Next, Gibson cloning methodology was used to fusion the cassette with B-MYB-N-Ter microhomologies to a pCRIS-PITChv2-BSD-dTAG (BRD4) vector (digested with MluI). The NEBuilder HiFi DNA Assembly protocol was followed. The number of pmols of the cassette with B-MYB-N-Ter michrohomologies fragment to clone and of the pCRIS-PITChv2-BSD-dTAG (BRD4) vector were calculated based on the length and weight using the next formula:

$$\mathbf{pmols} = (\text{weight in ng}) \times 1.000 \div (\text{base pairs} \times 650 \text{ daltons})$$

Next, the following reaction was set up on ice:

Table 38. Gibson assay cloning

Compound	Vector:insert=1:2
pCRIS-PITChv2-BSD-dTAG (BRD4) (1685) (digested with MluI)	0,1 pmols
Cassette with B-MYB-N-Ter michrohomologies B-MYB-N-Ter	0.2 pmols
NEBuilder HifI DNA assembly Master Mix	10 µl
Deionized H_2O	10-X µl
Total volume	20 µl

Samples were then incubated at 50°C for 15 minutes in a thermocycler. Then the samples were stores on ice for immediate use or at -20°C for subsequent transformation (2.2.2.1). The plasmid purified as described in (2.2.2.2) and the correct sequence was confirmed by sanger sequencing.

2.2.2.12 Golden gate cloning

The golden gate cloning assembly strategy was used to generate plasmid all in one: CRISPR-Cas9/B-MYB.N-Ter (Table 16), which expresses the Cas9 nuclease and two gRNAs cassettes, a N-ter B-MYB specific gRNA and a genetic PITCH-gRNA. First, the vector pX330A-1x2 was ligated to the annealed oligos which compound the N-ter B-MYB specific gRNA as described in (2.2.2.8) and transformed in competent cells as explained in (2.2.2.1) and plasmid was purified as described in (2.2.2.2). Then, the golden gate cloning reaction was prepared as follows:

Table 39. Golden gate assemby

Compound	Ammount (µl)
50 ng/µl pX330A-1x2 (with annealed oligonucleotides inserted)	1.5
100 ng/µl px330S-2-PITCh (1683)	1.5
10x T4 DNA Ligase reaction buffer	2
BsaI- HF	1
T4 ligase	1
ddH_2O	13
TOTAL	20

Samples were placed in a thermocycler under following conditions:

- ✓ 37°C for 5 min
- ✓ 16°C for 10min
- ✓ 4°C ∞

25X

Samples were transformed in competent cells as explained in (2.2.2.1) and plasmid purified as described in (2.2.2.2) and the correct sequence was confirmed by sanger sequencing.

2.2.2.13 Site directed mutagenesis

In order to introduce a point mutation in a gene, site-directed mutagenesis by PCR was performed. Primers were designed following the instructions of QuickChangeTM Site-Directed Mutagenesis Kit from Stratagene. A PCR was performed to insert the desired mutation, according to Table 40 and Table 41. The 10% of the PCR product was evaluated on an agarose gel. The vector template was digested by the enzyme DpnI (10 units) in a HF buffer for 1 hour at 37°C. The resulting product was then transformed in super competent TOP10 cell from Thermo Fischer. Single bacterial clones were cultured, plasmid DNA was purified and the site mutation was tested by sequencing.

Table 40. Pipetting scheme for site directed mutagenesis

Reagents	Volume (µl)
DNA template (50ng/ µl)	1
5xHF buffer	10
dNTPs (2mM)	5
Primer Forward (10 µM)	1
Primer Reverse(10 µM)	1
DMSO (final 10%)	5
Phusion Polymerase	1
ddH_2O	26
Total volume	50

Table 41. PCR temperature profile for site directed mutagenesis

Temperature	Time	Cycles
98°C	30 s	1
98°C 55°C 72°C	10 s 30 s 30 s/kb	18
72°C	300 s	1
4°C	∞	1

2.2.2.14 Isolation of genomic DNA

Cells were trypsinized in order to isolate genomic DNA, then resuspended in medium and transferred into a 15 ml falcon tube. Next, samples were centrifuged for 5 min 300x g, and the supernatant was discarded. The pellet was resuspended in 1 ml PBS and transferred to a 1.5 Eppendorf tube, and centrifuged for 5 min at 300 x g. Afterward, the pellet was resuspended in 300 µl tail buffer with 10 µl Proteinase K followed by an incubation step of 6 hours at 55 °C in constant shaking at 600 rpm. The samples were vortexed for 30s and incubated at 95 °C for 10 minutes in order to inactivate the Proteinase K. Next, samples were cool down and 166,7 µl 6 M NaCl were added, followed by 10 minutes of centrifugation at full speed (4°C), the supernatant was transferred into a new Eppendorf tube that contained 767 µl ice-cold 95% ethanol. Tubes were mixed by inversion 5 times and centrifuged one more time at full speed (4 °C). The supernatant was discarded and the pellet containing the gDNA was washed once with 700 µl ice-cold 70% ethanol and centrifuged at full speed for 5 min (4 °C). Next, the supernatant was removed and the samples were air-dried and pellets were resuspended in 30 µl TE buffer by 45 min incubation at 60 °C and finally, the gDNA samples were stored at -20 °C.

2.2.2.15 PCR of genomic DNA

For genotyping the degradation domain FKBP12 knock-in in *B-MYB*, genomic DNA was isolated from MDA-MB231 (as a control) and MDA-MB231-B-MYBdTAG cells, PCR reactions with specific primers for human *B-MYB* were performed according to Table 42 and Table 43. PCR products were mixed with 5x loading buffer and analyzed on 1% agarose gels (2.2.2.5).

Table 42. Pipetting scheme for PCR of genomic DNA

Reagents	Volume (µl)
DNA template (50ng/ µl)	1
5xHF buffer	10
dNTPs (2mM)	5
Primer Forward (10 µM)	1
Primer Reverse(10 µM)	1
DMSO (final 10%)	5
Phusion Polymerase	1
ddH_2O	26
Total volume	50

Table 43. PCR temperature profile for PCR of genomic DNA

Temperature	Time	Cycles
98°C	30 s	1
98°C 55°C 72°C	10 s 30 s 30 s/kb	18
72°C	300 s	1
4°C	∞	1

2.2.2.16 RNA isolation

Total RNA was isolated by using peqGOLD TriFast (Peqlab) following the manufacturer's instructions. The cells were taken from the incubator and placed on ice, the culture medium was aspired completely, and cells were lysed in 1ml of TriFast solution and transferred to a 1.5 ml tube and either frozen at -80 °C for a up to few weeks or incubated at RT for 5 minutes. Then, 200 µl chloroform were added, samples were mixed by vortexing for 20 seconds and incubated for 2 minutes on ice. To separate the mixture into three phases, samples were centrifuged for 10 minutes at 12,000xg and 4°C, the upper aqueous phase containing RNA was transferred into a new 1.5 ml tube. To precipitate RNA, 500 µl ice-cold isopropanol were added, mixed by inversion 5 times and incubated for 10 minutes on ice. Afterwards, the RNA was pelleted by centrifugation at 12,000 xg and 4 °C for 10 min. RNA pellet was washed twice by adding 1ml of ice-cold 75% ethanol and centrifuged at 7,000xg and 4°C for 5 minutes. Next, the ethanol was completely removed and the RNA pellet was air dried for 10 minutes at room temperature and resuspended in 25 µl RNase-free DEPC water. RNA concentration and purity were measured using the NanoDrop 2000 spectrophotometer, finally the isolated RNA was stored at -80 °C.

2.2.2.17 Reverse transcription of RNA into cDNA

For reverse transcription (RT) of RNA into cDNA, first 0.5 µl random hexamer primers primers were mixed with 2.5 µg of isolated RNA and filled up to 10 µl with DEPC water on ice and

denatured for 5 minutes at 70°C. The reaction was cooled down at 4°C, and 15 µl of the RT of the following mixture was added:

- 6.25 µl dNTPs (2 mM)
- 5 µl 5xRT buffer
- 0.5 µl RevertAid enzyme (200 U/µl)
- 0.5 µl RiboLock enzyme (40 U/µl)
- 2.75 ml RNase-free water

The reaction was mixed by pipetting and then incubated 1 hour at 37°C. The reaction was inactivated at 70°C for 15 minutes and cooled down at 4 °C. cDNA for RT-qPCR was diluted 1:16 ratio and stored at -20 °C.

2.2.2.18 Quantitative real-time PCR (qPCR)

Quantitative real-time PCR (qPCR) was used to analyze the relative mRNA expression of a specific gene normalizing to the expression of a housekeeping gene (relative mRNA expression). qPCR was then performed according to **Table 44** and **Table 45**. For setting up the qPCR reaction, master mix, primers and ddH_2O and water were thawed.

Table 44. qPCR master mix

Reagents	Vol (µl)
dNTPs (2mM)	3.5
10x Reprofast	2.5
SYBER Green (1:2000 in DMSO)	0.75
ddH_2O	11.45
Total Volume	18.2

Table 45. qPCR conditions

Reagents	Vol (µl)
Master Mix	18.2
Primer fwd (10 µM)	0.75
Primer rev (10 µM)	0.75
HisTaq 16 (5 U/µl)	0.3
Total Volume	20

To prepare the qPCR plate, 20 µl of the mix were pipetted in triplicates into a 96-well plate, following a template and then 5 µl of the corresponding cDNA (diluted 1:16) and water was used as non-targeted control instead of cDNA. The plate was sealed by using a transparent adhesive foil, and centrifuged shorly at 2000 x g for 1 min and the qPCR was run onto a Stratagene Mx3000P or a qTOWER^{3G} (Analytik Jena) qPCR machine following the next thermal profile:

Table 46. PCR temperature profile for qPCR

Temperature	Time	Cycles	
95°C	120s	1	Initialization
95°C 60°C 72°C	15s 30s 30s	40	Amplification
95°C 60°C 72°C	15s 30s 30s	1	Melting curve

The relative expression of a given gene in the sample of interest relative to the gene expression in a reference sample was calculated according to the following formula:

$$2^{-\Delta\Delta Ct}$$

with ΔCt = Ct (gene of interest) – Ct (housekeeping gene)

and ΔΔCt = ΔCt (sample) – ΔCt (reference)

The standard deviation of ΔΔCt was calculated by using the law of error propagation:

$$s = \sqrt{s_1^2 + s_2^2}$$

with s_1 = standard deviation of gene of interest

and s_2 = standard deviation of housekeeping gene

The error for $2^{(-\Delta\Delta Ct)}$ was calculated by using: $_2(-\Delta\Delta Ct \pm s)$

Finally, the error used for the error bars was calculated by using: $_2(-\Delta\Delta Ct \pm s) \_ _2(-\Delta\Delta Ct)$

2.2.2.19 qPCR for ChIP

qPCR along with chromatin immunoprecipitation (ChIP) (2.2.3.8) was used to quantify the enrichment of a specific DNA region upon the protein-specific immunoprecipitation, this calculation was made relative to the total amount of input DNA. Therefore, SYBR Select Master Mix (Thermo Fisher) was used, and set up as follows:

Table 47. ChIP-qPCR master mix

Reagents	Vol (µl)
SYBR Select Master Mix	10.0
Primer forward (10 µM)	0.4
Primer reverse (10 µM)	0.4
ChIP DNA	1.0
ddH_2O	8.2
Total Volume	20

The master mix without DNA sample was prepared and 19 µl were pipetted in triplicate into a 96-well plate, following a template scheme. Then, 1 µl of ChIP-DNA or 1 µl of ddH_2O (NTC) per well was added. The plate was seeded and spun for 30 seconds and the qPCR was run onto the Stratagene Mx3000P cycler or qTOWER^{3}G cycler following the next temperature conditions.

Table 48. PCR temperature profile for ChIP-qPCR

Temperature	Time	Cycles	
95°C	15 min	1	Initialization
95°C	30s		
60°C	1 min	40	Amplification
95°C	1 min		
60°C	30s	1	Melting curve
95°C	30s		

The % of input was calculated with $_2-\Delta Ct$, where:

ΔCt=(ChIP sample) C_T(input)

The error ΔCt was calculated by:

$$= \sqrt{s_1}^2 + {s_2}^2$$

Where s_1= input standard deviation and $s_{2=}$ ChIP sample standard deviation

The final error margin was calculated by:

$$2^{-(\Delta C_T + s)} - \% \; of \; input$$

2.2.3 Protein biochemistry

2.2.3.1 Whole cell lysates

Culture medium was discarded and cells were washed once with 10 ml ice-cold 1xPBS, then cells were scraped on ice with 10 ml ice-cold 1xPBS, transferred to a 15 ml falcon tube and centrifuged at 1,200 rpm and 4 °C for 5 min. The supernatant was aspired and the pellet was resuspended in a TNN lysis buffer with freshly added protease inhibitor cocktail (PIC) 1:1000, 1 mM PMSF, 1 mM DTT, and 10 mM ß-glycerophosphate, and transferred to a 1.5 Eppendorf tube. Samples were incubated on ice for 20 min and centrifuged at 14,000 rpm for 10 minutes at 4°C. the supernatant containing the proteins was transferred to a fresh tube and protein concentration was measured by Bradford assay 2.2.3.3. For Western Blot the samples were mixed with 3x electrophoresis sample buffer (ESB), boiled for 5 minutes at 95°C, and loaded on SDS gels or stored at -20°C.

2.2.3.2 Nuclear extracts

For co-immunoprecipitation of endogenous proteins, nuclear extracts were isolated. Cell plates were scraped off on ice with 10 ml 1xPBS, transferred to a falcon tube (4 plates per falcon), and centrifuged at 1200 rpm for 10 min at 4 °C. The supernatant was discarded and the pellet was mixed by pipetting 10ml of Buffer A which contains freshly added PIC 1:1000. Cells were incubated for 20 min on ice and then transferred and homogenized with 20 tight but slow up-and-down strokes using a glass Dounce homogenizer. Samples were transferred to a 10 ml falcon tube and centrifuged for 10 min at 2800 rpm, 4°C. The supernatant was removed and

the nuclei pellet was resuspended in 1ml of previously prepared Mix 1:1 Nuclear lysis Buffer and TNN with freshly added 1:1000 Pic and 0,5 mM DTT (1:2000). Samples were transferred to 1.5 ml tubes and incubated on ice for 20 minutes. Next, samples were centrifuged for 10 min at full speed and 4°C. The supernatant which contains the nuclear extracts was transferred to a new 1.5 ml tube, and the proteins were quantified as explained in 2.2.3.3. Samples were either immediately used for immunoprecipitation of endogenous proteins 2.2.3.5 or frozen with liquid nitrogen and stored at -80 °C.

2.2.3.3 Determination of protein concentration according to Bradford

To determine protein concentration, Bradford assay was used. 1 µl of whole-cell lysates or nuclear extracts were mixed with 100 µl of 0.15 M NaCl and 1 ml Bradford solution in semi-micro cuvettes. To generate a standard curve, 1 µl of a BSA dilution series was used. The extinction was then measured at 595 nm using a spectrophotometer. All measurements were made in duplicates. Protein concentrations were calculated by using a standard curve.

2.2.3.4 Nuclei isolation for ATAC-seq

Nuclei isolation was performed for Assay for Transposase-Accessible Chromatin using sequencing. Therefore, 100,000 MCF10A cells were washed with ice cold PBS and lysed in ATAC lysis buffer with freshly added PIC, and incubated on ice for 10 minutes. Samples were centrifuged at 500 g for 10 minutes at 4°C. The pellets were then used for transposition reaction 2.2.4.2.

2.2.3.5 Immunoprecipitation of endogenous proteins

For immunoprecipitation IP of endogenous proteins, 4.5 mg proteins were pipetted into a new 1.5 ml tube and completed to 1ml volume with HEPES 20mM. 2 µg of the corresponding antibody was added to the samples and incubated on the rotating wheel overnight at 4°C. For input 400 µg of the nuclear extracts were used, samples were heated with 0.5 volume of 3x ESB at 95 °C for 5 minutes and stored at -20°C for later use as input samples. On the next day, 25µl of pierce™ protein A/G beads were washed with 175µl TBS-T by using the magnetic rack. Beads were washed one more time with 1ml of TBS-T and supernatant was discarded. Next, the mixture of Antibody-Lysates was added to the tubes that contain the pre-washed beads. Samples were then incubated for 2h at 4°C in the rotating wheel. Tubes were placed in a

magnetic rack and supernatant was discarded and beads were washed three times in 1:1 Nuclear Lysis Buffer: HEPES 20nM and PIC 1:1000, each time 5 min in the cold room on the rotating wheel. After the last washing step, samples were transferred to fresh 1.5 ml tubes, the beads were boiled in 40µl 3x ESB for 5 min at 95 °C. To perform western blot 2.2.3.7 samples were centrifuged for 5 min at full speed at RT, and 20 µl of the supernatant which contains the immunoprecipitated proteins was loaded, the input was also loaded on 8% SDS-gels.

2.2.3.6 Proximity ligation assay (PLA)

To study protein proximity between endogenous proteins, proximity ligation assay (PLA) was performed using the DuolinkTM PLA Technology (Sigma Aldrich). Cells were seeded in 18-well ibidi slides, after incubation and treatment time cells were washed once in a 10 cm dish filled with 1xPBS and fixed in PSP for 10 min at RT. Next, cells were rinsed twice shortly and once for 3 minutes with 1xPBS, then permeabilized for 5 minutes in 1xPBS with 0.2% Triton-X100. Afterward, cells were washed twice in 1xPBS and blocked in PBS with 3% goat serum and 0,2% Tween-20 for 20 minutes at room temperature. The blocking solution was removed and cells were incubated with desired primary antibodies diluted in the blocking solution overnight at 4 °C in a humidified chamber. On the next day, the primary antibody solution was removed and cells were washed twice for 5 minutes with 1x PBS. Then, cells were incubated with 20 µl/well of the PLA Probe Anti-Mouse PLUS and Anti-Rabbit MINUS diluted 1:5 in antibody diluent for 1 hour at 37°C in a humidified chamber. Cells were washed two times for 5 minutes in wash buffer A, then cells were incubated with ligase (1 U/µl) diluted 1:40 in ligation buffer for 30 minutes at 37°C in a humidified chamber. Next, slides were washed twice with buffer A for 5 minutes and incubated with polymerase (10 U/µl) diluted 1:80 in amplification buffer for 120 min at 37 °C in a humidified chamber. Cell nuclei were stained with Hoechst 33258 diluted 1:1000 in PBS for 5 minutes at room temperature, the slides were washed once with washing buffer B for 10 minutes and once with 0.01x buffer B for 1 minute. Buffers were carefully removed and one drop of ImmuMount was added per well and slides were immediately imaged using an inverted Leica DMI 6000B.

2.2.3.7 Western Blot

SDS polyacrylamide gel electrophoresis (SDS-PAGE)

Sodium dodecyl sulfate polyacrylamide gel electrophoresis (SDS-PAGE) was carried out using the system Mini-Protean® III from Biorad. A separation gel (8%-12%) was prepared as specified in table Table 49. The separated gel was overlaid with water and after polymerization, a stacking gel (5%) Table 49 was poured on top of the separating gel and a 10- or 15-well comb was inserted. The polymerized gel was placed into the electrode assembly and samples were loaded onto the gel. Gels were run with 1x SDS-running buffer with constant amperage (35 mA/gel) for 1.5 hours approximately.

Table 49. Ingredients for gels preparation

Reagents	Separationg gel			Stacking gel
	8%	10%	12%	5%
ddH_2O	4.6 ml	3.8 ml	3.2 ml	3.0 ml
1.5 M Tris pH 8.8	2.6 ml	2.6 ml	2.6 ml	-
0.5 M Tris pH 6.8	-	-	-	1.25 ml
30% Acrylamide/ProtoGel	2.6 ml	3.4 ml	4.0 ml	0.67 ml
20% (w/v) SDS	50 µl	50 µl	50 µl	25 µl
10% (w/v) APS	50 µl	50 µl	50 µl	25 µl
TEMED	5 µl	5 µl	5 µl	2.5 µl

Immunoblotting

To transfer the proteins from polyacrylamide gels to polyvinylidene fluoride (PVDF) membranes, the Mini-Trans Blot system from Bio-Rad was used following the manufacturer's instructions. The PVDF membrane was first activated in 100% methanol for 1 minute. To prepare the membrane-gel-sandwich blotting pads, Whatman papers and the pre-activated PVDF membrane were flooded in cold 1x blotting buffer. The blotting sandwich was assembled as follows: Starting on the black side of the cassette, blotting-pad, two Whatman papers, PVDF membrane, polyacrylamide gel, two Whatman papers, and a blotting-pad. Afterward, the cassette was closed and placed into the electrode module with the black side of the cassette towards the black side of the module and a frozen cooling unit was placed in the blotting tank and filled with pre-cooled 1x blotting buffer. The transfer was conducted at constant amperage of 250 mA per blotting tank for 90 minutes. The successful transfer of proteins to the PVDF membrane was confirmed by Ponceau S staining for a few minutes. In order to avoid unspecific binding of proteins, membranes were first blocked either with 5% BSA or milk powder in TBS with 0.1% Tween 20 (TBS-T) for 1 hour at RT in constant shaking. Membranes were then

incubated with specific primary antibodies diluted in blocking solution overnight at 4°C. On the next day, the primary antibody was removed and membranes were washed one with TBS-T for 10 minutes and twice with TBS-T for 5 minutes at room temperature in constant shaking. Then, membranes were incubated with secondary HRP-conjugated antibodies diluted in blocking solution for 1h at RT. Three additional washed steps with TBS-T were performed for 10 minutes and twice with TBS-T for 5 minutes at room temperature in constant shaking. Finally, membranes were incubated for 1 minute with freshly prepared enhanced chemiluminescence (ECL) solution and wrapped in a plastic foil and exposed to X-ray films in the darkroom or to the ImageQuant 800 (Amersham Biosciences).

2.2.3.8 Chromatin-immunoprecipitation (ChIP)

Cross-linking and cell lysis

After cells were culture and treated as appropriate, dishes were placed on ice, DNA and proteins were cross-linked by the addition of 405 µl 37% formaldehyde dropwise to the medium. Dishes were incubated at 10 minutes at room temperature with gently slowly shaking. Then, 1.8 ml of glycine 1M were added to the plates and incubated at RT for 5 minutes on a slow shaker. Cells were placed back on ice and washed twice with 20 ml ice-cold 1xPBS. After the second wash, 5-8 ml ice-cold 1xPBS with freshly added PMSF (1:100) and PIC (1:1000) were added to the cells. Scraped cells of various dishes that contain a number of cells of $5x10^7$ were pooled in 50ml falcon tubes. Cells were centrifuged at 1200rpm for 8 min at 4°C, the pellet was resuspended in 3ml Lysis buffer with freshly added PMSF (1:100) and PIC (1:1000) and incubated on ice for 20 min. Pooled cells containing $5x10^7$ were centrifuged at 1200 rpm for 5 minutes at 4°C. Supernatants were removed and pellets were then frozen with Liquid Nitrogen and subsequently stored at -80 °C.

Fragmentation of chromatin by sonication

Cell pellet was thawed on ice for sonication and resuspended in 1.5ml Lysis buffer II with freshly added PMSF (1:100) and PIC (1:1000) and incubated on ice for 10 minutes. To shear DRA, lysed nuclei were transferred to a new 15 ml falcon tube with the upper part at 12.5 ml cut off. Samples were placed in a beaker previously filled with ice and water, sonication was performed for a total of 15 minutes using a Branson Sonifier equipped with a microtip, following the next settings: 25% amplitude, 10 s ON, and 45 s OFF (duration: 82.5 min per sample/per 5 x 10^7

cells). Next, samples were placed on ice in a cold room, 60 µl were taken off in order to estimate the chromatin size. The sample was then centrifuged at max speed for 15 min at 4°C, 50 µl of the supernatant were transferred to a new 1.5 ml tube.

Determination of DNA concentration and analysis of successful fragmentation

Cross-ling was reversed by the addition of 2 µl 5 M NaCl and 1 µl RNase A (10 mg/ml) and incubated overnight in a thermomixer at 65°C in constant shaking at 550 rpm. Next, samples were briefly cooled down at RT, 2 µl of Proteinase K (10 mg/ml) were added and samples were incubated at 45°C for 2 hours while shaking at 550 rpm. Samples were filled up with 500 µl of TE1X, 1 ml phenol chloroform-IAA (25:24:1) were added, samples were briefly vortexed and spun at 16.100 for 5 min at RT. The upper phase was pipetting into a new 2 ml tube and 50 µl of sodium acetate 2M PH5,6, 1.5 ml 100% ice-cold ethanol, and 1 µl of glycogen were added. Tubes were mixed by inversion and frozen at -80°C for 90 minutes. Afterwards, the samples were taken from the -80°C freezer and directly centrifuged at 16.100g for 20 min at 4°C. The supernatant was discarded and the pellet was washed once with 500 µl of 70% ice-cold ethanol and samples were spun at 16.100g for 5 minutes at 4°C. The samples were air-dried for 10 minutes and resuspended with 50 µl TE1X. DNA concentration was measured using a NanoDrop2000.

To analyze DNA fragment size, 20 µl of DNA were mixed with 5x loading buffer and loaded on a 1.2% agarose gel, using a 100bp ladder. When the size of fragmented DNA was between 150-300 bp, the fragmented chromatin was centrifuged at max. speed for 15 min at 4°C. Supernatants were taken, and aliquots of 100 µg for ChIP-qPCR or 240 µg for ChIP-seq were achieved using Lysis Buffer II (PIC 1:1000, PMSF 1:100). Aliquots were frozen in liquid nitrogen and placed at -80°C for later use.

Immunoprecipitation

For immunoprecipitation step, 30 µl (ChIP-qPCR) or 90 µl (ChIP-seq) Protein G Dynabeads were washed three times with 1 ml BSA-PBS (5 mg/ml) using the DynaMag-2 Magnet rack (Thermo Fisher). Beads are resuspended in 1ml BSA-PBS. Primary antibody was added 3 µg (ChIP-qPCR) or 9 µg (ChIP-seq), non-specific IgG was used as a negative control, samples were incubated overnight on a rotating wheel at 4°C. Beads were three times washed with 1 ml BSA-PBS and

resuspended in 30 µl or 90 µl BSA-PBS. The diluted 500-1000 µl chromatin was added to the antibody-coupled beads and incubated on a rotating wheel for 6h at 4°C. For input, 1% of chromatin used for IP was pipetted into a fresh 1.5 ml tube and stored at 4°C.

Subsequently, beads were washed three times with Wash Buffer I (PIC 1:1000, PMSF 1:100), three times with Wash Buffer II (PIC 1:1000, PMSF 1:100) and another three times with Wash Buffer III (PIC 1:1000, PMSF 1:100), in every washing step cells were placed 5 min on a rotating wheel at 4°C. A final wash step with 1x TE Buffer (PIC 1:1000, PMSF 1:100) was done and samples were transferred to a fresh 1.5 ml tube and then placed in the magnetic rack. The supernatant was removed completely and proteins were eluted from the beads by the two times addition of 250 µl of freshly prepared Elution Buffer and incubation on a rotating wheel at RT for 15 min each time.

Reversal of cross-links and DNA purification

To revert DNA-Protein binding 16 µl 5 M NaCl (final concentration: 160 mM) and 1 µl 10 mg/ml RNase A (final concentration: 20 µg/ml) were added to the eluates (500 µl in total) and incubated for one hour at 37°C and then 65°C overnight with constant shaking at 550 rpm. On the next day, 5.2 µl 0.5 M EDTA (final concentration: 5 mM) and 10.3 µl 10 mg/ml Proteinase K (final concentration: 200 µg/ml) were added and incubated at 45 °C for 2 h. Next, DNA was purified by using the QIAquick PCR Purification Kit (Qiagen) according to the manufacturer's instructions and eluted in 50 µl EB buffer. 1 µl of ChIP DNA sample was used in qPCR as stated in 2.2.2.19.

2.2.4 Next-generation sequencing (NGS)

2.2.4.1 ChIP-sequencing (ChIP-seq)

Chromatin immunoprecipitation for ChIP-Seq was performed as described in 2.2.3.8. First, purified ChIP-DNA was quantified in duplicate by using the Quant-iT PicoGreen dsDNA Assay Kit (Thermo Fisher) following the manufacturer´s instructions. Samples were measured using a black 96-well plate with F-bottom (Greiner). A standard curve was prepared by diluting the lambda DNA (100 µg/ml) and used to calculate the DNA concentrations. Input DNA was diluted

1:10 using EB buffer from (Qiagen). The fluorescence intensity of the samples was measured using the Tecan Infinite M200 plate reader.

The Quantified ChIP DNA was diluted in EB buffer (QIAquick Kit) to a volume of 50 µl. 10ng of the purified ChIP DNA was used, and the DNA libraries were generated using the NEBNext® Ultra II DNA Library Prep Kit for Illumina® (New England Biolabs) according to the manufacturer's instructions. Size selection (150 bp) was performed by the use of Agencourt AMPure XP beads (Beckman Coulter). The PCR amplified DNA libraries were purified also by the use of Agencourt AMPure XP beads. DNA library was amplified by 12-15 PCR cycles using i5/i7 index primers from the NEBNext® Multiplex Oligos for Illumina® (Dual Index Primers Set 1) kit (New England Biolabs). DNA library size and concentration were analyzed using the Fragment AnalyzerTM Automated CE System (Advanced Analytical) with the DNF-474 High Sensitivity NGS Fragment Analysis Kit (1 bp – 6,000 bp) (Advanced Analytical). Libraries were pooled to an equimolar ratio and sequenced on the NextSeq 500 platform (Illumina).

2.2.4.2 ATAC-seq

After the nuclei were isolated as shown in 2.2.3.4, a transposition mix was prepared in advance (25 µl 2X TD buffer, 2.5 µl TDE1 Nextera transposase (Illumina)), 16.5 µl PBS, 0.5 µl 1% digitonin, 0.5 µl 10% Tween-20, and 5 µl of nuclease free water). The mix was added to the nuclei and incubated at 37°C for 30 mins. Afterwards, the DNA was purified by using the MinElute PCR purification kit (Qiagen), and a PCR with approximately 10-13 cycles was performed using the NEBNext High Fidelity 2X PCR Master Mix (NEB) and Ad1_noMX and Ad2.1–2.12 barcoded primers described in (Buenrostro et al., 2013). Size selection of the libraries was performed by the use of Agencourt AMPure XP beads (Beckman Coulter). Library quality and fragment size distribution was analyzed on a fragment analyzer (Advanced Analytical). Paired end 2 x 75 bp sequencing was performed on the NextSeq 500 platform (Illumina).

2.2.5 Data acquisition and statistical analysis

2.2.5.1 ATAC-seq Analysis

Data acquisition and statistical analysis of ATAC-seq were performed by Prof. Dr Stefan Gaubatz. First, the base calling was performed with Illumina's CASAVA software or FASTQ Generation software v1.0.0 and the FastQC script was used to test sequencing quality. The

resulting read files were imported to the Galaxy Web-based analysis portal (Afgan et al., 2018) and Bowtie2 with default parameters was used to map the reads to the human (hg19 assembly) genome (Langmead & Salzberg, 2012). The paired reads were filtered by a Phred score cutoff of 30 and mitochondrial reads were removed. The ATACseq peak calling was carried out with Genrich (https://github.com/jsh58/Genrich). Differential analysis was performed within Galaxy using featurecounts and Limma-voom using a minimal log2 fold change of +/- 0 and adjusted p-value of <0.035 as a threshold (Liu et al., 2015). Nucleosome calling was performed with NucleoATAC (Schep et al., 2015). Deeptools2 was used to plot heat maps and density profiles of ATACseq, ChIPseq and CUT&RUN data (Ramírez et al., 2016). Deeptools bamcoverage was used to normalize bigwig files with a bin size of 10 and normalized to counts per million (CPM). Density matrices were generated by means of computeMatrix function, using the BigWig files to compute the called reads centered on ATAC-seq peak summits, YAP peak summits or on the TSS of MMB-target genes (Fischer et al., 2016). Subsequently, heatmaps and profiles were plotted with plotHeatmap and plotProfile tools. Gene browser tracks from ATAC-seq data were loaded into the Integrated Genome viewer (Robinson et al., 2011). Motif analysis was carried out with chromVAR (Schep et al., 2017). The relative position of ATAC-seq peaks to known human genes was determined by ChIPseeker within Galaxy.

2.2.5.2 ChIP-seq Analysis

Data acquisition and statistical analysis of ChIP-seq were performed by Prof. Dr Stefan Gaubatz. As for ATACseq analysis the base calling was performed with Illumina's CASAVA software or FASTQ Generation software v1.0.0 and the FastQC script was used to test sequencing quality. The resulting read files were imported to the Galaxy Web-based analysis portal (Afgan et al., 2018). Alignment was performed with Bowtie2 with default parameters to map the reads to the human (hg19 assembly) genome (Langmead & Salzberg, 2012). Peaks were called with MACS2 (callpeak–nomodel–broad). Bigwig files were generated by bamcoverage (Deeptools) and density matrices were generated by means of computeMatrix to calculate scores per genome regions. Consequently, heatmaps, profiles and metagene plots were plotted with plotHeatmap and plotProfile. ChIP-seq data for the histones H3K4me1, H3K4me3 and H3K27ac from Pattschull et al. (2019) were used to identify enhancers and promoters. We used the feature bedtools intersect to overlap the ChIP-seq data from histones in order to identify

enhancers. Gene tracks from ChIP-seq data were shown by using the Integrated Genome viewer (Robinson et al., 2011). Active promoters were defined by being in a region of ± 1 kb around annotated transcriptional start sites and positive enrichment for H3K4me3 overlapping with H3K27ac without H3K4me1 enrichment. Enhancers were defined as not being within 1 kb of a transcription start site and positive enrichment for H3K4me1 overlapping with H3K27ac without H3K4me3 enrichment.

For p63 ChIP-seq, the peaks were called with MACS2 in narrow peak mode. ChIPseeker was used to identify closest genes to the detected ChIP-seq peaks.

2.2.5.3 Data availability

ATACseq and ChIPseq datasets are available at the NCBI's Gene Expression Omnibus (Edgar et al., 2002) under the accession number: GSE193704.

2.2.5.4 Statistical Analysis

Unless stated otherwise, data are presented as mean ± standard deviation (SD). For statistical analysis, Prism 9.0 (GraphPad) was used. Statistical tests to determine significance are indicated in the corresponding figure. For comparison between two experimental groups two-tailed Student's t-test was used. P-values ≤ 0.05 were considered statistically significant and marked by asterisk: * P ≤ 0.05; ** P ≤ 0.01; *** P ≤ 0.001; **** P ≤ 0.0001. P-values > 0.05 are labeled as not significant (ns). In box plots, the central lines represent the median.

3. Results

3.1 Endogenous YAP is required for G2/M cell cycle transition

In previous publications of our laboratory (Pattschull et al., 2019) in murine lung adenocarcinoma KPL cells and in untransformed human breast epithelial cells (MCF10A), it was shown that YAP and the MMB complex co-regulate a subset of genes involved in G2 and mitosis phases. YAP induces the expression of a set of G2/M genes, including B-MYB, and also promotes its chromatin binding to promoters of genes relevant for G2 and mitosis. Additionally, the use of an untransformed human breast epithelial cell line MCF10A cells which express doxycycline-inducible YAP5SA where a constitutive allele of YAP that cannot be inhibited by the Hippo kinases is expressed (von Eyss et al., 2015; Zhao et al., 2007) led to an increased cell cycle progression (Pattschull et al., 2019). Due to that YAP has been previously associated to cooperate with MYC and E2F to promote S phase entry (Croci et al., 2017; Kapoor et al., 2014; Shen & Stanger, 2015), in the first part of this thesis, I addressed the question of whether YAP is required for G2-M transition at endogenous levels. Therefore, I evaluated the progress of the cell cycle after inhibition of YAP with a YAP-TEAD binding suppressor: verteporfin (Feng et al., 2016). In the first set of experiments, MCF10A cells were double thymidine blocked and released at the indicated times with or without verteporfin treatment to inhibit YAP and TEAD binding (Figure 6A). Cell cycle progression was evaluated through flow cytometry (FACS) (Figure 6B). As expected, the percentage of cells in G2/M increased 4h and 6h after release from the thymidine block. In contrast, inhibition of YAP-TEAD interaction led to a lower increment of the percentage of cells in G2/M. (Figure 6C). These results are consistent with a described role for YAP in the expression of G2/M genes (Pattschull et al., 2019). Additionally, no significant changes in S and G1 phases were observed through FACS.

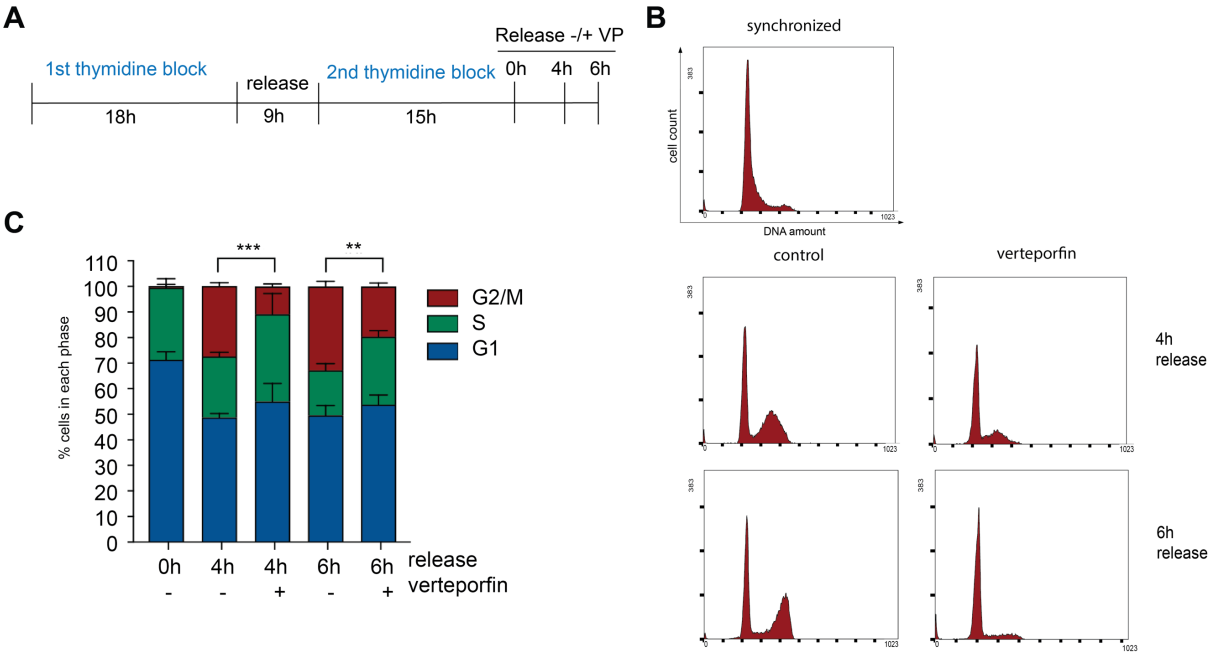

Figure 6. YAP is required for cell cycle progression

(A) Scheme of the experiment. MCF10A cells were double thymidine blocked and then released in the presence or absence of verteporfin (VP) for 4 or 6 hours. (B) The fraction of cells in the different phases of the cell cycle was analyzed by flow cytometry. (C) Quantification of FACS data from three independent experiments, the error bars depict SEM. n=3 biological replicate. Student's t-test. * = $p<0.05$, ** = $p<0.01$, *** = $p<0.001$

To identify cells in S phase, 1 hour before finishing the release time, bromodeoxyuridine BrdU was incorporated into the cells for 1 hour at 37°C, and cells were stained through immunofluorescence using an antibody that recognized BrdU as described in (**Table 14**). Notably, the results by immunofluorescence provided a more specific insight for the analysis of cells in S phase in comparison to the FACS results. Interestingly, a marked and significant difference of S phase positive cells was found between untreated cells and verteporfin-treated cells at 4h of release, specifically from 42% to 10 % and at 6h from 34% to 12% (**Figure 7A**). In order to identify cells in late G2 and mitosis, staining of phosphorylated histone H3 (pH3), a marker for mitotic cells which is exclusively expressed during late G2 and mitosis. Consistently with the previous FACS results, the percentage of cells in mitosis was reduced after the suppression of the YAP-TEAD complex, at 4h release from 5,2% to 2% and at 6h from 7,5% to 3,5% (**Figure 7B**). **Figure 7C** shows representative photos of cells in S phase (above) and in mitosis (below). Next, selected YAP target genes (*CTGF* and *CYR61*) and co-regulated YAP-MMB target genes (*CDC20* and *BIRC5*) were investigated following the same set of experiments shown in **Figure 7A**. mRNA expression of *CTGF* and *CYR61* confirm the inhibition of YAP activity

by verteporfin treatment. In addition, YAP-MMB target genes were also significatively downregulated after verteporfin treatment (Figure 7D). In summary, the inhibition of the endogenous activity of YAP results in decreased cell cycle progression, affecting G2/M phases as well as S phase, resulting in delayed cell cycle progress. These results suggest that YAP endogenous activity plays an important role in regulating cell cycle gene expression and cell cycle progression.

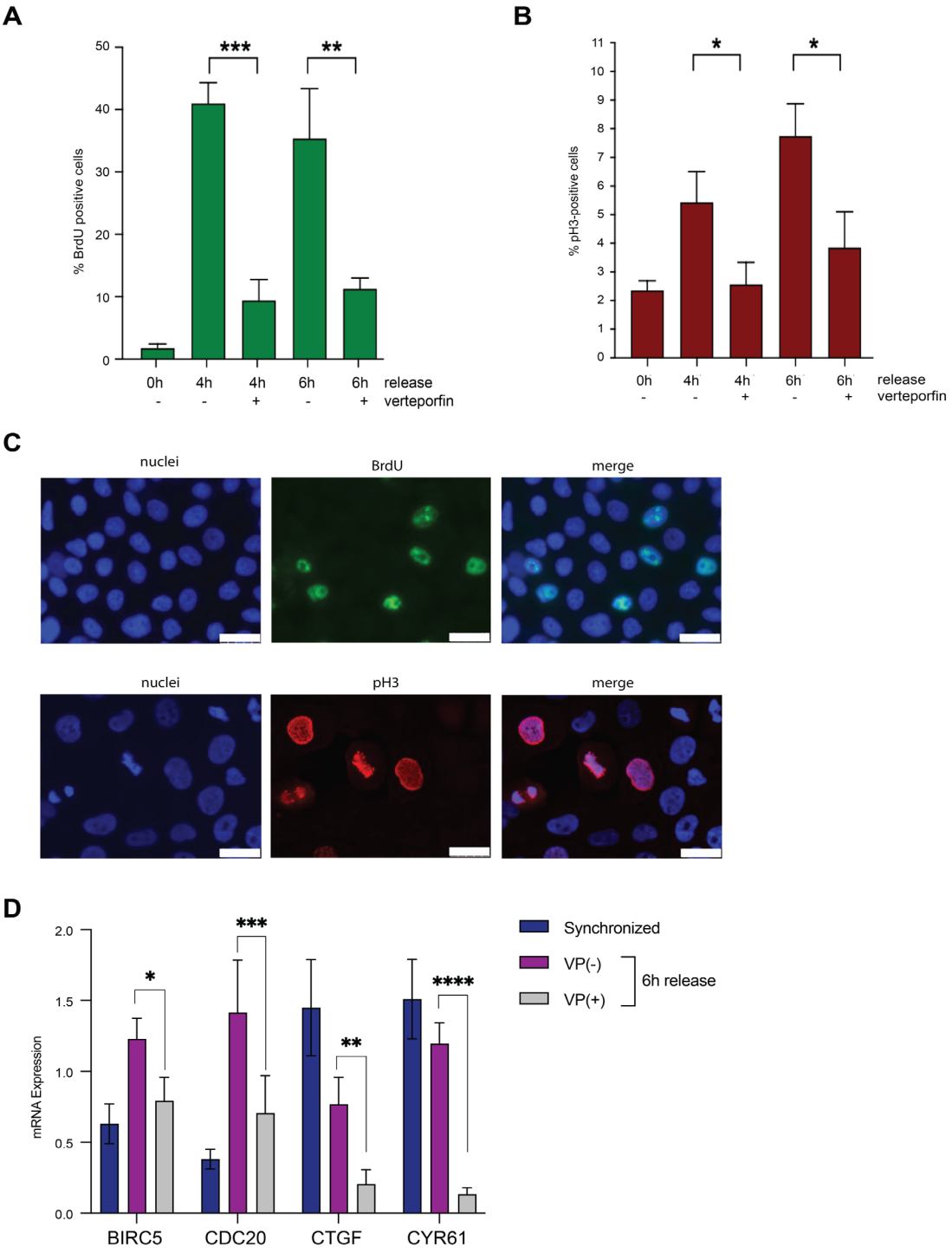

Figure 7. YAP is required for S and G2/M cell cycle phases

(A) Quantification of BrdU positive cells and (B) cells stained for phosphorylated histone H3. Error bars indicate standard deviation (SD). Per condition, 500 cells were counted. (C) Representative images of immunostaining for BrdU (green, above) and for pH3 (red, below), nuclei are stained with Hoechst (blue). Scale bar: 25 µm. (D) mRNA expression of YAP and YAP-MMB target genes relative to GAPDH was analyzed by RT-qPCR. Error bars represent the SDs of three independent replicates. Statistical significance was tested using the Student's t-test, two-tailed. All experiments: n=3 biological replicates. * = p<0.05, ** = p<0.01, *** = p<0.001, ****= p< 0.0001

3.2 Endogenous B-MYB is required for the progression of the cell cycle

Next, in order to determine whether the acute loss of endogenous B-MYB activity could have a similar effect on cell cycle progression as the observed results after endogenous YAP inhibition, we generated a stable cell line to induce degradation of endogenous B-MYB. To introduce the degradation tag, I used the PITCh (Precise Integration into Target chromosome) system in which DSBs, are generated in the genome at the 5' end of B-MYB and in the donor CRIS-PITCH (v2) vector by CRISPR-cas9 (Sakuma et al., 2016). This vector contains the endonuclease Cas9, a gRNA directed to the first exon of B-MYB and a common PITCH directed gRNA. The donor FKBPV-2A/BSD cassette contains the degradation domain FKBPV and a blasticidin resistance cassette to be inserted into the genome by microhomology-mediated end joining (MMEJ) stimulated by the microhomologous ends on the CRIS-PITCH (v2) vector and generated by the Cas9 (Figure 8A). Once both vectors were correctly generated and sequenced as described in (2.2.2.11 & 2.2.2.12) they were transfected into MDA-MB231 cells, this cell line was used as a tumor model cell line that expresses high levels of B-MYB. Selection, single-cell cloning, genotyping by qPCR, and sequencing was performed as indicated in (2.2.2.14 & 2.2.2.15) In regards to the dTAG degradation system (Nabet et al., 2018), protein degradation occurs by dTAG13, a degrader targeting the mutant degradation domain $FKBP12^{F36V}$ which is fused to an endogenous protein. This leads to the rapid, reversible and selective degradation of target proteins by the activation of the proteasome cascade through the CRBN E3 ligase complex (Figure 8B). Selected homozygous dTAG-B-MYB clones were treated or not with dTAG13 for 1,4,6,8 and 24 hours in order to evaluate the effective endogenous degradation of B-MYB (only one example clone is shown). As a control MDA-MB231 wild type (WT) cells were treated for 8 hours with dTAG13. Degradation of endogenous B-MYB was detectable after 1 hour of dTAG13 treatment and was stronger in the next time points. As expected in the WT cell line no effect on B-MYB was observed after 8 hours of treatment with dTAG13 compared to the untreated condition (Figure 8C). Additionally, immunofluorescence was performed and cells were stained

using antibodies directed at the HA-tag fused to endogenous B-MYB, which confirmed the effective degradation of endogenous B-MYB in MDA-MB231-B-MYB/dTAG cells (**Figure 8D**).

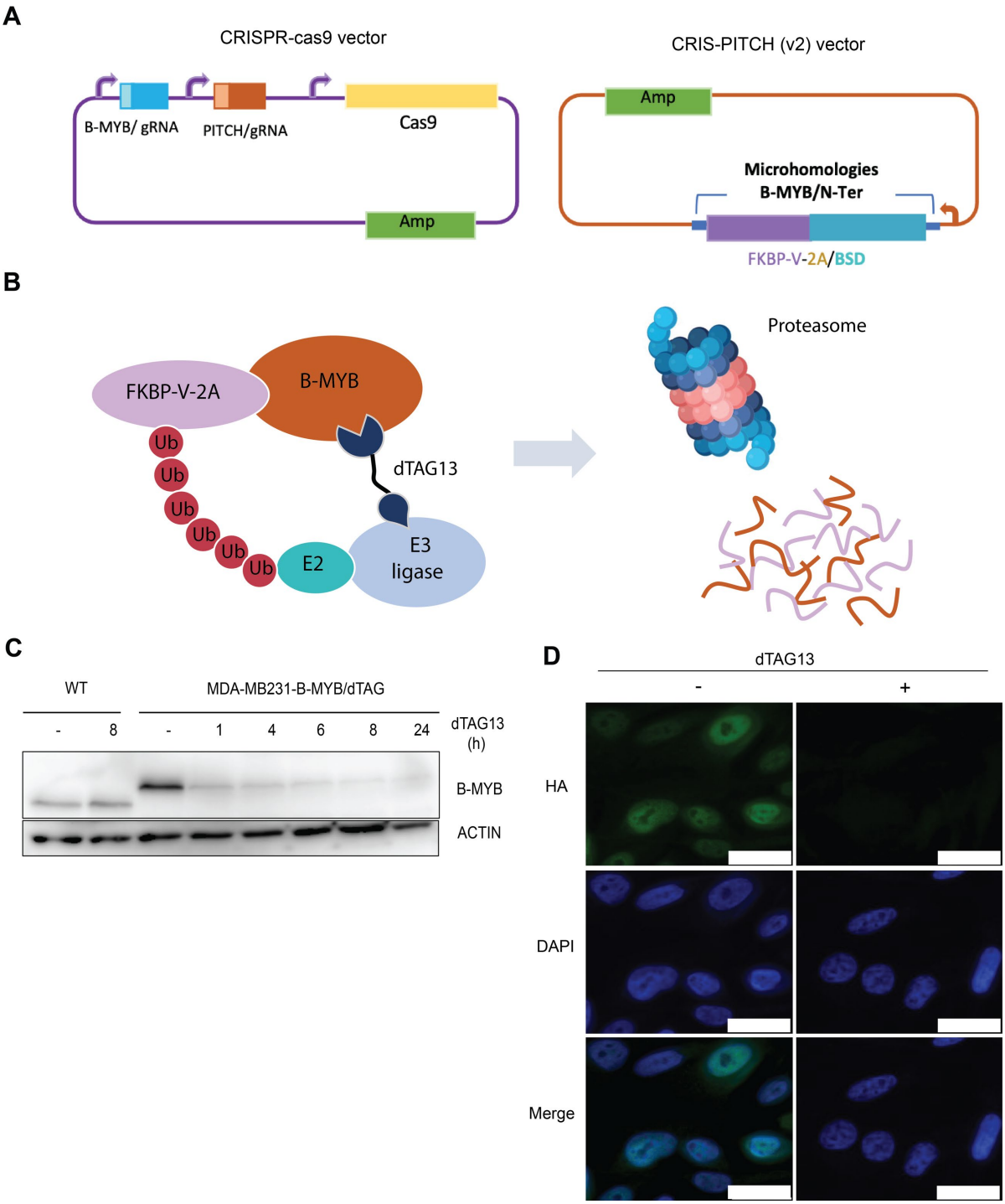

Figure 8. Endogenous degradation of B-MYB through dTAG system

(A) Schematic illustration of the plasmids CRISPR-cas9 (Left) and CRIS-PITCH (v2) (Right). The plasmid CRISPR-cas9 contains a gRNA directed at the amino-terminus of B-MYB and a commonly usable PITCH-gRNA. This vector also contains the Cas9 expression cassette which will generate the DSBs in the genome and in the donor vector CRIS-PITCH (v2) vector (right) which harbors the microhomologies at

B-MYB N-terminus, the degradation domain (FKBP-V-2A) and the blasticidin resistance cassette. (B) Schematic depiction of the strategy to degrade endogenous B-MYB through the dTAG system. (C) MDA-MB 231 WT and B-MYB/dTAG cells were treated or not with dTAG13 (500nM) for the indicated times. Lysates were immunoblotted with the indicated antibodies. Actin was used as a loading control. (D) Representative images of immunofluorescence analysis before and after dTAG13 treatment for 24 hours. HA antibody targeted the HA-tag of endogenous B-MYB (Green), nuclei are stained with Hoechst (blue). Scale bar: 25 µm. n=3 biological replicates.

It has been previously reported that knockdown of B-MYB in murine embryonic stem cells (mES) results in a delayed transition through G2/M phases (Tarasov et al., 2008). To address whether acute degradation of B-MYB has similar effects on cell cycle transition of human MDA-MB231-cells, cells were double synchronized in G1/S by double thymidine block and subsequently released and treated with dTAG13 simultaneously for 6h, 8h or 10h (Figure 9A). FACS results indicated that the percentage of cells in G2/M increased after degradation of B-MYB, at 8 hours of release from 64% to 71% and at 10 hours from 57% to 66%. Whereas, a significant decrease in the percentage of cells in G1 phase of the next cell cycle after degradation of B-MYB compared with control cells was found. After 8 hours of release and more markedly after 10 hours of release and dTAG13 treatment the percentage of cells in G1 phase of the next cell cycle was less increased from 29% to 19% (Figure 9B,C). These results indicate that B-MYB absence could promote the accumulation of cells in G2/M, leading to a delay in the transit from mitosis to the beginning of the next cell cycle in G1 phase which is evidenced by a decrease on G1 phase rates (Figure 9D).

In summary, these findings independently illustrate a role for endogenous YAP and B-MYB to fully continue and lead cell cycle progression. Inhibition or depletion of either YAP or B-MYB resulted in cell cycle delays. Specifically, after YAP inhibition S phase rates decreased affecting cell cycle progression through S phase to G2/M, which was evidenced also by the decreased amount of cells in G2/M. B-MYB degradation led to the accumulation of cells in G2/M, which delayed re-entry of cells into the next G1 phase.

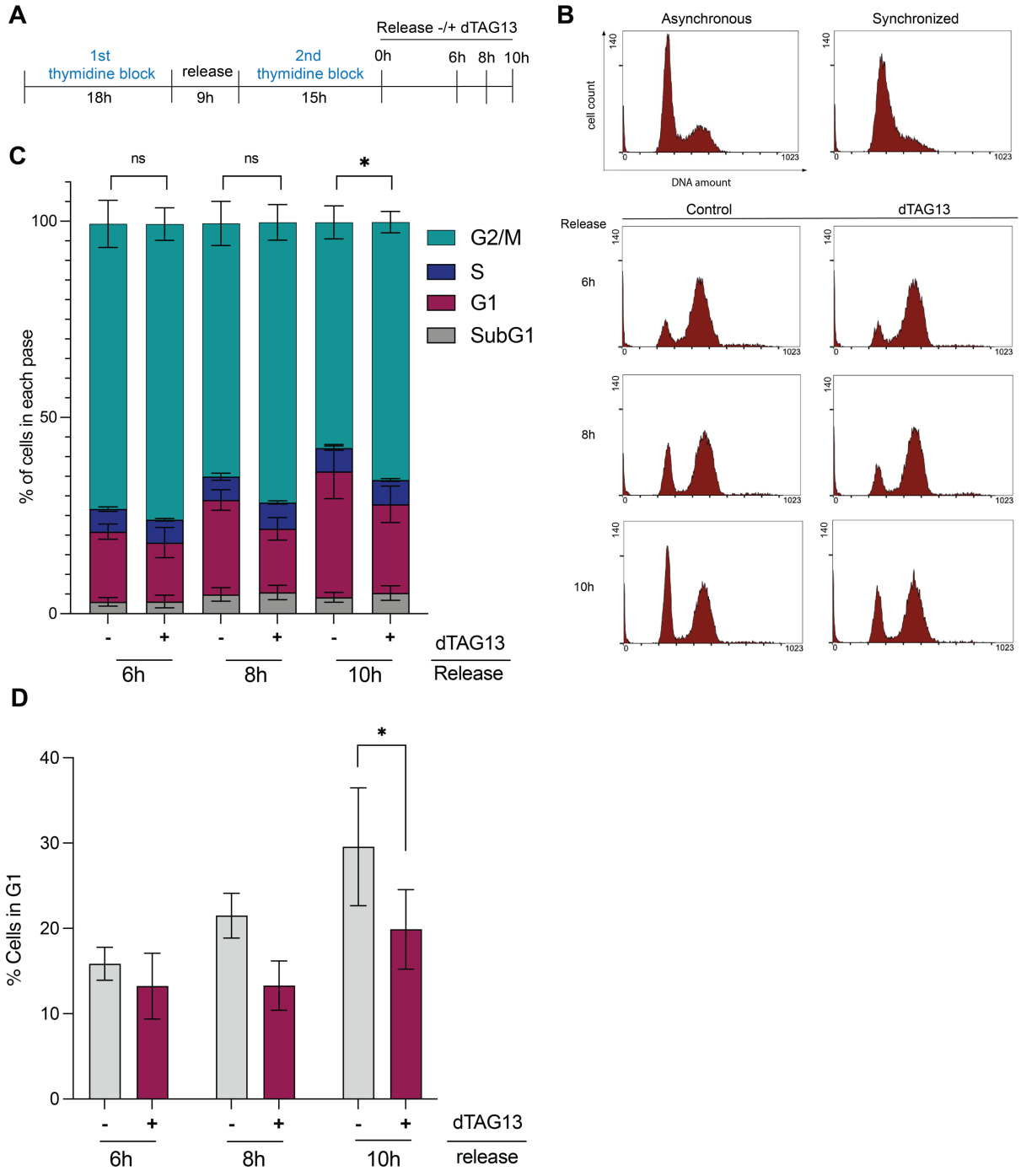

Figure 9. Endogenous degradation of B-MYB leads to defects in cell cycle progression

(A) Scheme of the experiment. MDA-MB231-B-MYB/dTAG cells were double thymidine blocked and then released in the presence or absence of dTAG13 for 6, 8 or 10 hours (B) The fraction of cells in the different phases of the cell cycle was analyzed by flow cytometry. (C) Quantification of FACS data from three independent experiments, the error bars depict SEM. Statistical significance for differences in the amount of G2/M cells was assessed by one-way ANOVA T-Test. (D) Quantification of cells in G1 phases. The means and SD of three independent experiments are depicted. All experiments: n=3 biological replicates. Statistical significance was tested using the Student's t-test, two-tailed. ns= not significant, * = p<0.05, ** = p<0.01, *** = p<0.001, ****= p< 0.0001

3.3 B-MYB is required for cell migration of MDA-MB 231 cells

Due to the shown oncogenic role of B-MYB in different human cancers as in promoting not only cell proliferation but also cell migration (Fan et al., 2018; Jin et al., 2017) we asked the question of whether the endogenous degradation of B-MYB could have effects on the ability of MDA-MB 231 cells to migrate. First, I determined if MDA-MB231-B-MYB/dTAG cells migration is affected by the degradation of B-MYB through dTAG13 treatment. Migration was measured using a well-established trans-well assays where serum-starved cells migrate through a trans-well membrane to a complete serum medium. Migrated cells were stained with crystal violet and evaluated by microscopy. Additionally, wild-type MDA-MB231-WT cells were analyzed in parallel to exclude off target effects on migration of the dTAG13 treatment by itself. I observed that degradation of B-MYB significantly decreases cell migration in comparison with untreated cells. In contrast, we did not observe any reduction in cell migration after dTAG13 treatment in the MDA-MB231-WT cells, showing that the obtained reduction of migration in the B-MYB-dTAG cell line is due to the effective degradation of B-MYB (**Figure 10A,B**). To further prove that the observed reduction on migration was due to B-MYB degradation, I performed rescue assays. To do so, I generated MDA-MB231-B-MYB/dTAG cells expressing doxycycline-inducible B-MYB by infection with lentiviral pINDUCER-B-MYB-WT. With this cell line, I can simultaneously induce the endogenous degradation of B-MYB upon dTAG 13 treatment and induce overexpression of B-MYB-WT after doxycycline treatment (**Figure 10C,D**). The reduced migration after degradation of B-MYB was rescued by the simultaneous overexpression of B-MYB-WT through doxycycline treatment, where we observed that B-MYB expression trigger to migration (**Figure 10E,F**). Taken together these results suggested that B-MYB effectively has a role on the oncogenic ability of MDA-MB231 cells to migrate, where the endogenous depletion of B-MYB lead to a reduction on the number of migrating cells.

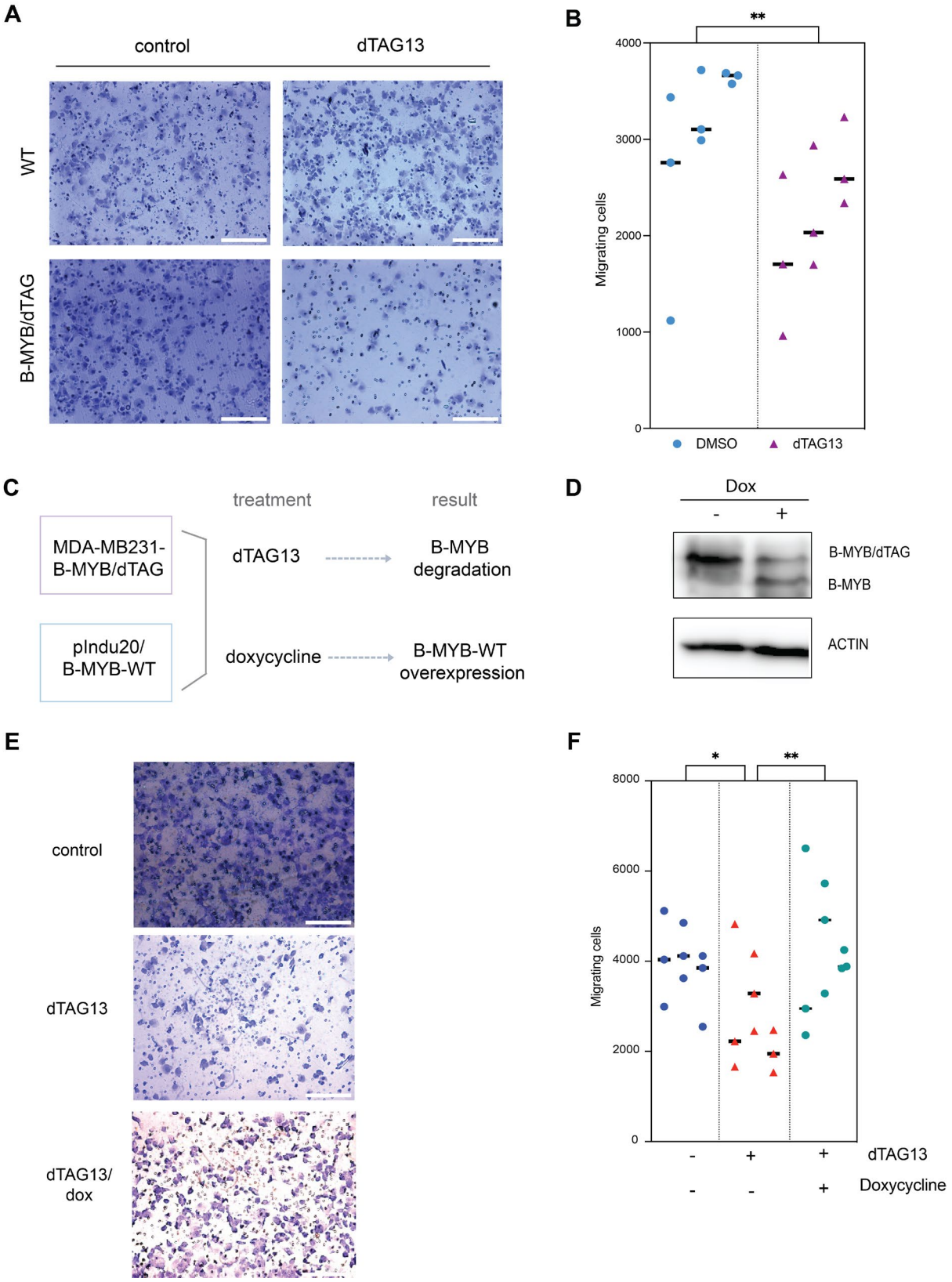

Figure 10. B-MYB has a role in migration of MDA-MB 231 cells

A) Example photos of transwell migration assay in MDA-MB 231 wild type and MDA-MB231-B-MYB/dTAG cells with and without dTAG 13 treatment. Scale bars: 50 µm. B) Quantification of migrating cells. n=3 biological replicate. Analysis in WT cells was performed once, quantification is not shown. C)

Scheme explanation of MDA-MB231-B-MYB/dTAG-Pindu20-B-MYB/WT cell line and effects of the corresponding treatments. D) Protein lysates after and before doxycycline 0.01 µg/ml treatment for 48 hours to induce expression of B-MYB WT. ACTIN was used as a loading control. E) Example photos of transwell migration assay in MDA-MB231-B-MYB/dTAG-Pindu20-B-MYB/WT cells treated with dTAG13 or dTAG13/ doxycycline or untreated. Scale bars: 50 µm .F) Quantification of migrating cells. n=3 biological replicates. Statistical significance was tested using the Nested: ANOVA one-way. * = p<0.05, ** = p<0.01, *** = p<0.001, ****= p< 0.0001 n=3 biological replicates

3.4 YAP and B-MYB roles in CHK1 inhibitor sensibility

The proteinase CHK1 inhibits the cell-cycle progression by phosphorylation of CDC25 as a response to DNA double-strand breaks in order to block cell cycle progression. This phosphorylation targets CDC25 for degradation and therefore inhibits the activity of CDK2/CDK1 leading to cell cycle arrest at intra-S and G2/M checkpoints (Wang et al., 2002; Zhao et al., 2002) (Figure 11A). Recently, combined therapies for cancer targeting CHK1 have been used in order to battle chemoresistance and abrogate tumor growth (Bartucci et al., 2012). Precisely, prexasertib is a CHK1 inhibitor (CHK1i) that leads to the inhibition of checkpoint control 1 triggering to a hurried cell cycle progression which causes premature mitosis during late S phase (Blosser et al., 2020; Branigan et al., 2021). MMB-FOXM1 complex and CDK1 have been associated with an enhanced sensibility to CHK1i by driving premature mitosis during late S phase leading to a replication catastrophe (Branigan et al., 2021) (Figure 11A). Given this role of the MMB complex, I asked whether B-MYB degradation could affect sensitivity to CHK1i in our endogenous leaded degradation system. I observed that MDA-MB231-B-MYB/dTAG cells without dTAG13 treatment (-dTAG) were sensible to CHK1i treatment with an IC50 (nM) of 15.17 nM. Interestingly, after targeted degradation of B-MYB with dTAG13 treatment (+dTAG) a clear loss of sensibility was observed with an IC50 (nM) of 53.78 (Figure 11B). Through crystal violet staining we could show that after simultaneous treatment with CHK1i and dTAG13 the amount of stained cells stay was constant from 100nm to 500nm CHK1i treatment indicating cell resistance. In contrast, in the no dTAG13 treatment condition, a clear reduction of cells was observed at the three CHK1i concentrations (100,200 and 500nM) denoting sensitivity (Figure 11C,D). Together, these results suggest that degradation of B-MYB in the MDA-MB231 cells confers resistance to CHK1i, corroborating previous findings that indicated that the MMB-mediated premature mitosis causes sensibility of cancer cells to CHK1i.

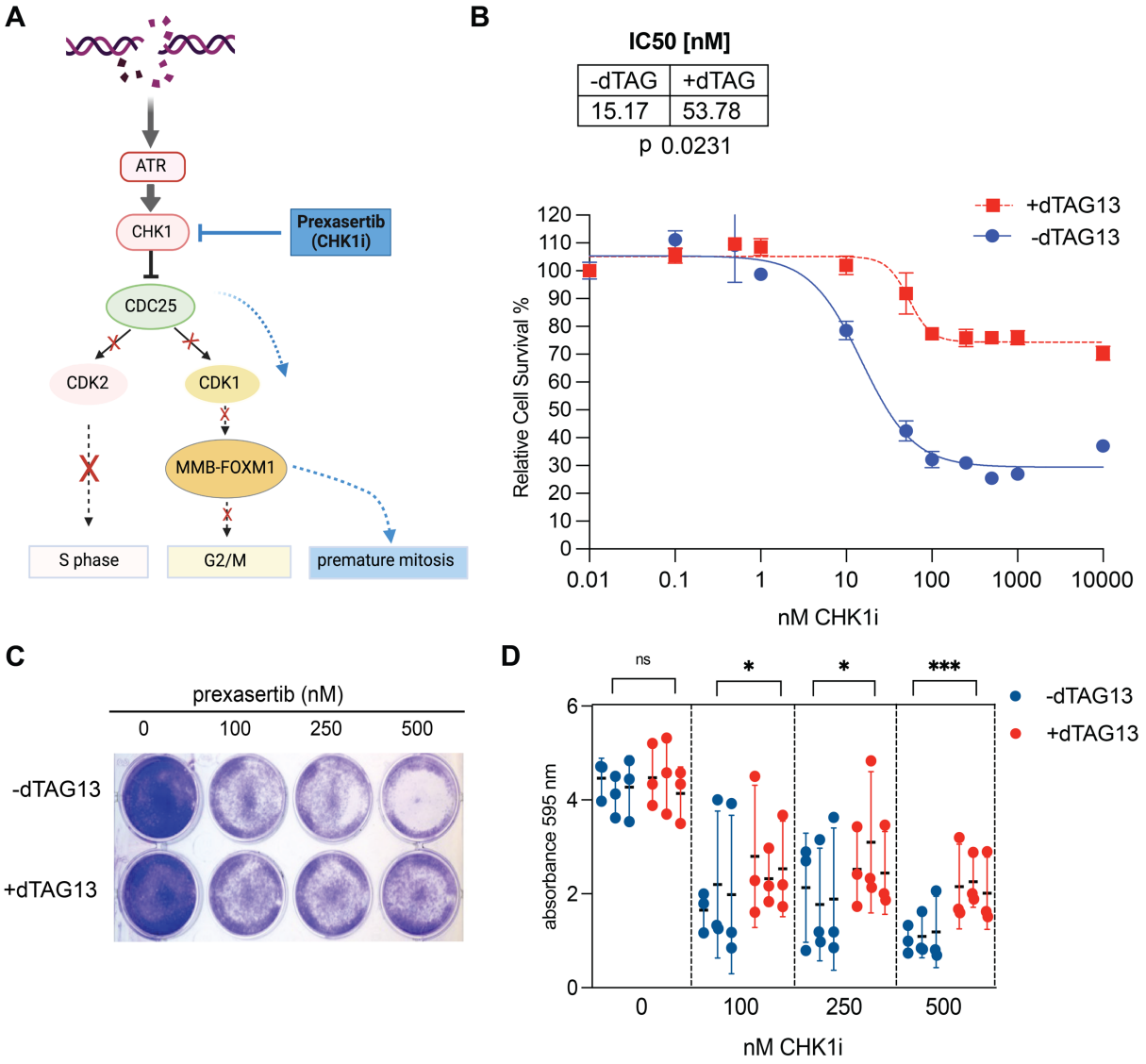

Figure 11. Endogenous degradation of B-MYB leads to CHK1 inhibitor resistance in MDA-MB231 cells.

A) Scheme illustration of checkpoint control 1 by CHK1. B) MTT assay of MDA-MB231-B-MYB/dTAG cells treated with different concentrations of CHK1i for 48h. Cells were first pretreated or not for 24h with dTAG13, and kept in treatment during the MTT assay for a total of 72h, to induce degradation of B-MYB. C) Representative photos of Crystal violet stained cells treated with different concentrations of CHK1i for 48h, before and after treatment with dTAG13 during 72h. D) quantification of C. B,C,D n=3 biological replicate Statistical significance was tested using the Student's t-test, two-tailed. * = p<0.05, ** = p<0.01, *** = p<0.001, ****= p< 0.0001. B Experiment and quantification was done by Nataliia Sira (B.Sc. student).

Since we observed that B-MYB expression is necessary for cells sensitivity to CHK1i, we then asked if the MMB target genes after CHK1 inhibition were upregulated. Therefore, we next evaluated gene expression in cells arrested in G1/S arrested by thymidine treatment and released in the cell cycle with or without CHK1i medium (**Figure 12A**). Expression of example MMB target genes: *CDC20*, *AURKA,* and *KIF23* were quantified. A significative gene

upregulation consequence of CHK1i treatment at 4h and 6h of release was found (Figure 12B), this indicates that inhibition of CHK1 hyperinduces transcription of MMB-regulated genes which mRNA products may be more stable. Next, we pretreated MDA-MB231-B-MYB/dTAG cells with dTAG13 for 24 haours and simultaneously treated them with CHK1i for 4 hours in order to evaluate if the degradation of B-MYB could prevent the hyperinduced expression of MMB target genes due to the inhibition of CHK1. Contrary to the expected downregulation of genes regulated by MMB complex after the degradation of B-MYB, we found no significant changes in gene expression of those genes by the degradation of B-MYB (Figure 12C). On the other hand, after releasing G1/S arrested cells with verteporfin to inhibit YAP-TEAD interaction and CHK1 inhibition simultaneously (Figure 12D) MMB and YAP target genes were less induced. No significant effect is observed in cells treated only with VP. All this suggests that YAP contributes to the premature hyper-upregulation of G2/M genes after CHK1 inhibition (Figure 12E). Therefore YAP seems to be involved in sensitivity to CHK1i as well as MMB complex.

Taken together, our findings point to the role of B-MYB leaded sensitivity to CHK1 inhibition which may mediate the premature mitosis observed by the overexpression of G2/M genes after CHK1i treatment. In addition, YAP appears to be involved in the accelerated transcription of G2/M genes after the inhibition of CHK1. Depletion of B-MYB by endogenous degradation led to cell resistance to CHK1i indicating that B-MYB activity is required to facilitate CHK1i sensitivity. Surprisingly, the degradation of B-MYB does not affect the CHK1i-mediated increased expression of MMB target genes, probably due to shorter dTAG13 treatment not being sufficient to observe detectable changes in mRNA levels or due to overlapping functions of transcription factors that co-regulate G2/M genes after CHK1 inhibition.

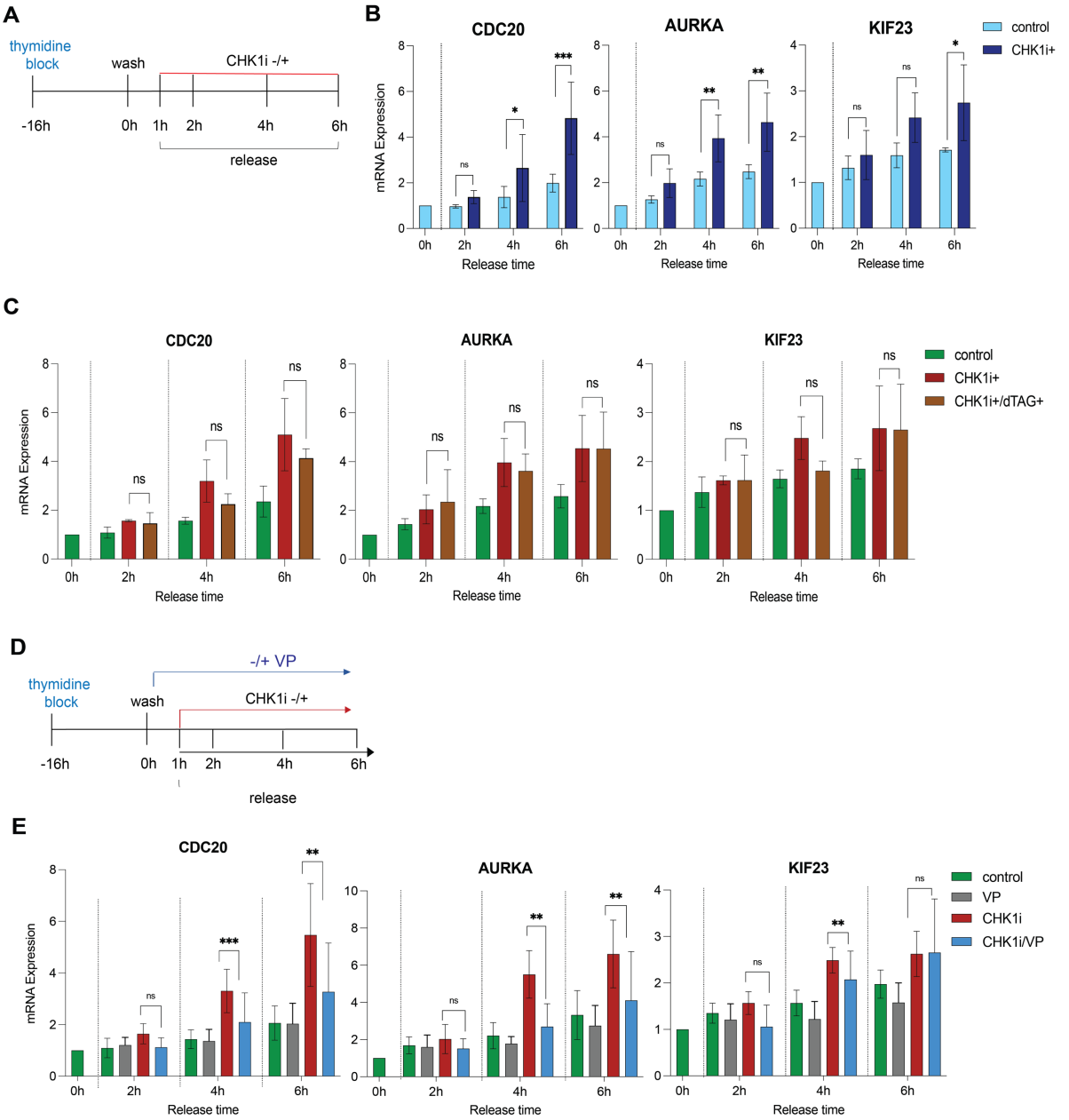

Figure 12. YAP and B-MYB are involved in prexasertib sensibility in MDA-MB231 cells

A) Scheme of the experiment. MDA-MB231-B-MYB/dTAG cells were thymidine blocked and then released at the indicated times in the presence or absence of CHK1i (B) and/or pretreated with dTAG13 for 24h(C). B,C) mRNA expression of representative MMB target genes B) before and after CHK1i C) with or without dTAG13 pre-treatment. D) Scheme of the experiment. MDA-MB231-B-MYB/dTAG cells were thymidine blocked and then released in the presence or absence of CHK1i and verteporfin at the indicated times. E) mRNA expression of representative MMB target genes before and after CHK1i and verteporfin treatment at the indicated times. Gene expression was analyzed relative to *GAPDH* and it was analyzed by RT-qPCR. Error bars represent the SDs of three independent replicates. Statistical significance was tested using the Student's t-test, two-tailed. B,C,E n=3 biological replicate. ns= not significant, * = p<0.05, ** = p<0.01, *** = p<0.001, ****= p< 0.0001 C,D,E) Experiments were done by Natalie Siri (B.Sc. student).

3.5 Overexpression of YAP can lead to genome-wide changes in chromatin accessibility

Given that YAP and MMB activate the expression of G2/M genes in MCF10A cells, we wanted to investigate if YAP-mediated transcription of MMB target genes results from global changes in chromatin accessibility. To answer this question an *assay for transposase-accessible chromatin with sequencing* (ATAC-seq) was performed in two biological replicates. Untransformed human breast epithelial MCF10A cells which express doxycycline-inducible YAP5SA were used. In these cells a constitutive allele of YAP that cannot be inhibited by the Hippo kinases is expressed (von Eyss et al., 2015; Zhao et al., 2007). In previous studies in our group, it was identified that the induced expression of YAP5SA by doxycycline treatment results in upregulation of MMB target genes as *CDC20*, *AURKA* and *TOP2A* (**Figure 13A**) (Pattschull et al., 2019).

Interestingly, the induction of YAP5SA resulted in evident changes in chromatin accessibility in the genome of MCF10A cells (**Figure 13B,C**). We identified that upon YA5SA induction 23,890 peaks were newly accessible ATAC-seq peaks “opened” and 13,612 peaks were less accessible “closed” in comparison with the no doxycycline-treated cells (control). In contrast, 111,403 peaks “flat” were accessible in both conditions and showed no change after YAP5SA expression. These flat regions correspond mainly to transcriptional start sites and intergenic regions which seem not to change upon expression of YAP5SA (**Figure 13D**). The majority of the newly opened and closed peaks mapped to intergenic and intronic regions and few of them were found in promoter regions of annotated genes (**Figure 13D**). Transcription factor motifs associated with the YAP5SA-induced changes in chromatin accessibility statuses were identified by chromVAR (Schep et al., 2017) (**Figure 13E,G,F**). The newly open chromatin regions after YAP5SA induction were enriched for binding sites that correspond to TEAD proteins and to the Activator Protein-1 (AP-1) family of transcription factors. These findings are consistent with previous reports showing that YAP is recruited to the chromatin through TEAD proteins where TEAD and AP-1 could as well interact at enhancer regions to regulate transcription of YAP-regulated genes (Liu et al., 2016; Zanconato et al., 2015) (**Figure 13E,G**). Remarkably, the regions that became less accessible after YAP5SA expression were highly enriched for binding motifs for the p53 family of transcription factors, suggesting that regulation of p53 family, could be involved in the YAP mediated rearrangement on chromatin landscape (**Figure 13F,G**). In summary, we show here

that YAP5SA expression leads to more (open) and less (close) accessible regions which could represent a key to understanding how YAP regulates transcription of cell cycle genes.

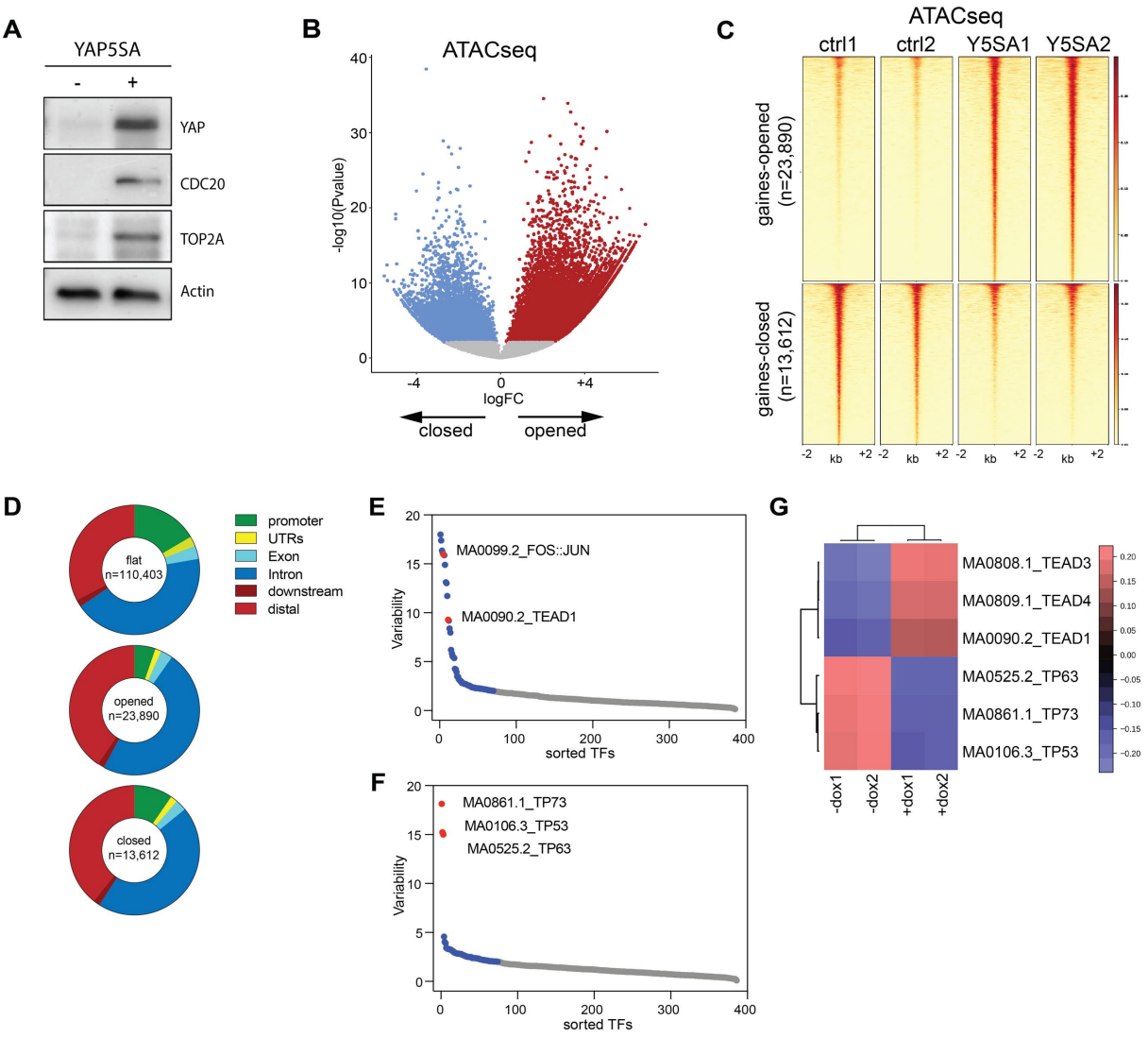

Figure 13. Changes in chromatin accessibility by YAP overexpression

MCF10A cells expressing doxycycline-inducible YAP5SAwere treated with (+) or without (-) doxycycline to induce YAP5SA. A) The expression of YAP, CDC20, and TOP2A was analyzed by immunoblotting. Actin was used as a loading control. B) volcano plot of ATAC-seq data after YAP5SA expression YAP5SA expression. C) Heatmap showing upregulated and downregulated ATAC-seq peaks in a window of -2kb to +2kb centered on the middle of the peak. 23,890 regions were newly opened, 13,612 were newly closed, and 110,403 were unchanged (flat) at q<0.035. 2 biological replicates per condition. D) Distribution of ATAC-seq peaks relative to annotated and known genes in the genome. E,F) ChomVAR chromatin variability scores for ATAC-seq data, showing the most enriched transcription factors motifs. For open regions TEAD (E) and for closed regions p53-family were significantly found (F). G) Heatmap showing motif enrichment for open and closed regions.

3.6 YAP overexpression leads to the opening of chromatin on YAP-regulated enhancers but not at MMB-regulated promoters

As described previously after YAP5SA expression, we found that chromatin got newly closed or opened. Classifying the changed regions revealed that those regions corresponded mainly to enhancer regions, while fewer changes happened at promoters (**Figure 14A**). To further investigate whether the chromatin regions that were opened after YAP5SA expression corresponded to YAP binding regions we analyzed the *Cleavage Under Targets and Release Using Nuclease* (CUT&RUN) data set from MCF10A cells before and after YAP5SA expression (Liss, unpublished data) (**Figure 14B, D**). 21,027 high confidence YAP peaks were identified after induction of YAP5SA with doxycycline and those peaks mainly corresponded to distal, intragenic and intergenic regions, consistent with previous ChIP-seq data from (Pattschull et al., 2019) (**Figure 14B**). Putative enhancers were defined as H3K4me-1 positive, H3K4me3 negative regions in a distance of more than 1kb to the transcription start site (TSS). Following these parameters 34,469 putative enhancer regions were identified in MCF10A cells (**Figure 14C**). The enhancer regions were clustered based on YAP enrichment YAP-high (YAP-bound) regions and YAP-low regions (non-YAP bound). Chromatin accessibility in YAP-bound regions was found to be increased after YAP5SA expression through ATAC-seq analysis, while non-YAP bound regions did not evidence changes in chromatin accessibility (**Figure 14E**). These findings prove that YAP5SA expression induces chromatin opening specifically at its own YAP-bound enhancers. Evaluation of previous ChIP-seq data of the histone markers H3K27ac and H3K4me1 from Pattschull et al., 2019, revealed that YAP-bound enhancers became hyper-active after YAP5SA induction (**Figure 14E**).

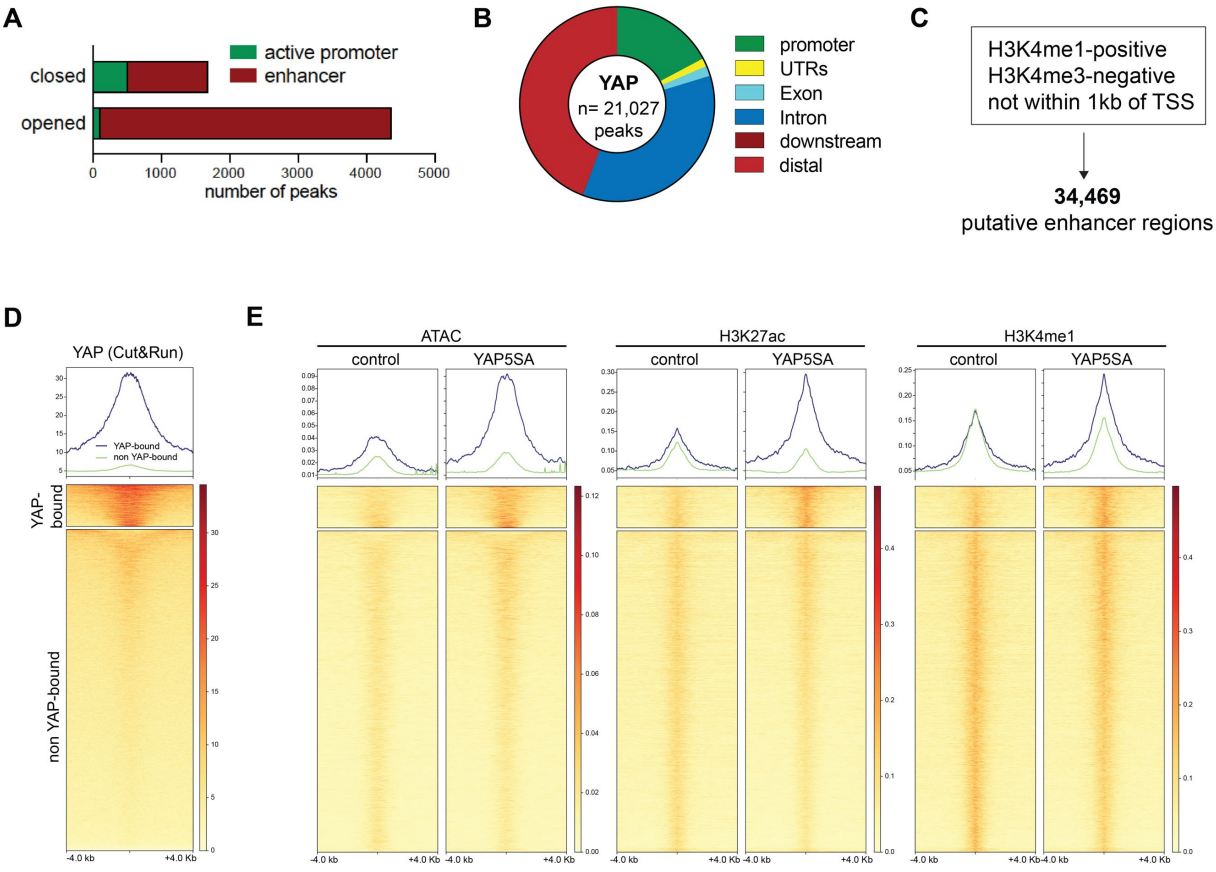

Figure 14. YAP mediates chromatin opening at its regulated enhancers

A) Sorting of newly open and closed regions in relation to active promoters or enhancers. B) MCF10A cells expressing doxycycline-inducible YAP5SA were treated with and without doxycycline. Cut and Run-seq data set from (Liss, unpublished data) showing YAP peaks after YAP5SA induction. C) number of YAP regulated putative enhancer regions according to position with respect to TSS and histone markers. D,E) Heatmaps showing enrichment at high YAP bound regions (up) or at low YAP bound regions (down), D) Cut&Run of YAP enriched peaks, E) ATAC-seq signal and enrichment of H3K27ac and H3K4me1 peaks in a window of -4kb to +kb centered on the middle of the peak.

Next, putative enhancers were clustered according to their accessibility determined by ATAC-seq. Clustering of primed and active enhancers based on YAP enrichment by CUT&RUN confirmed that accessibility at YAP-bound regions increased upon expression of YAP5SA (**Figure 15A**). By plotting the enrichment of H3K27Ac at YAP bound enhancers we could show specificity in the distribution of YAP peaks in relation to H3K27ac, where the center of YAP-peaks is flanked by two H3K27ac peaks that gain acetylation when YAP5SA is expressed (**Figure 15B**). Together, these data suggest that YAP binds to a subset of putative enhancers in MCF10A cells leading to their chromatin opening and activation.

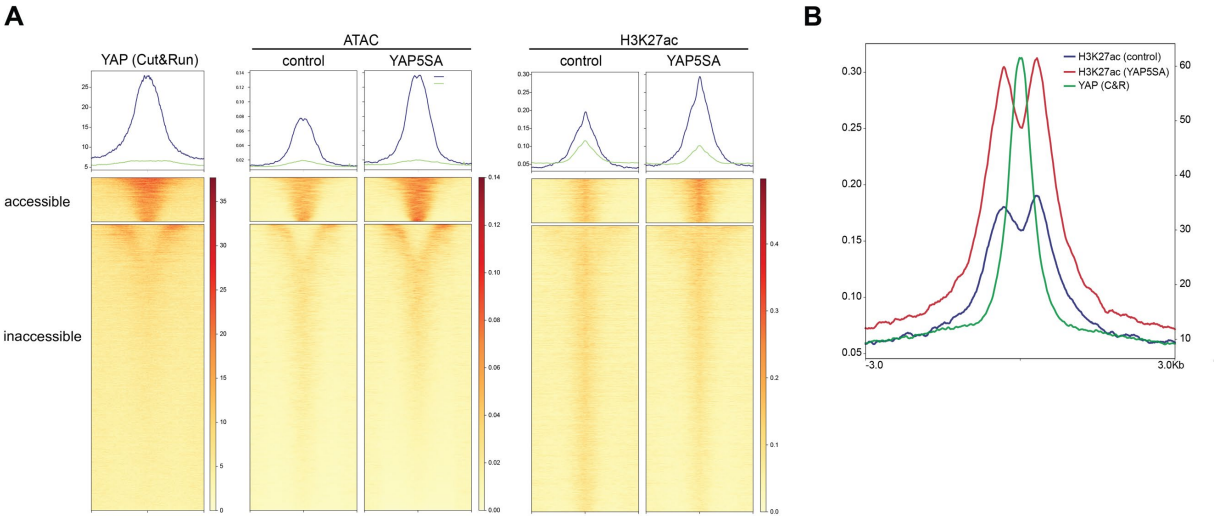

Figure 15. YAP bound regulated enhancers became active after YAP5SA expression
A) MCF10A cells expressing doxycycline-inducible YAP5SA were treated with doxycycline (YAP5SA) and without (control) doxycycline. Heatmaps showing clustered enhancers, classified as accessible (up) or inaccessible (down). ATAC-seq, ChIP-seq for H3K27ac, and YAP Cut&Run are presented. B) Line plots depicting enrichment of H3K27Ac at YAP binding sites (in enhancers), showing the distribution of YAP peaks in relation to H3K27ac evidencing gain of acetylation due to YAP5SA expression.

Given that previous studies have shown that binding of YAP to enhancers promotes B-MYB chromatin association to promoters of MMB-target genes (Pattschull et al., 2019), we wanted to investigate how YAP5SA-activated enhancers regulate gene expression of YAP and MMB coactivated cell cycle genes. The ATAC-seq results show that TSS regions of YAP and MMB target genes are already accessible in the control condition. A slightly reduced occupancy at the -1 nucleosome was found after YAP5SA expression (**Figure 16A**). No significant changes were found in nucleosome positioning and H3K4me3 enrichment at the TSS of MMB-YAP target genes, after YAP5SA expression. Additionally, the increased binding of B-MYB and FOXM1 at TSS regions of MMB-YAP target genes following YAP5SA expression overlaps with the already accessible regions (**Figure 16A**). As ChIP-seq signals also revealed that LIN9 binds to TSS in control cells before induction of YA5SA, this could explain the constitutive accessibility at these regions. These results indicate that activation of YAP and MMB target genes is associated with the YAP5SA mediated chromatin opening at enhancer regions, while the remodeling and chromatin opening at the TSS of these genes seems to be independent of YAP expression.

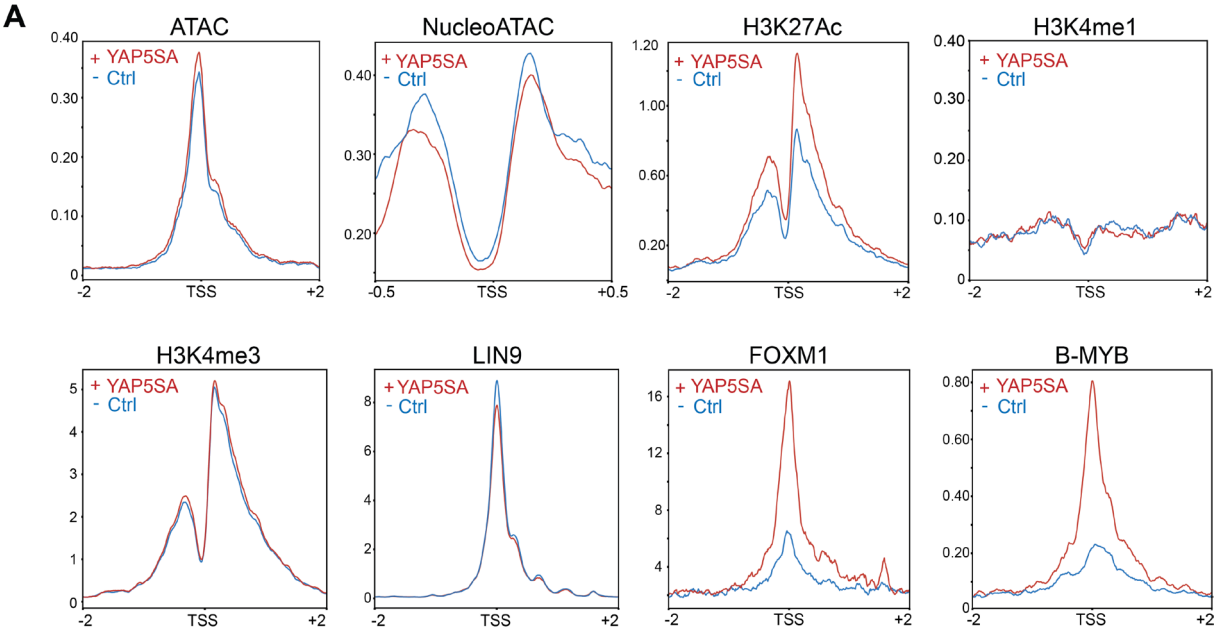

Figure 16. Promoter regions of MMB target genes remain accessible after YAP5SA expression
A) Line plots depicting chromatin accessibility (ATAC), nucleosome signal (NucleoATAC) and the levels of the indicated proteins (by ChIP-seq) at the TSS of MMB target genes in uninduced MCF10A-YAP5SA cells (-ctrl) and after induction of YAP5SA by doxycycline (+YAP5SA).

3.7 A role of YAP-regulated enhancers to facilitate initiation of transcription at CDC20 locus

To investigate how YAP and MMB co-regulate gene expression, we selected a well-known YAP-MMB target gene, *CDC20*, as a model gene. YAP binds to two distal enhancers of CDC20 and through chromatin looping those enhancers interact with the promoter region, where B-MYB binding is induced by YAP5SA expression to regulate *CDC20* expression (Pattschull et al., 2019) (**Figure 17A**). Chromatin accessibility and acetylation of H3K27ac at the two enhancers are increased by YAP5SA expression (**Figure 17B**).

In order to better understand how YAP-bound enhancers regulate the expression of *CDC20*, the enhancers were inactivated by the use of a CRISPR interference system (CRISPRi), where CRISPR/dCas9 was fused to the KRAB transcriptional repressor domain (dCas9-KRAB) (**Figure 17C**). An MCF10A-YAP5SA cell line that stably expresses doxycycline-inducible dCas9-KRAB with a nonspecific control guide RNA or a set of five guide RNAs that target dCas9-KRAB to the two CDC20 enhancers was created by our group (Bennedikt Gantert, 2019) (**Figure 17C,D**). Notably, the expression of CDC20 was significatively reduced when its two enhancers were silenced, indicating that the YAP-regulated enhancers of CDC20 are required for YAP-mediated CDC20

mRNA expression (**Figure 17E**). To evaluate whether enhancer activity is required for cell cycle dependent under endogenous YAP expression in synchronized MCF10A cells, MCF10A Cas9-KRAB cells with guide RNAs specific for the CDC20 enhancers where double synchronized with thymidine as described in (2.2.1.17) and release into the cell cycle. CDC20 expression was low in synchronized cells and highest when cells were released from the block, as expected. Interestingly, when the CDC20 enhancers were silenced, the induction of CDC20 was not reduced (**Figure 17F**). Thus, the YAP-bound enhancers are necessary for the YAP5SA-mediated increase in CDC20 expression, but not for cell-cycle-dependent expression of CDC20 under conditions where only endogenous YAP is present in untransformed cells, which may be different in tumor cells where YAP seems to have crucial roles in cell cycle progression.

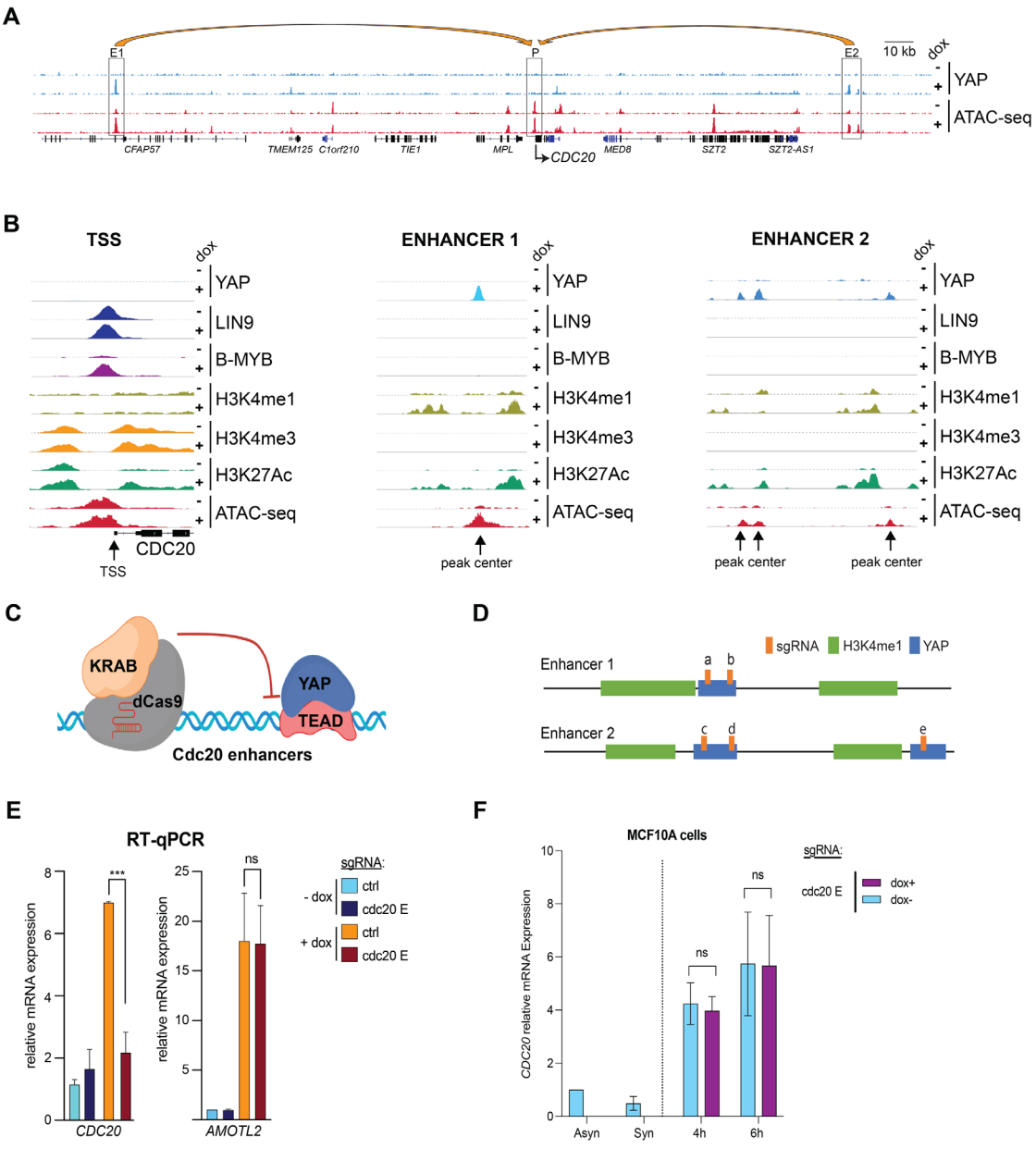

Figure 17. Silencing of CDC20 enhancers limits the expression of CDC20

A) Gene browser of CDC20 showing binding of YAP to the two enhancers (E1 and E2) by ChIP-seq and chromatin accessibility by ATAC-seq in untreated MCF10A-YAP5SA cells (-) and in cells expressing YAP5SA (+). Long-range interactions between the CDC20 promoter and enhancers as determined by 4C-seq are indicated by arrows (Pattschull et al., 2019). B) Gene browser of CDC20 at TSS and enhancers regions, showing ATAC-seq and ChIP-seq for YAP, B-MYB, LIN9 and histone modifications untreated MCF10A-YAP5SA cells (-) and in cells expressing YAP5SA (+). C) Scheme for the dCas9/KRAB system targeting CDC20 enhancers. D) Scheme depicting CDC20 enhancers (E1 and E2) and the respective position of sgRNAs (a-e) in relation to the YAP and H3K4me1 peaks as determined by ChIP-seq E) MCF10A-YAP5SA-Cas9-KRAB cells expressing either a control (ctrl) or enhancer specific guide RNAs (CDC20 E) were treated with doxycycline (+dox) to induce the expression of YAP5SA and Cas9-KRAB or were left untreated (-dox). The expression of *CDC20* and *AMOTL2* relative to *GAPDH* was analyzed by RT-qPCR. Error bars: SD of four independent replicates. F) MCF10A-Cas9-KRAB cells expressing the specific guide RNAs (CDC20 E) were double thymidine blocked and released into the cell cycle at the indicated times, and treated with doxycycline (+dox) for 48 hours to induce the expression of Cas9-KRAB or were left untreated (-dox). The expression of *CDC20* relative to *GAPDH* was analyzed by RT-qPCR. Error bars: SD of three independent replicates. Student's t-test. * = $p<0.05$, ** = $p<0.01$, *** = $p<0.001$, ns = not significant

As we observed the reduced expression of *CDC20* after silencing of its enhancers we next confirmed that the silencing of *CDC20* enhancers prevents enhancer activation. ChIP-qPCR assays were performed to study the chromatin marks associated with enhancers transcriptional activation (acetylated H3K9, H3K27, H4 and H2A.Z). Following YAP5SA expression, histone acetylation at CDC20 enhancers was increased, which was clearly prevented when Cas9-KRAB was co-expressed targeting enhancers through specific guide RNA. These results confirm the activation of *CDC20* enhancers by YAP5SA expression and reveal that silencing of enhancers by Cas9-KRAB interferes with YAP-induced activity at enhancers (Figure 17E, Figure 18A).

To address the effects of silencing the of *CDC20* enhancers on promoter activity (Figure 18B), ChIP-qPCR was performed. The qPCR results revealed that silencing of enhancers reduced B-MYB binging to the CDC20 promoter, but did not completely prevent it (Figure 18C). Furthermore, occupancy of RNA Pol II was also evaluated after silencing of CDC20 enhancers. Specifically, we tested the recruitment of RNA Pol II phosphorylated at Ser5 (p-Ser5) which is associated with promoter escape to initiate transcription, and of RNA Pol II phosphorylated at Ser2 (p-Ser2) which occurs during pause release leading to elongation through gene bodies (Larochelle et al., 2012). Based on a previous report where YAP was found to modulate promoter-proximal pause release (Galli et al., 2015), we expected reduced levels of p-Ser5 Pol II and increased levels of p-Ser2 pol II in the *CDC20* gene body after YAP5SA expression.

Strikingly, p-Ser5 pol II accumulated at the TSS of CDC20 after YAP5SA expression and this effect was remarkably reduced by silencing of *CDC20* enhancers (Figure 18C). p-Ser2 Pol II enrichment increased in the *CDC20* gene body and at the TES after YAP5SA induction, which was slightly reduced after inhibition of the enhancers (Figure 18C). These results suggest that the inhibition of *CDC20* enhancers decreases the YAP5SA-mediated accumulation of paused Pol II at *CDC20* promoter leading to progression of the transcription, which could also result in reduction of p-Ser2 Pol at gene body and consequently a decrease of transcription elongation as a secondary effect of the reduced initiation, after silencing of *CDC20* enhancers.

In another set of ChIP-qPCR experiments, we tested whether the inhibition of *CDC20* enhancers affects the histone modifications associated with gene activation at the *CDC20* promoter. To do so we tested the acetylation of H3K9, H3K27, H4 and H2A.Z. Acetylated histones showed a bimodal distribution around the TSS and importantly the enrichment of H3K9, H4 and H2A.Z increased after YAP5SA expression. Interestingly the inhibition of *CDC20* enhancers reduced only the acetylation of H3K9, indicating that this histone modification could be dependent on enhancers regulation, while acetylation of H2A.Z and H4 was not prevented by silencing of *CDC20* enhancers. Intriguingly the H3K27 acetylation increased after the disruption of enhancers (Figure 18D).

Taken together, the results of this thesis indicate that YAP5SA-mediated activation of *CDC20* enhancers has effects on RNA Pol II occupancy and B-MYB binding to the promoter, and that it has a more direct impact on H3K9-acetylation at the CDC20 promoter than on acetylation of H4, H2A.Z and H3K27.

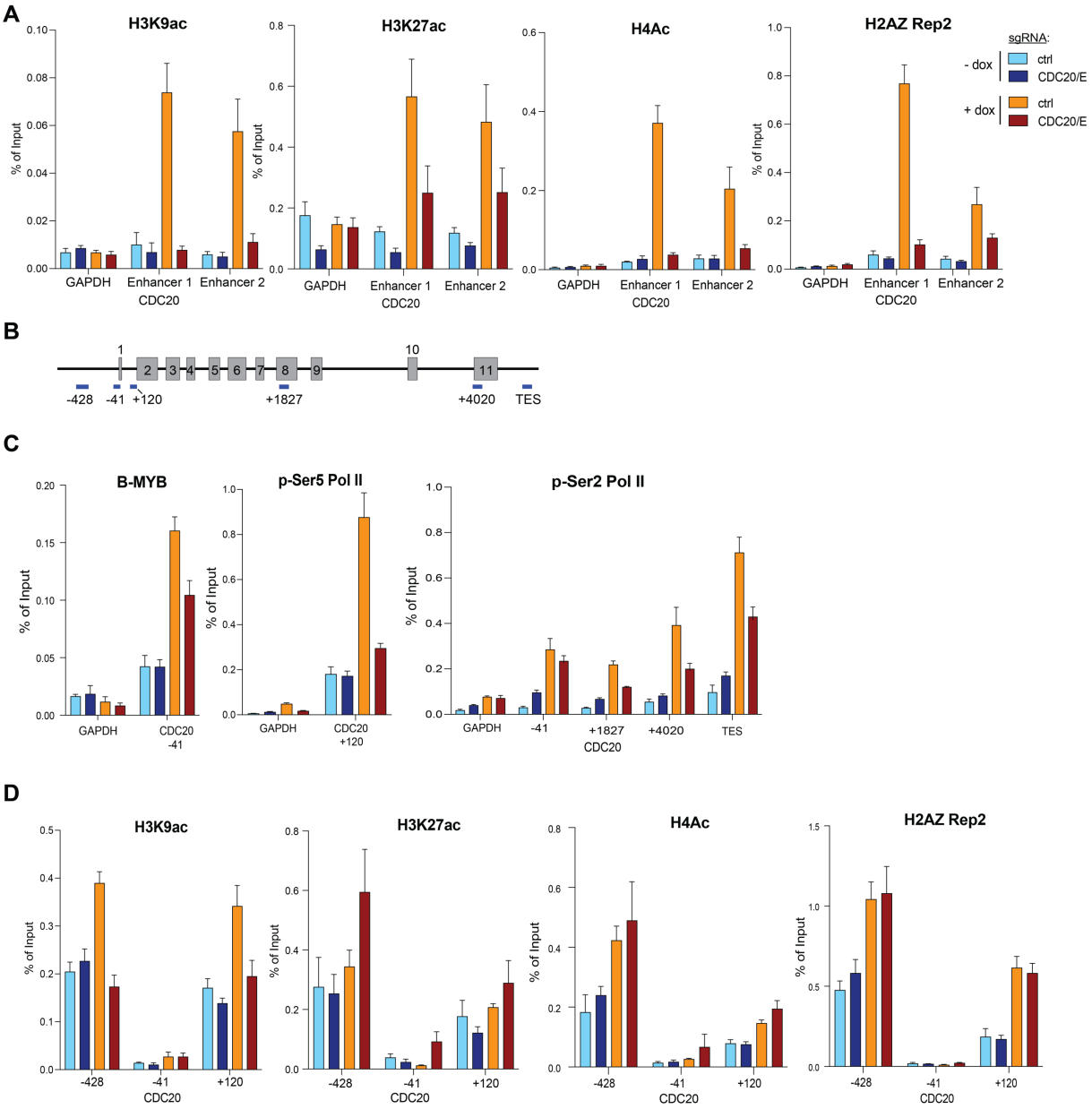

Figure 18. Enhancers of CDC20 facilitate histone modifications and transcription

(A) ChIP-qPCR for H3K9Ac, H3K27Ac, H4Ac and H2A.Zac at the two CDC20 enhancers in MCF10A-YAP5SA-Cas9-KRAB cells before and after YAP5SA induction with doxycycline and with either a control guide RNA (ctrl) or enhancer-specific guide RNAs (CDC20 E) showing that targeted CRISPRi interferes with enhancer activation by YAP5SA. B) Scheme of the CDC20 locus and the position of amplicons used for ChIP-qPCR. C,D) ChIP-qPCRs of cells treated as in A), regions analyzed at CDC20 indicated locus for C), B-MYB, p-Ser5 Pol ll and p-Ser2 Pol ll and for D) H3K9Ac, H3K27Ac, H4Ac and H2A.Zac antibodies, *GAPDHS* promoter served as a negative control. Mean and SDs of technical replicates of a representative experiment are shown (n=2).

3.8 Overexpression of YAP leads to increased initiation and elongation of transcription of MMB target genes

To gain further insights into the role of YAP in leading changes in Pol II occupancy in a larger set of genes, genome-wide occupancy of p-Ser5 Pol II, p-Ser2 Pol II, and unphosphorylated Pol II were measured by ChIP-seq. Consistent with our last findings, p-Ser5 Pol II enrichment was increased at TSS proximal regions of MMB-YAP target genes after YAP5SA expression. ChIP-seq signal for p-Ser2 Pol II showed also higher levels in gene bodies and especially in TES of MMB target genes after YAP5SA expression, correlating with previous results where YAP leads to pause-release (Galli et al., 2015). Levels of unphosphorylated Pol II were also increased at MMB targets by YAP5SA but less than p-Ser5 Pol II and p-Ser2 Pol II (Figure 19A). By plotting the fold enrichment of unphosphorylated Pol II, p-Ser5 Pol II and p-Ser2 Pol II we found that p-Ser5 presented the biggest and significative increase in cells expressing YAP5SA (Figure 19B). Those findings are represented by genome browser tracks of selected MMB target gene examples as *CCNF, TOP2A, NEK2* and *CDC20* (Figure 19C).

In summary, these findings indicate that YAP5SA expression promotes the initiation of transcription of MMB-YAP target genes, which extends and complements previous studies where YAP was mainly associated with regulation of pause-release and transcriptional elongation.

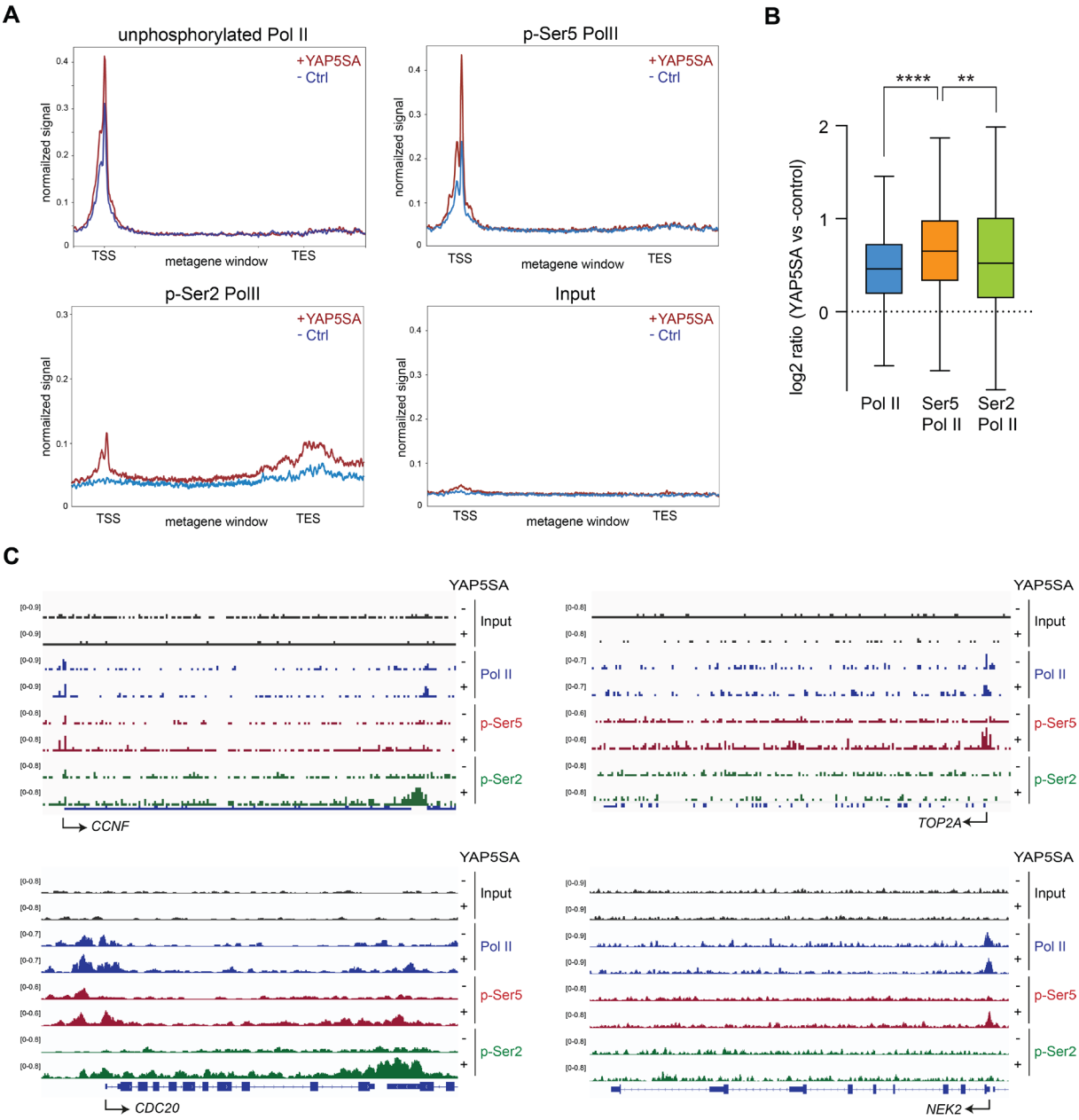

Figure 19. Overexpression of YAP leads to increased initiation and elongation of transcription of MMB target genes.

A) Metagene plots of unphosphorylated RNA Pol II and RNA Pol II phosphorylated at serin 5 (p-Ser5 Pol ll), serine 2 (p-Ser2 Pol ll), and unphosphorylated Pol ll, MCF10A/YAP5SA cells treated with doxycycline to induce YAP5SA expression (+YAP5SA) and control cells (-Ctrl) from TSS to TES of MMB-regulated genes. B) Boxplot representing the fold enrichment at MMB-regulated genes of unphosphorylated Pol II , Ser5 Pol II in a window of -500bp to +500bp from TSS, and Ser2 Pol II in a window of +500 to +3000 bp in cells expressing YAP5SA. Student's t-test. * = p<0.05, ** = p<0.01, *** = p<0.001, ns = not significant. C) Genome browser ChIP-seq tracks of *CCNF, TOP2A, NEK2,* and *CDC20* demonstrating enhanced phosphorylation of Ser5 Pol II at the TSS after induction of YAP5SA by doxycycline (+), untreated cells are shown as (-).

In order to address the relevance of the direct interaction between YAP and B-MYB in YAP5SA-induced transcriptional initiation and elongation of MMB target genes we used the already described MY-COMP (for B-MYB-YAP competition), a fragment of B-MYB that interferes within YAP and B-MYB binding. We used a previously characterized MCF10A cell line which co-expresses tamoxifen-inducible ER-YAP2SA and doxycycline-inducible MY-COMP (MCF10A-ER-YAP2SA/MY-COMP cells) (Figure 20A) (Grundl et al., 2020). ChIP-qPCR assays using antibodies specific for p-Ser5 Pol II and p-Ser2 Pol II revealed that YAP2SA led to increased RNA Pol II phosphorylated at Ser5 at the TSS of selected YAP/ MMB-target genes, which is consistent with our previous finding (Figure 19C). Importantly, when MY-COMP was co-expressed the induced pSer5 Pol II was prevented (Figure 20B). Moreover, MY-COMP induction also prevented the YAP2SA-mediated increase of p-Ser2 Pol II towards the CDC20 gene body (Figure 20C).

In summary, our results demonstrate that the YAP and MMB interaction is also necessary for the YAP-mediated increased Ser5 phosphorylation of Pol II at the TSS and for the Ser2 phosphorylation of Pol II at gene body of *CDC20*, which leads to increased initiation and the consequently boosted elongation of transcription of these genes resulting in hyperactivation of MMB-target genes.

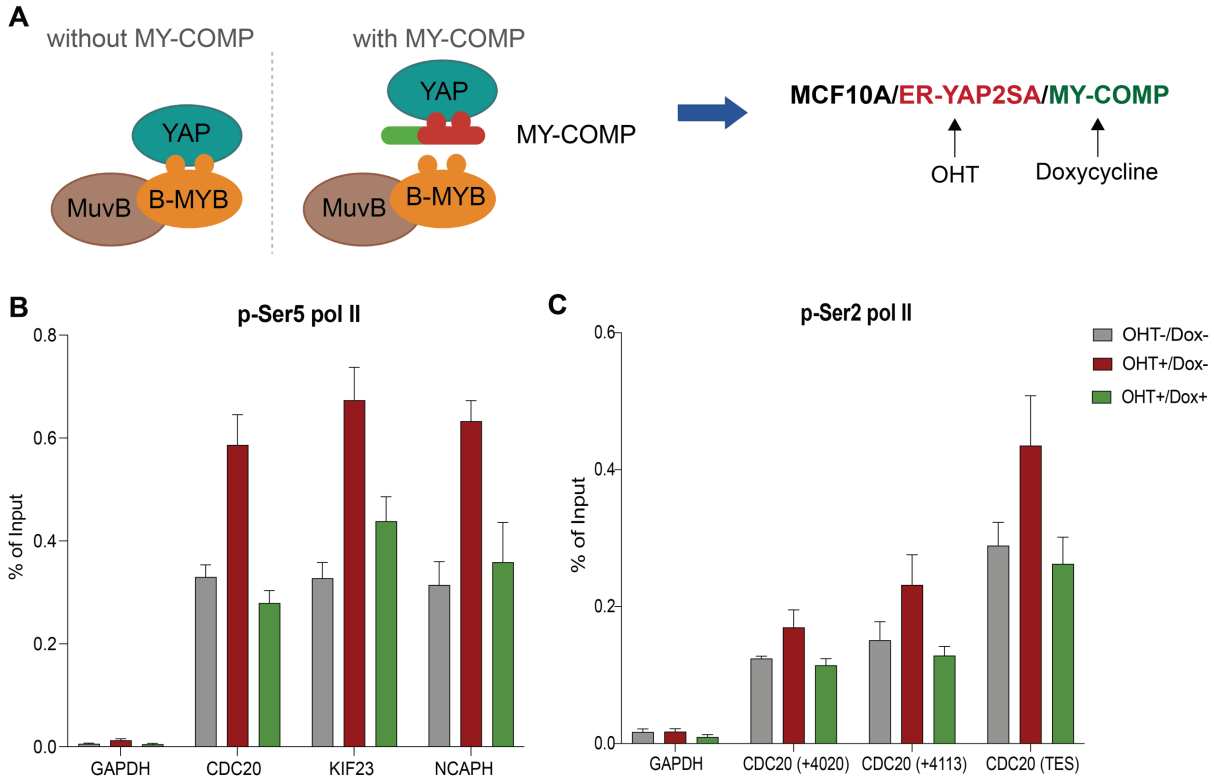

Figure 20. Interaction of YAP and MMB is necessary for YAP leaded initiation and elongation of transcription.

A) Scheme depicting the disruption of the YAP-B-MYB interaction by MY-COMP and the necessary treatments in MCF10A/ER-YAP2SA/MY-COMP cells to induce YAP and MY-COMP. B,C) ChIP-qPCR analysis for B) p-Ser5 Pol II at TSS of selected MMB target genes, and for C) p-Ser2 Pol II at gene body and TES of CDC20. MCF10A-ER-YAP2SA-MY-COMP cells were treated with 4-OHT and doxycycline as indicated. Mean and SDs of technical replicates of a representative experiment are shown (n=2).

3.9 YAP5SA promotes the binding of CDK7 to promoters of MMB target genes, which is prevented after the silencing of enhancers, particularly in CDC20

As previously described, the induction of YAP increased phosphorylation of RNA Pol II at Ser5 at TSS of MMB-target genes. This led to the assumption that the main kinases that phosphorylate RNA Pol II (CDK7, CDK8 and CDK9) may be involved in the YAP-mediated increase of initiation and elongation of transcription shown in section 3.8. We used the MCF10A-cells expressing ER-YAP2SA, to induce fast activation of YAP by 4-OHT treatment. Induction of ER-YAP2SA at different time points is shown for YAP and some YAP-MMB target genes (**Figure 21A**). Expression of YAP-MMB target genes increased as expected after YAP2SA induction and this effect was reduced by the inhibition of CDK7 and CDK9 using well-established kinase inhibitors. In contrast, inhibition of CDK8 had little effect on gene expression (**Figure 21B**). The effect of

CDK7 inhibition has a larger impact on basal and YAP-induced expression of selected YAP-MMB target genes (Figure 21B).

To further evaluate the inhibition of CDK7,8 & 9 in a shorter treatment that could exclude indirect effects in cell cycle progression due to CDK inhibition, we used the ATR-CHK1 pathway inhibition in MDA-MB231 cells as a tool to achieve rapid activation of MMB-target genes, in a similar experiment as showed in (Figure 12A). As it was shown previously in Figure 12A,B inhibition of CHK1 in MDA-MB-231 cells released from G1/S block promoted hyperactivation of MMB-target genes after release. Notably, inhibition of CDK7 and CDK9 but not of CDK8, abolished CHK1i-mediated activation of MMB-target genes. (Figure 21C,D). Inhibition of CDK9 reduced induction of CDC20 and AURKA but had less effect on TOP2A induction. Based on a report where CDK7 stabilizes YAP (Cho et al., 2020), we analyzed YAP protein expression but found that YAP expression levels were not affected by inhibition of CDK7 or CHK1 (Figure 21E).

Together, these results suggest that CDK7 and CDK9 could be involved in the increased initiation and elongation of transcription mediated by YAP. We focus our studies on the role of CDK7 on YAP-mediated regulation of MMB target genes and we also confirmed that CDK7 inhibition does not lead to YAP-reduced levels which could otherwise account for the lower induction of MMB target genes after CDK7 inhibition.

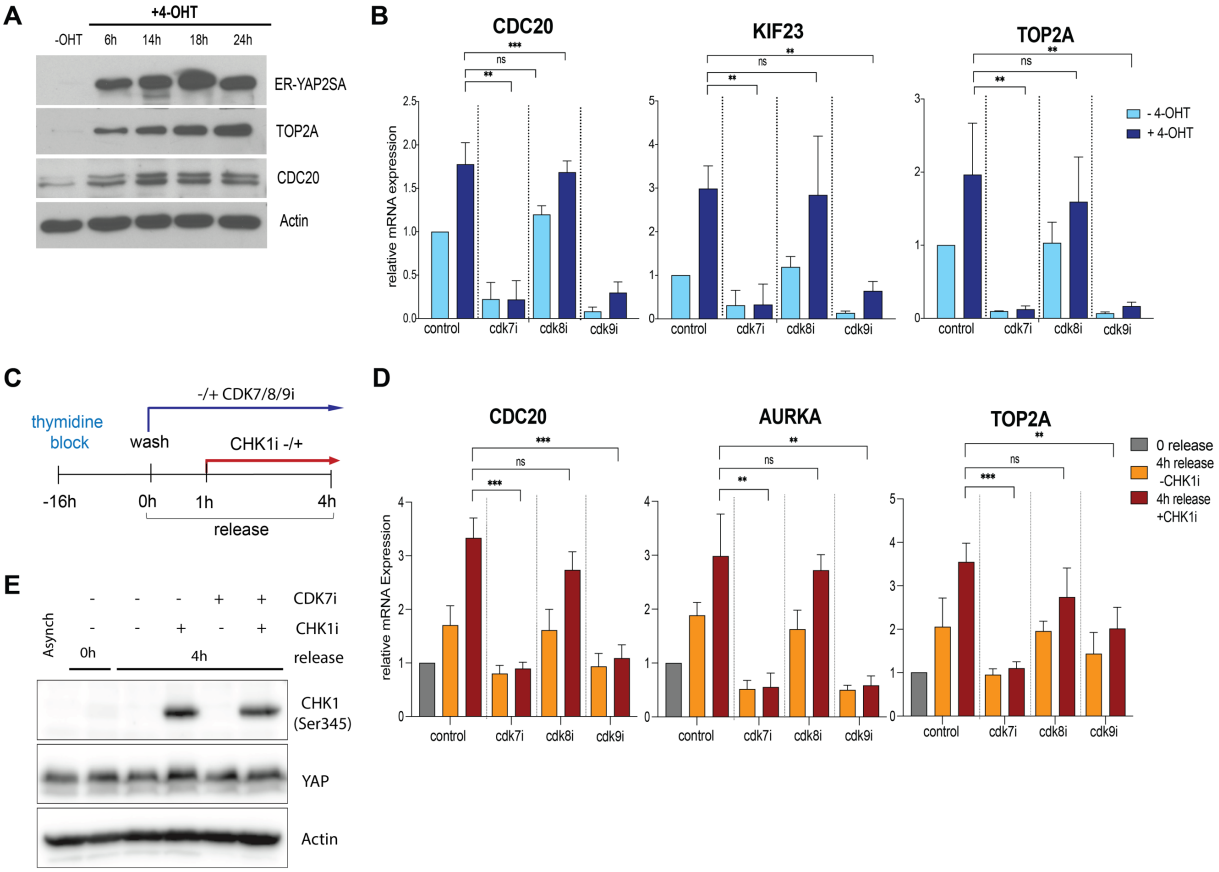

Figure 21. Inhibition of CDK7 and CDK9 decreases activation of MMB target genes

A) Lysates of MCF10A-ER-YAP2SA cells treated with 4-OHT to induce ER-YAP2SA, at the indicated time points. The expression of the indicated proteins was analyzed by immunoblotting and Actin served as a loading control. B) MCF10A-ER-YAP2SA cells were treated with or without 4-OHT for 14 hours in the presence of the indicated CDKs inhibitors or with DMSO (control). The expression of *CDC20*, *KIF23,* and *TOP2A* relative to *GAPDH* was analyzed by RT-qPCR. Error bars: SD of three independent replicates. C) scheme presenting the experiment where MDA-MB-231 were released from a single thymidine block in the presence or absence of CDK inhibitors. One hour later cells were treated or not with CHK1i. After 4 hours of release, RNA was isolated and expression of *CDC20*, *AURKA,* and *TOP2A* relative to *GAPDH* was analyzed by RT-qPCR. Error bars: SD of three independent replicates. E) Lysates of cells treated as described in C (just with CDK7i) for the indicated proteins were analyzed by immunoblotting, Actin served as a loading control. Student's t-test. * = p<0.05, ** = p<0.01, *** = p<0.001, ns = not significant. A) was done by Doerthe Gertzman (M.Sc student).

3.10 Overexpression of YAP enhances the proximity of CDK7 and LIN9

Based on the effect of YAP overexpression on increased Pol II Ser5 phosphorylation by CDK7 and consequently the enhanced initiation of transcription, we evaluated protein interaction and proximity. Specifically, to address whether CDK7 interacts with YAP and with the MMB complex, co-immunoprecipitation experiments were performed in MCF10A-YAP5SA cells with and without doxycycline treatment. This experiment showed no detectable biochemical

interaction between YAP and CDK7 and between CDK7 and B-MYB. XPD was used as a positive control since CDK7 and XPD both are subunits of the TFIIH complex (Rimel & Taatjes, 2018)(**Figure 22B**). Next, we evaluated protein proximity through proximity ligation assays (PLA) using antibodies directed to CDK7 and to the LIN9 subunit of MMB and to CDK7 and YAP. Close proximity was found between CDK7 and LIN9 after YAP5SA expression, indicating that YAP enhances the proximity of CDK7 to LIN9 (**Figure 22 C,D**). Additionally, CDK7 and YAP proximity was also induced by YAP overexpression consistent with the fact that more nuclear YAP is expressed and could be in proximity to CDK7 and also promotes the proximity of CDK7 to the MMB complex.

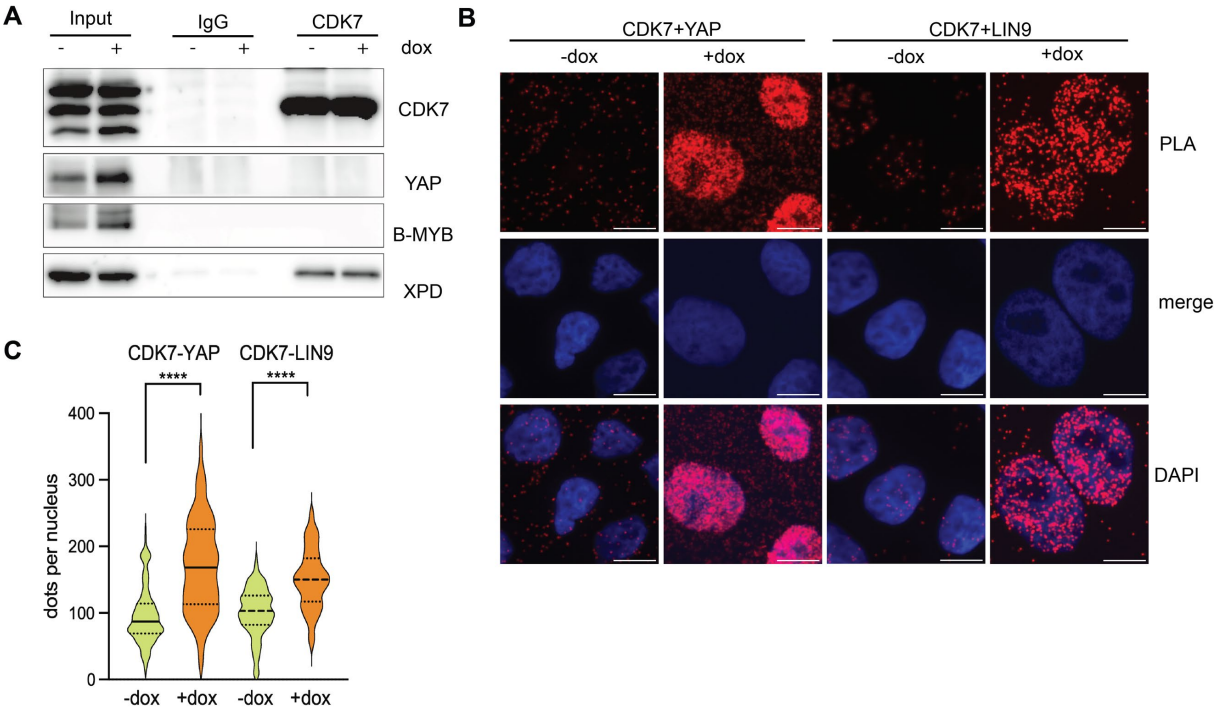

Figure 22. YAP5SA expression enhances the proximity of CDK7 with LIN9 and YAP

A) Nuclear lysates of MCF10A-YAP5SA treated or not with doxycycline for 48h were subjected to immunoprecipitation with CDK7 antibody. Proteins were separated by SDS-PAGE and detected by immunoblotting using the indicated antibodies. XPD was used as a positive control of interaction with CDK7. Immunoprecipitations with nonspecific IgG served as a negative control. 3% of the lysates were immunoblotted as input control. B) Example photos of proximity ligation assays (PLA) of YAP and CDK7 and pf LIN9 and CDK7 in MCF10-YAP5SA cells treated with or without doxycycline. Scale Bar 50um. C) Quantification of PLA (n=2 independent experiments). Student's t-test. * = $p<0.05$, ** = $p<0.01$, *** = $p<0.001$, ns = not significant. A) was done by Julius Thomas (M.Sc student).

3.11 YAP5SA promotes the binding of CDK7 to promoters of MMB target genes

To determine whether YAP5SA expression influences CDK7 promoter binding, ChIP-qPCR assays were performed. CDK7 recruitment to promoters of selected MMB target genes was increased after YAP5SA expression (Figure 23A). As a marked increased binding of CDK7 to the promoter of *CDC20* was identified, we asked if the regulation of *CDC20* enhancers may have a role in CDK7 promoter binding. Interestingly, YAP5SA-induced binding of CDK7 to the *CDC20* promoter was prevented by CRISPRi-mediated silencing of the enhancers which is similar to the binding of p-Ser5 Pol ll at this locus (Figure 23B, Figure 18C). Taken together these data suggest a role for the YAP-bound enhancers in the recruitment of CDK7 to MMB-regulated promoters which could lead to the subsequent phosphorylation of Pol II at Ser5. Finally, we found that B-MYB and YAP interaction was relevant for the binding of CDK7 to promoters of additional MMB target genes (Figure 23C), because after the disruption of the interaction of YAP and B-MYB by the induction of MY-COMP with doxycycline, we observed reduction on the chromatin binding of CDK7 to promoter of G2/M genes, indicating that the interaction between YAP and B-MYB is necessary to induce CDK7 chromatin binding (Figure 23C).

In summary, here we demonstrate that YAP5SA expression increases the binding of CDK7 to promoters of MMB target genes, which is in concordance with evidenced increase in phosphorylation of RNA Pol II at Ser5 as a known function of CDK7. Interestingly, the interaction of YAP and MMB complex seems to play a role in the recruitment of CDK7 to promoters by YAP5SA.

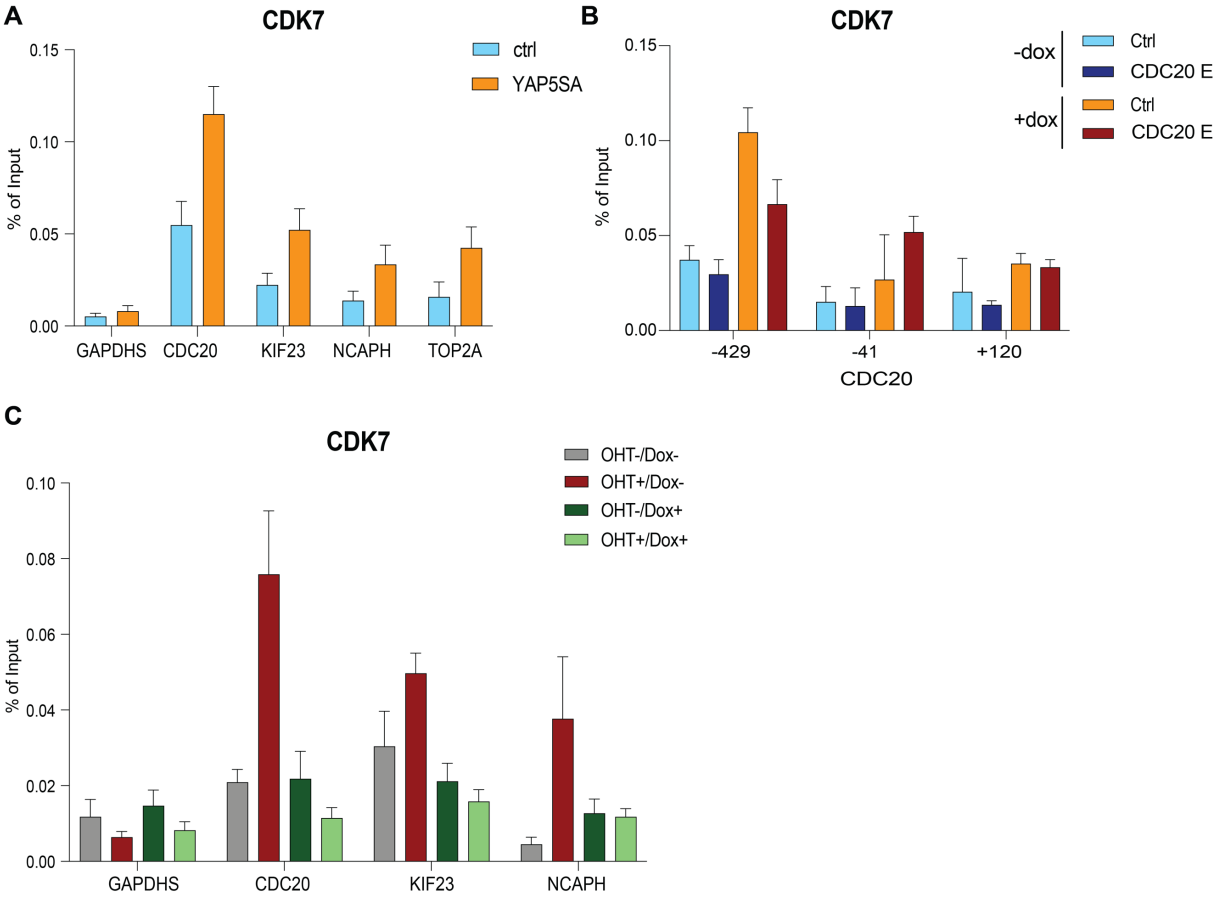

Figure 23. CDK7 chromatin binding is reduced after CDC20 enhancers silencing and after interfering with the B-MYB and YAP interaction

A) MCF10A-YAP5SA cells before (Ctrl) and after YAP5SA induction (YAP5SA). ChIP-qPCR for CDK7 at promoter regions of indicated MMB target genes. B) ChIP-qPCRs for CDK7 at CDC20 indicated locus as in Figure 13B for CDK7, before and after doxycycline treatment in MCF10A-YAP5SA-Cas9-KRAB cells expressing either a control guide RNA (Ctrl) or enhancer-specific guide RNAs (CDC20 E). C) ChIP-qPCR analysis for CDK7 at promoters of selected MMB target genes in MCF10A-ER-YAP2SA-MY-COMP cells that were treated with 4-OHT and doxycycline as indicated. Mean and SDs of technical replicates of a representative experiment are shown (n=2). GAPDHS promoter served as a negative control.

3.12 YAP5SA induces loss of chromatin accessibility at ΔNp63-bound regions and mediates p63 downregulation

As described above, the induction of YAP5SA also led to the closing of chromatin regions that contain binding motifs of the p53 family. Because it has been reported that MCF10A cells express p53 and p63 but not p73, and p53 is expressed at low levels in unstressed cells (Carroll et al., 2006; Uzunbas et al., 2019; Yoh et al., 2016) this thesis focuses on p63 and its role in the closing of chromatin at its bound regions induced by YAP5SA expression. First, it was of our interest to evaluate if loss of chromatin binding by p63 leads to the reduced chromatin

accessibility following YAP5SA expression. By ChIP-seq, 1213 binding sites for p63 were found in the control condition (q-value < 0.01), and a strong overall reduction in p63 chromatin binding sites was detected after the induction of YAP5SA with doxycycline in comparison to the control untreated cells (Figure 24A). By comparison with ATAC-seq, about 50% of accessible p63-binding regions became inaccessible after YAP5SA expression (Figure 24B). Thus, reduced chromatin accessibility is correlated with reduction of p63 chromatin binding, suggesting that p63 binding is necessary to keep the chromatin accessible (Figure 24C).

Previous ChIP-seq data from Pattschull et al., 2019 were used to analyze histone modifications of MCF10A-YAP5SA expressing cells and control cells, in order to determine if YAP5SA expression correlates with chromatin status changes at p63 binding sites. Interestingly, a decrease in H3K27 acetylation was found at p63 binding sites, suggesting a reduced enhancer activity upon YAP5SA induction. Effectively the H3K4me1 markers probed that the regions where the p63 binding was reduced after YAP5SA expression corresponded to enhancers and as expected the histone modification for active promoters H3K4me3 was not highly enriched in both conditions (Figure 24D). Together, our results indicate that YAP leads to the loss of p63 binding which could consequently explain the chromatin closing indicating that p63 binding is required to maintain the accessibility of chromatin at its binding regions. Additionally, the newly inaccessible regions correspond mainly to enhancers of p63 target genes that after YAP5SA expression also became inactive as evidenced by decreased H3K27 acetylation (Figure 24D).

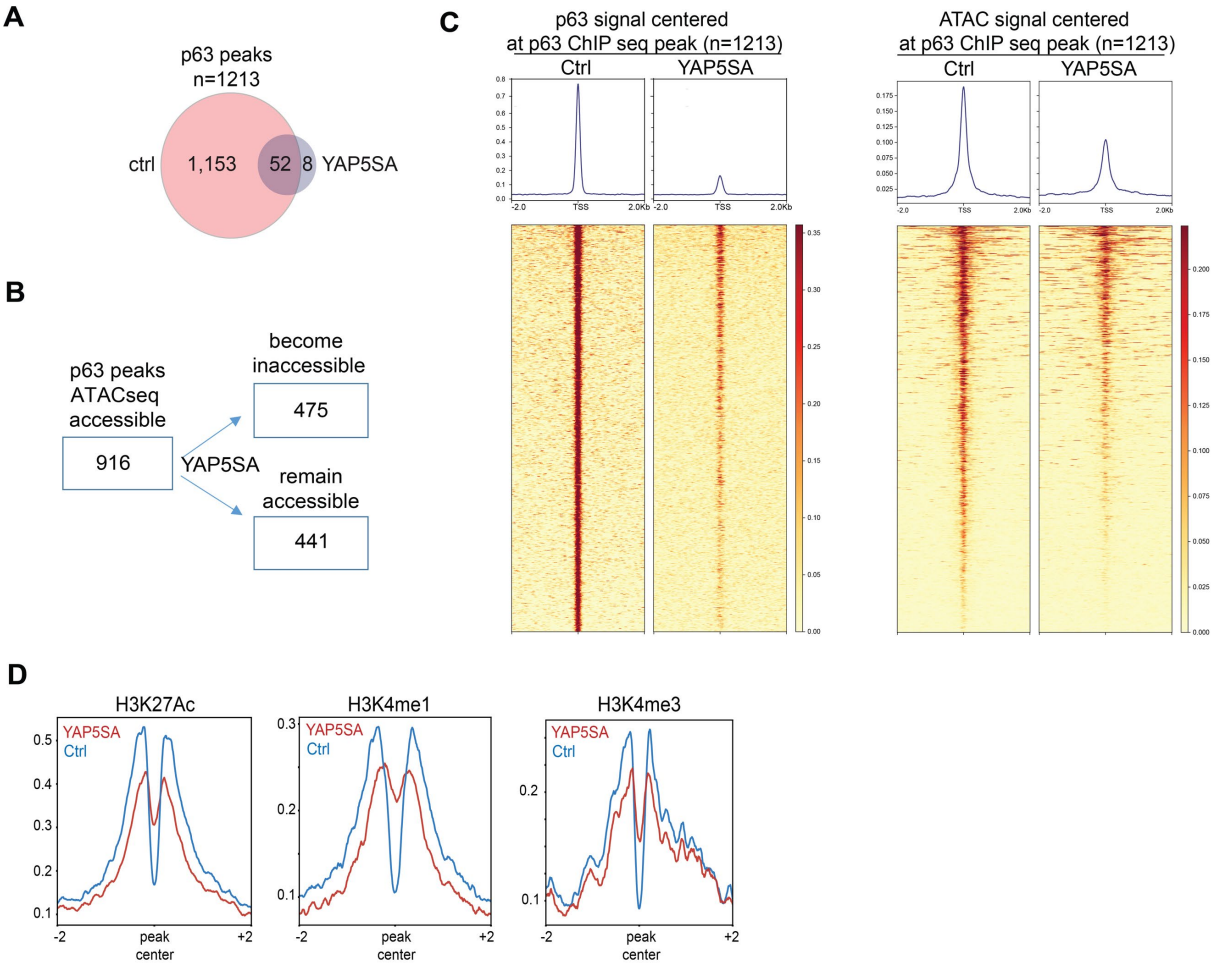

Figure 24. YAP5SA overexpression induces reduction on p63 binding

A) Summary of genome-wide localization depicting p63 binding sites determined by ChIP-seq using a p63 antibody in MCF10A cells before (Ctrl) and after YAP5SA expression (YAP5SA). B) the accessibility of p63 binding peaks was compared with ATAC-seq. C) Heatmaps showing p63 enrichment and chromatin accessibility at p63 peaks before and after YAP5SA expression in a window of -2kb to +2kb centered on the middle of the peak. D) Line plots showing enrichment of the H3K27Ac, H3K4me1, and H3K4me3 signal at p63 binding sites in MCF10A cells control and expressing YAP5SA. ChIP-seq data are from Pattschull et al., 2019.

Genome browser tracks for example p63 target genes (*IRF6* and *MINK1*) depict the loss of p63 chromatin binding at its enhancers together with reduced H3K27 acetylation and chromatin closing after YAP5SA expression (**Figure 25A**). Through ChIP-qPCR we corroborate that p63 binding to enhancers of its target genes *IRF6, DLG5, MINK1* and *SYNPO* is lost upon YAP5SA induction (**Figure 25B** & **Figure 24A**). Additionally, RT-qPCR verified that loss of p63 chromatin binding upon YAP5SA expression also led to the downregulation of the corresponding p63 target genes (**Figure 25C**). Importantly, ΔNP63 expression was also highly reduced after YAP5SA expression. *AMOTL2* is a direct target gene of YAP and it was used as a control of YAP5SA

induction and as expected it was strongly overexpressed after doxycycline treatment and YAP5SA induction. In summary, YAP5SA overexpression leads to downregulation of ΔNp63 and as a consequence also to downregulation of ΔNp63 target genes.

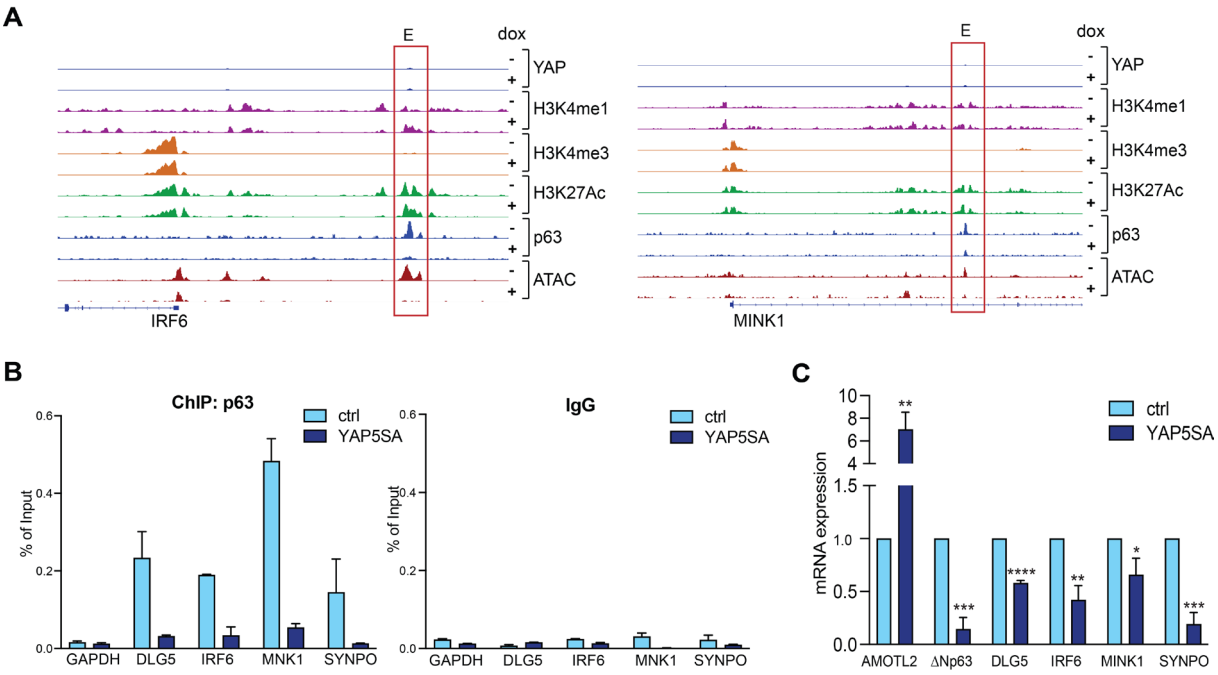

Figure 25. YAP5SA expression mediates the downregulation of p63 genes

A) Genome browser tracks of genome localization of p63 target genes as *IRF6* and *MINK1,* depicting ChIP-seq and ATAC-seq data in MCF10A-YAP5SA cells before (-) and after (+) expression of YAP5SA. B) ChIP-qPCR for p63, showing binding of p63 to enhancers or of? some selected target genes in MCF10A-YAP5SA cells before and after the induction of YAP5SA. Nonspecific immunoglobulin G (IgG) served as a control of enrichment. Mean and SDs of technical replicates of a representative experiment (n=2) C) Expression of *AMOTL2* a YAP target gene, *ΔNp63,* and selected target genes of ΔNp63 were analyzed by RT-qPCR relative to *GAPDH.* Data represent means from biological triplicates, error bars represent SDs (n=3). Student's t-test. * = p<0.05, ** = p<0.01, *** = p<0.001, ns = not significant.

To test if the downregulation of the ΔNp63 mRNA after YAP5SA expression was also evident in protein levels, we performed immunoblots after indicated time points of YAP5SA induction with doxycycline. A strong reduction in the expression of ΔNp63 after doxycycline treatment was found, especially after 24 and 48 hours of treatment (**Figure 26A**). Furthermore, we used MCF10A cells that stably express a hormone inducible ER-YAP2SA fusion protein, to evaluate in another YAP inducible systems the protein expression of ΔNp63 upon YAP2SA induction. Robust downregulation of ΔNp63 was also observed in this cell line after YAP2SA activation through 4-OHT treatment (**Figure 26B**). This confirmed the reduced protein expression of

ΔNp63 by YAP expression. To evaluate if the reduction of ΔNp63 expression could be due to an increased turnover by the proteasome, cells were treated with the proteasome inhibitor MG132. Downregulation of ΔNp63 by YAP was also observed after inhibition of the proteasome by MG132, indicating that the reduction of ΔNp63 expression is not due to proteasomal degradation (**Figure 26C**). As a control, we observed that MG132 treatment stabilized p53, which is known to be regulated by proteasome degradation. As we have observed the decreased protein expression of ΔNp63 after YAP5SA expression we next evaluated the mRNA levels of p63, ΔNp63, p53, and AMOTL1, after treatment with doxycycline at indicated time points. Expression of p63 and the most abundant isoform ΔNp63 was severely reduced after 16h of YAP5SA induction in concordance with previous experiments (**Figure 25C**), moreover p53 mRNA expression was slightly reduced (**Figure 26D**). Finally, we tested if the knockdown of YAP/TAZ altered the expression of ΔNp63. It was found that co-depletion of YAP and TAZ led to upregulation of *ΔNp63* and its target gene *IRF6* (**Figure 26E**).

Collectively, our results revealed that YAP overexpression leads to a reduction of ΔNp63 protein levels. Conversely, we also evidenced that the depletion of YAP led to upregulation of ΔNp63 expression showing that YAP overexpression is necessary to mediate ΔNp63 depletion.

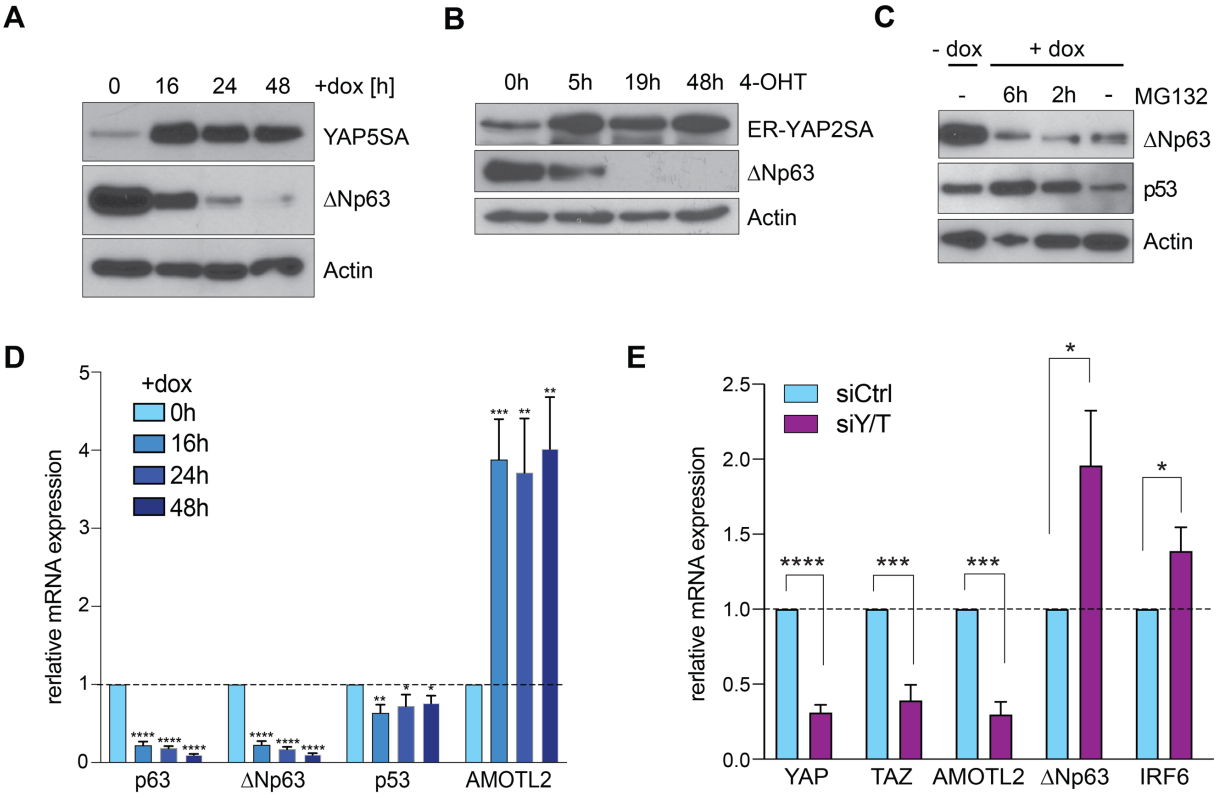

Figure 26. YAP5SA expression leads to downregulation of ΔNp63 and its target genes
MCF10-YAP5SA cells were untreated (-dox) or treated with doxycycline at the indicated time points to induce expression of YAP5SA. A) Expression of YAP and ΔNp63 was evaluated by immunoblotting. Actin served as a loading control. B) MCF10A-ER-YAP2SA cells were untreated (-OHT) or treated with OHT to activate ER-YAP2SA for the indicated time points. The expression of YAP and ΔNp63 was analyzed by immunoblotting. Actin served as a loading control. C) MCF10A-YAP5SA cells were untreated or treated with doxycycline to induce YAP5SA and simultaneously treated with the proteasome-inhibitor MG132. The expression of the indicated proteins was analyzed by immunoblotting. Actin served as a loading control. D) RT-qPCR of MCF10A-YAP5SA cells before and after YAP5SA induction, at the indicated time points. The expression of the indicated genes was analyzed relative to *GAPDH.* Data presented as means from biological triplicates, error bars represent SDs (n=3) E) MCF10A-YAP5SA cells were transfected with a control siRNA (siCtrl) or with siRNAs specific for YAP and TAZ (Y/T). The expression of the indicated genes was analyzed by RT-qPCR. Data presented as means from biological triplicates, error bars represent SDs (n=3). Student's t-test. * = p<0.05, ** = p<0.01, *** = p<0.001, ns = not significant. A,B,C,D) Quantification was done by Magdalena Vogel (B.Sc. student).

3.13 Downregulation of p63 contributes to the oncogenic activities of YAP

To gain further insights into the role of ΔNp63 downregulation mediated by YAP overexpression, we generated a cell line where the expression of ΔNp63 was induced by a tet-inducible system when cells were treated with doxycycline (**Figure 27A**). Simultaneous overexpression of YAP and ΔNp63 after doxycycline treatment was evidenced, and different concentrations of doxycycline were tested to achieve levels of YAP5SA and ΔNp63 that are not excessively high in comparison to endogenous expression (**Figure 27B**) The concentration of doxycycline chosen for further experiments was 0.1 μg/mL. These levels result in moderate ΔN63 expression in MCF10A/YAP5SA/ΔN63 cells. In MCF10A/YAP5SA cells the selected concentration leads to YAP induction and ΔNp63 downregulation (**Figure 27C**). Importantly, restoring ΔNp63 expression reverts the downregulation of ΔNp63 target genes by YAP5SA induction for most of the studied p63 target genes: *DLG5, IRF6, MINK1*, and *SYNPO* (**Figure 27D**).

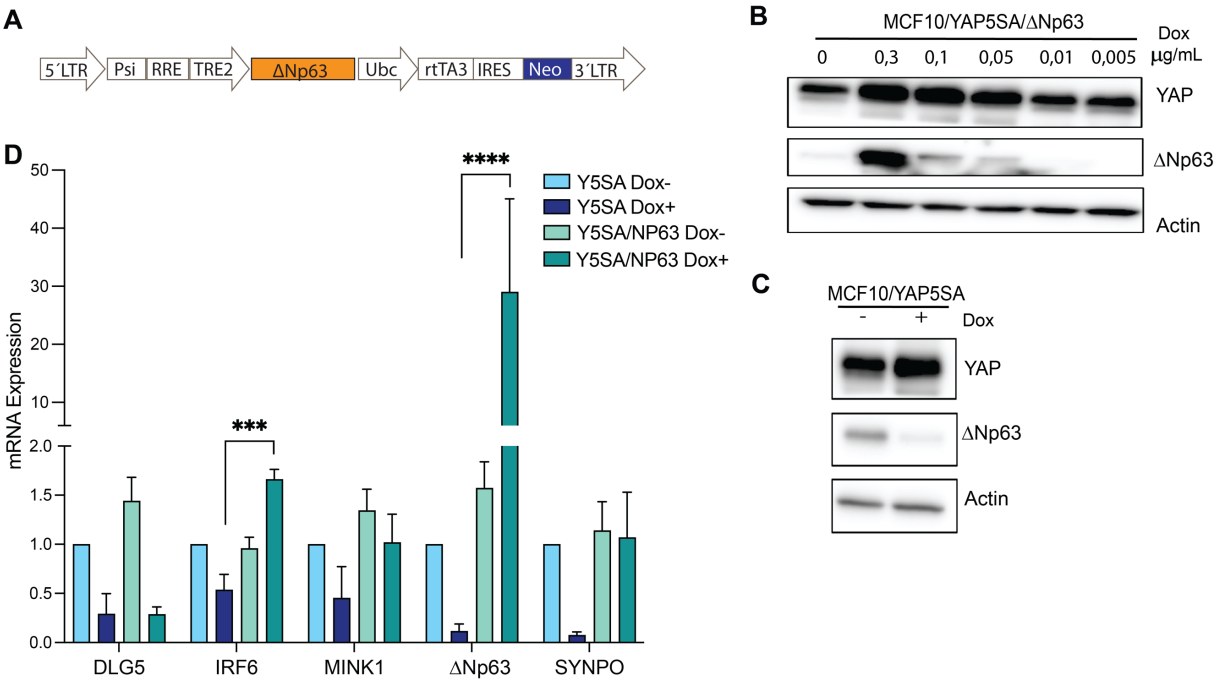

Figure 27. Lentiviral restoration of ΔNp63 expression

A) Scheme of pIndu20 construct to lead the doxycycline-inducible overexpression of ΔNp63. B) Lysates of MCF10A/YAP5SA and MCF10A/YAP5SA/ΔNp63 cells before and after doxycycline treatment were analyzed by immunoblotting. C) MCF10A/YAP5SA were treated with 0,1 µg/mL to corroborate that at this concentration YAP5SA is induced and ΔNp63 is still downregulated by YAP5SA expression. B,C) Lysates were analyzed by immunoblotting. The expression of YAP and ΔNp63 was analyzed, and Actin served as a loading control D) RT-qPCR of MCF10A-YAP5SA and MCF10A/YAP5SA/ΔNp63 cells before and after doxycycline treatment. The expression of the indicated genes was analyzed relative to *GAPDH.* Data presented as means from biological triplicates, error bars represent SDs (n=3). Data presented as means from biological triplicates, error bars represent SDs (n=3). Student's t-test. * = p<0.05, ** = p<0.01, *** = p<0.001, ns = not significant

To identify if the downregulation of ΔNp63 contributes to the oncogenic activities induced by YAP, we first tested YAP-mediated mammosphere formation in MCF10A cells (Pattschull et al., 2019; Zanconato et al., 2018). We identified that the ectopic expression of ΔNp63 did not reduce the formation of mammospheres (**Figure 28A,B**). Similarly, changes in the cell cycle profile after YAP5SA expression were comparable with the simultaneous induction ΔNp63. Specifically, after YAP5SA induction the fraction of cells in G1 decreased and the fractions of cells in S phase increased, and this effect was not rescued by the expression of ΔNp63 (**Figure 28C,D**).

.

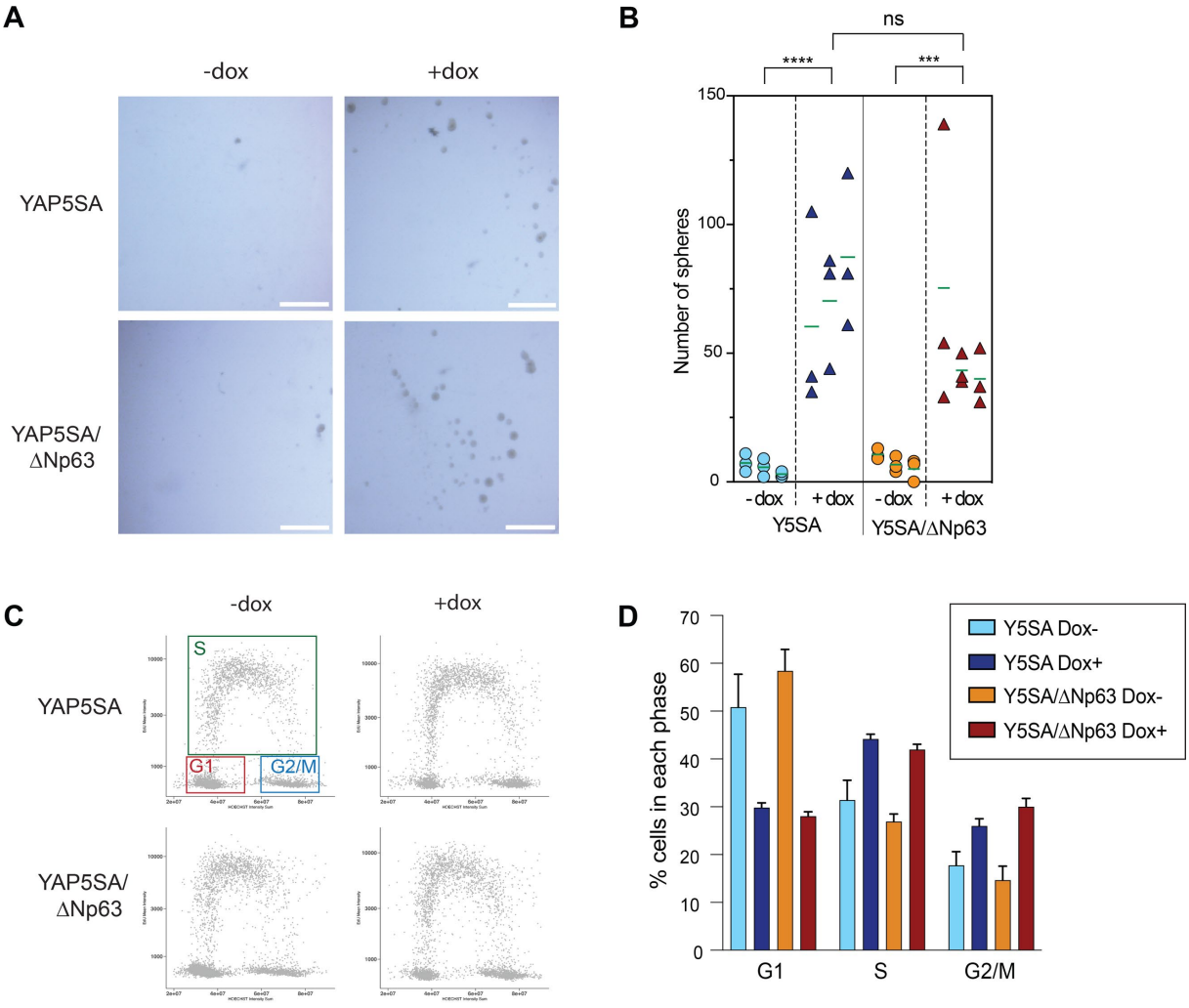

Figure 28. Effects of P63 overexpression on mammosphere formation and cell cycle

A) Representative images of primary mammosphere formation assay in MCF10A-YAP5SA and MCF10-YAP5SA-ΔNp63 treated as described. Scale bar: 80 µm. B) Quantification of spheres, represents the means and SDs of three biological replicates. C) Cell cycle analysis of MCF10A-YAP5SA and MCF10A-YAP5SA-ΔNP63 cells stained with EdU and Hoechst. The percentage of cells in the different phases of the cell cycle is shown. D) Quantification of C. Mean and SDs of two biological replicates of a representative experiment (n=2). Student's t-test. * = p<0.05, ** = p<0.01, *** = p<0.001, ns = not significant.

Through the integration of RNA-seq from Pattschull., et al 2018 and the p63 ChIP-seq data sets, we could identify a set of YAP and p63 co-regulated genes. The p63-bound identified genes are involved in biological processes related to cell-cell communication, cell junction organization, development, and wound healing (**Figure 29A**). Thus, we next investigated the effect of ΔNp63 downregulation on YAP-induced cell migration. We found that the expression of YAP5SA

induces migration of MCF10A cells. However, in the case when ΔNp63 expression was restored the number of migrating cells was strongly reduced (Figure 29B,C).

Thus, the downregulation of p63 is critical for the ability of YAP to enhance cell migration. To evaluate if the depletion of p63 without YAP overexpression was sufficient to induce cell migration of MCF10A cells, p63 was downregulated by RNAi (Figure 29D). Cells depleted of p63 expression were not able to migrate compared to cells transfected with a control siRNA (Figure 29 E,F). Together these results indicate that not only the depletion of ΔNp63 is necessary for migration but also the YAP increased expression.

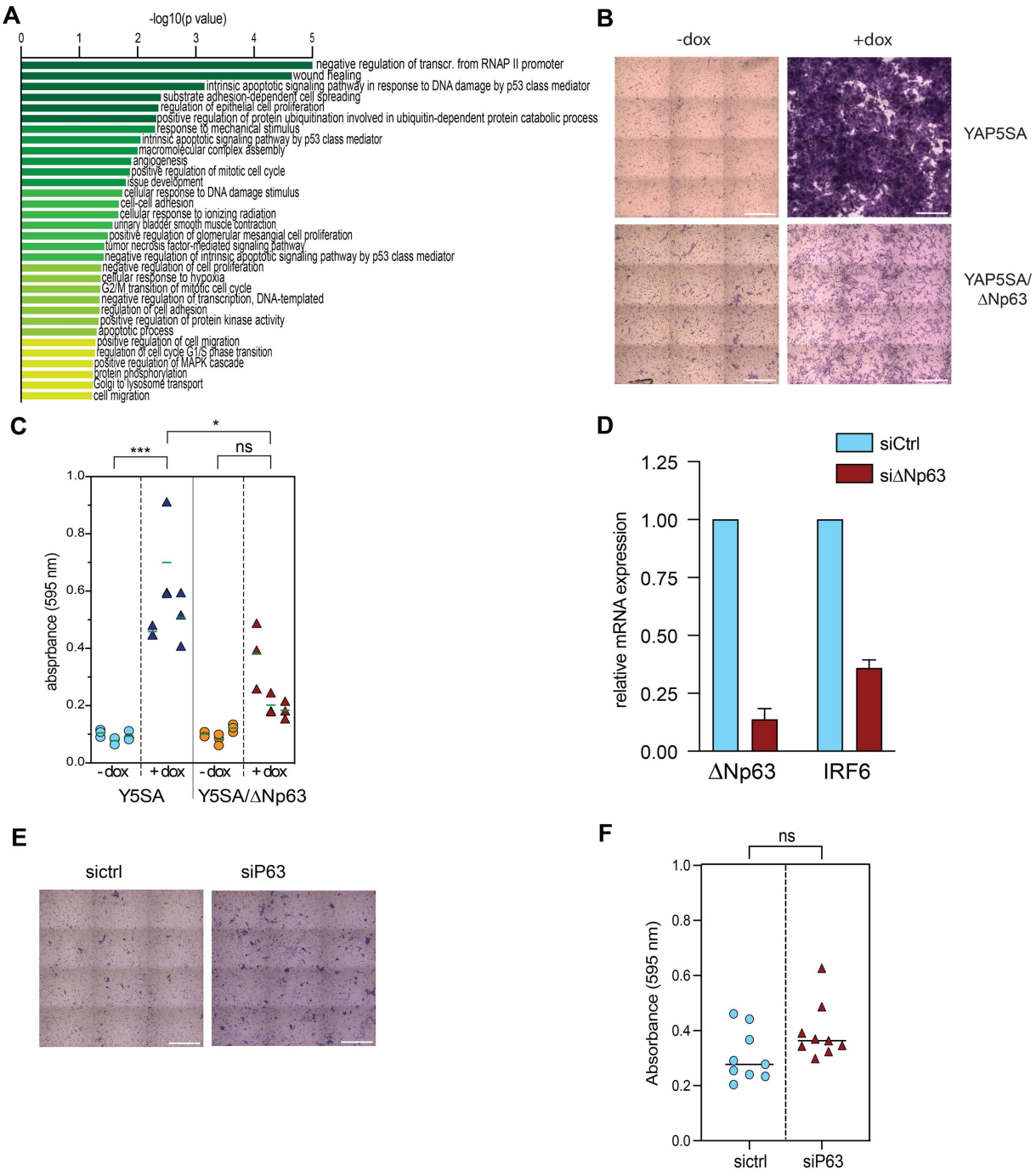

Figure 29. ΔNP63 downregulation mediated by YAP is necessary to promote cell migration

A) Metascape analysis of YAP and p63 co-regulated genes by integration of p63 ChIP-seq and YAP5SA RNA-seq data sets. The identified genes are involved in diverse biological processes. B,C) Transwell migration assay of MCF10A-YAP5SA and MCF10A-YAP5SA-ΔNp63 cells before and after doxycycline treatment, to either induce only YAP5SA or simultaneously induce YAP5SA and ΔNp63. B) Representative images from crystal-violet stained transwell layers Scale bar: 150 µm. C) Crystal violet was extracted and quantified at 595nm. Data represent three biological replicates, each performed in technical replicates. D) MCF10A-YAP5SA cells were transfected with a control siRNA (siCtrl) or with siRNAs specific for ΔNP63. The expression of the indicated genes was analyzed by RT-qPCR relative to *GAPDH*. Data presented as means from technical triplicates of a representative experiment. Error bars

represent SDs (n=3). E,F) Transwell migration assay of MCF10A cells transfected with siCtrl or siΔNP63. E) Representative images from crystal-violet stained transwell layers. Scale bar: 150 µm. F) Crystal violet was extracted and quantified at 595nm. Data represent three biological replicates, each performed in technical replicates. Student's t-test. * = $p<0.05$, ** = $p<0.01$, *** = $p<0.001$, ns = not significant.

4. Discussion

4.1 G2/M gene hyperactivation led by YAP and B-MYB is essential for sensitivity to CHK1i

Since a previous publication by our laboratory described the direct association of YAP with the Myb-MuvB complex MMB (Pattschull et al., 2019), the first part of this thesis addressed the role of YAP in the transcriptional activation of G2/M genes in order to regulate cell cycle progression in unperturbed cells. After inhibiting the interaction of YAP and TEAD, we found that the cell cycle progression of MCF10A cells was diminished especially affecting the S phase and mitosis as well as the expression of G2/M genes. These data are consistent with our previous finding that the overexpression of YAP5SA activates G2/M genes by stimulating the activity of the MMB complex. Mechanistically, by binding to distant enhancers YAP promotes the chromatin association of B-MYB, leading to the formation of the MMB complex and induction of MMB target genes (Pattschull et al., 2019). In addition, YAP also enhances the expression of B-MYB, contributing to an increased rate of mitosis and to hyperproliferation (Grundl et al., 2020; Pattschull et al., 2019; Wei et al., 2019). Data in this thesis suggest that the same mechanism is relevant for cell cycle progression of unperturbed MCF10A cells.

In a previous pan-cancer transcriptome analysis, the expression of components of the DREAM/MMB pathway such as FOXM1 and B-MYB were associated with sensitivity to the CHK1 inhibitor prexasertib (CHK1i) (Blosser et al., 2020), and more recently it was reported that the MMB-FOXM1 complex mediates drug sensitivity to CHK1i by leading to premature mitosis, it has thus been suggested that the dysregulation of the S to M transition is necessary for CHK1 inhibitor sensitivity (Branigan et al., 2021). Here we show that the YAP-TEAD interaction is required for the hyper-induction of mitotic gene expression following the treatment with CHK1i (Figure 12B,D). Thus, YAP appears to be involved in the expression of genes required to lead the premature mitosis induced by CHK1 inhibition. In order to further investigate the role of B-MYB in gene hyperactivation and sensitivity to CHK1, we generated a genetic tool to allow for the rapid degradation of B-MYB In the human beast cancer cell line MDA-MB231 by fusing it to a degradation domain (FKBPV-2A). The advantages of this method are the rapid induced degradation which is not lethal for the cells avoiding the difficulties of other methods such as siRNAs that commonly have off-target effects. Therefore, treatment with dTAG13 triggered the

effective and rapid degradation of B-MYB (Figure 8). Depletion of B-MYB resulted in resistance of MDA-MB231 to CHK1i treatment, confirming that the MMB complex and specifically B-MYB is required for CHK1i cell sensitivity also in these cells. It has been suggested that B-MYB promotes hyperactivation of mitotic genes and premature mitosis in response to CHK1i (Branigan et al., 2021). Similarly, data from Saldivar et al., 2018 suggested a role of B-MYB-FOXM1 in premature cyclin B expression and G2/M progression (Saldivar et al., 2017; Saldivar et al., 2018). However, data in this thesis suggest that B-MYB could lead to sensitivity to CHK1i independent of its role as a transcription factor in G2/M: First, although MMB target genes implicated in mitosis were upregulated after CHK1 inhibition, unexpectedly, after the degradation of B-MYB the expression of its target genes was not affected. Secondly, loss of B-MYB had only relatively mild effects on cell cycle progression and only led to a subtle delay from G2/M into the next cell cycle. Another function of B-MYB that could explain the effect the B-MYB in sensitivity to CHK1i is for instance the described role for B-MYB in maintaining replication fork progression in embryonic stem cells (ESCs) (Lorvellec et al., 2010). More recently it was found that B-MYB promotes the ATM response to replication stress (Blakemore et al., 2021). Thus, future work should aim to identify the molecular mechanisms by which B-MYB leads to CHK1 sensitivity, presumably by regulating intra S phase events.

B-MYB has been associated not only with cell cycle proliferation but also with cell motility. Indeed, the ability of MDA-MB231 cells was reduced after degradation of B-MYB, suggesting a role of B-MYB in cell migration also in the context of breast cancer. Moreover, after performing rescue assays, the ability of cells to migrate was restored. Similar results were found in A549 lung cancer cells expressing high levels of B-MYB, where B-MYB was found to promote cell motility and invasion (Fan et al., 2018). In the same study, a mechanism was suggested in which B-MYB leads to the downregulation of the insulin-like growth factor binding protein 3 (IGFBP3) a mitogenic suppressor in order to mediate cell migration. Low expression of IGFBP3 appears to be necessary for stimulating cell proliferation and migration. Together these findings support the idea that B-MYB expression in cancer promotes migration, however it will still be necessary to evaluate the mechanism of this regulation in breast cancer. Initially, it could be tested if in this cell context (MDA-MB231) the B-MYB-induced migration is due to a negative regulation over IGFBP3 or other related proteins that could lead to activation of ERK and Akt which have crucial roles in cell proliferation, survival, and migration.

In conclusion, we corroborate that B-MYB and YAP play important roles during cell cycle progression of MDA-MB231 and MCF10A cells respectively, whereas premature transcription of G2/M genes was detected to be dependent on YAP upon CHK1i treatment as a part of pharmacological strategies to lead cancer cells into replication catastrophe. In MDA-MB231 cells loss of B-MYB particularly reduced cell migration and confers cell resistance to CHK1 inhibition providing insights into resistance mechanisms.

4.2 YAP induces changes in chromatin accessibility and activity

The second part of this thesis provides new insights into YAP-induced changes in chromatin accessibility which can determine levels of gene expression. Importantly we demonstrated that YAP5SA induced widespread changes in chromatin defined as opening (more accessible chromatin) and closing (inaccessible chromatin). Motif analysis revealed that TEAD and FOS-JUN consensus sites are enriched in opened regions, corresponded to which have been previously identified as YAP partners to mediate its chromatin binding to promote tumor cell proliferation and transformation (He et al., 2021; Liu et al., 2016; Zanconato et al., 2015). Interestingly, mapping of the open regions revealed that they corresponded mainly to enhancers (Figure 14) which is consistent with previous reports which state that YAP regulates transcription through its binding to enhancers (Cebola et al., 2015; Chen & Liu, 2019; Galli et al., 2015). Additionally, to opening of chromatin at enhancers, enhancers activity was also increased by YAP, in concordance with a recent publication were it was found that YAP activation induces the histone H3K27 acetylation and chromatin opening in a liver context (Wu et al., 2022).

On the other hand, our data implicate also that YAP led to chromatin closing, where intriguingly the motif analysis revealed enrichment for consensus sites for the p53 family of transcription factors, suggesting that the p53 family, comprised of the three members p53, p63, and p73, could play a role in shaping the YAP-mediated enhancer landscape. In this thesis, we focus on p63 because p53 is expressed at low levels in unstressed cells and also because MCF10A cells do not express p73 (Carroll et al., 2006; Uzunbas et al., 2019). it was of interest to study the role of YAP on p63 activity and chromatin closing due to the potential of p63 to act as both an oncogene and a tumor suppressor. The results are discussed in detail in the section (4.5).

Our results implicate that YAP overexpression generates changes in chromatin accessibility, supporting the previous idea that YAP can interact with factors of chromatin-remodeling complexes that control the accessibility of target genes such as GAGA, Ncoa6, Mediator, SWI/SNF, TET1 and Nucleosome Remodeling and Deacetylase (NuRD) (Bayarmagnai et al., 2012; Beyer et al., 2013; Kim et al., 2015; Qing et al., 2014; Skibinski et al., 2014; Wu et al., 2022). Genomic studies on cardiomyocytes expressing a constitutively active form of YAP, revealed that YAP induction mediated an increment in chromatin accessibility and gene expression necessary for development and cell proliferation (Monroe et al., 2019). More recently in liver, YAP was found to regulate TET1 to coordinate genome-wide epigenetic reprogramming. In particular, TET1 is a member of the TET family of DNA methyltransferases, which was found to interact with TEAD proteins to elicit regional DNA demethylation, facilitating histone H3K27 acetylation and chromatin opening in YAP target genes to facilitate transcriptional activation (Wu et al., 2022). However, the effects of YAP on chromatin rearrangement as a mechanism to regulate MMB-target genes and its role on cell cycle gene activation remains unclear.

Screening for epigenetic factors may identify additional co-factors and mechanisms for enhancer activation and gene control by YAP. Screening for co-factors could be performed with transposase-accessible chromatin with visualization assay (ATACsee), a recently developed transposase-based imaging technology that through fluorescently labeling of the accessible genome transforms allows the detection of open chromatin sites by microscopy (Chen et al., 2016).

4.3 YAP regulates enhancers to facilitate RNA pol II Ser5 phosphorylation to induce transcription of G2/M genes

The findings of this thesis go beyond previously published data that have shown that YAP regulates gene transcription through binding to distal enhancer regions of cell cycle genes (Cebola et al., 2015; Galli et al., 2015; Lopez-Hernandez et al., 2021; Pattschull et al., 2019; Zanconato et al., 2015) by extending our understanding of how YAP regulated enhancers control transcription. Specifically, by using CRISPR interference we show that induction of CDC20 is prevented upon inhibition of two YAP-bound enhancers confirming the importance of these regulated enhancers in CDC20 gene expression. In addition, by combination with ChIP-

qPCR, we demonstrated that activation of the YAP-bound enhancers promotes the recruitment of RNA Pol II to the TSS of CDC20 and the subsequent phosphorylation of RNA Pol II at Ser5. Efficient phosphorylation of the RNA Pol II at Ser5 at *CDC20* promoter depends on the activation of the two YAP-bound enhancers. At MMB target genes YAP increases the binding of Ser5-phosphorylated Pol II more than that of Ser2-phosphorylated Pol II. Phosphorylation of Pol II at Ser5 is related to promoter escape which is a fundamental step for the initiation of transcription (Core & Adelman, 2019) while the phosphorylation of Pol II at Ser2 through the gene body has been linked to pause release and consequent elongation of transcription (Bowman & Kelly, 2014). Our findings complement previous studies that have associated YAP with RNA Pol II recruitment and control of pause-release stimulating transcription elongation by RNA Pol II through BRD4 and CDK9 (Galli et al., 2015; Zanconato et al., 2018). Transcription pausing guarantees a checkpoint that ensures the release of fully activated and mature Pol II through the promoter region allowing rapid activation of gene expression to keep up with the varied cell stimuli (Adelman et al., 2009; Core & Adelman, 2019). We hypothesize that YAP promotes Pol II ser5 phosphorylation in addition to controlling pause-release in order to balance initiation with elongation as a response to the high demand on mRNA processing due to induced transcription by enhancers hyperactivation.

Another notable finding from this thesis concerns the YAP and MMB interaction promoting the initiation and elongation of transcription (**Figure 20**). Specifically, the disruption of YAP and MMB interaction led to a decrease in enrichment of RNA pol II phosphorylated at Ser5 and Ser2 at promoter regions of YAP and MMB target genes and at CDC20 gene body respectively. Mechanistically YAP and MMB interaction was shown to stimulate B-MYB chromatin binding (Pattschull et al., 2019), indeed we proved that this interaction is also necessary when YAP is overexpressed to activate the transcription machinery specifically during initiation and elongation of transcription by the RNA-pol II.

Remarkably, silencing of CDC20 enhancers in synchronized MCF10A cells that express endogenous levels of YAP did not prevent cell cycle-mediated expression of *CDC20*. This indicated a specific requirement for the YAP-bound enhancers CDC20 under conditions of high levels of YAP expression (**Figure 17F**), where YAP mediates chromatin opening and enhancer activation. Interestingly, it was previously found in YAP endogenous conditions (**Figure 7D**)

that inhibition of YAP-TEAD in synchronized cells decreased the expression of CDC20 when the cells were released, suggesting a role for endogenous YAP in CDC20 expression. Based on recent studies that indicate that enhancer reprogramming promotes adaptation of cancer cells to cellular changes during tumor progression (Fagnocchi et al., 2018), we argue that under these conditions CDC20 expression may be either regulated by other set of enhancers or via promoters bound by transcription factors as the MMB complex in response to cell cycle progression. As YAP has been reported as an oncogene and its overexpression is associated with uncontrolled cell proliferation in many cancer types (Harvey et al., 2013; Yu et al., 2015; Zanconato et al., 2016; Zheng & Pan, 2019), our results point that YAP overexpression hyperactivates enhancers which are the mechanism by which YAP induce rapidly initiation of transcription. The enhancers activated by YAP might extend to a cancer context in light of the high overexpression of YAP in cancer cells. Future work should aim to identify enhancer activity of YAP-regulated enhancers, directly through measurement of eRNAs sequencing, which can be directly analyzed by PRO-sequencing (Dukler et al., 2017). Furthermore, it would be of great interest to test whether the transcription of YAP regulated enhancers RNAs are relevant and affect the transcription of cell cycle genes. Conversely, as YAP bound enhancers have been recently linked to regulation of cellular proliferation (Li et al., 2021), it remains of interest to characterize the specific roles of these YAP-regulated enhancers in cancer development.

4.4 A role for CDK7 in YAP-mediated activation of MMB-target genes

After the chemical inhibition of CDK7, CDK9 and CDK8 we observed that only the inhibition of CDK7 and CDK9 had inhibitory effects on the expression of YAP-MMB target genes. Although CDK8 has been reported as a co-activator of transcription (Alarcon et al., 2009; Donner et al., 2010; Hirst et al., 1999; Knuesel et al., 2009) it seems not to have a role in transcription of YAP-MMB target genes. The role of YAP in controlling transcriptional elongation by CDK9 recruitment has been previously described by (Galli et al., 2015), thus we focused our next set of experiments on exploring the role of CDK7 in YAP-mediated activation of transcription. Specifically, we used THZ1 to perform rapid and effective inhibition of CDK7, which revealed that YAP-induced expression of MMB target genes was abolished, elucidating the dependence on CDK7 activity. The chemical inhibition of CDK7 by THZ1 has been proposed as a promising strategy in cancer therapy (Fisher, 2019; Wang et al., 2015). However, it is of relevance to consider that CDK7 inhibition may have a global effect on gene transcription. And as CDK7 is a

subunit of the CAK complex (Cyclin-dependent kinase (CDK) Activating Kinase) which activates CDK1, CDK2, CDK4 and CDK6 to regulate cell cycle (0), the inhibition of CDK7 may have effects on cell cycle transition (Lolli & Johnson, 2005; Malumbres, 2014). Thus, it remains to be shown whether YAP and CDK7 association specifically regulates MMB target genes during cell cycle progression. Although CDK7 has recently been shown to phosphorylate YAP in the nucleus and prevent its proteasomal degradation (Cho et al., 2020), in our experimental scheme, we did not observe any effect of CDK7 inhibition on YAP protein levels (Figure 21E).

While proteomic analysis and co-immunoprecipitations did not show a direct biochemical interaction between CDK7 and YAP or MMB, PLA assays evidenced increased proximity between CDK7 and MMB when YAP5SA was expressed. We speculate that the interaction of CDK7 with YAP and the MMB complex may be indirect and dynamic. In addition, by ChIP-qPCR assays, we found that YAP stimulated binding of CDK7 to promoters of selected YAP-MMB target genes. Importantly, the binding of CDK7 to CDC20 promoter was reduced after silencing of the two enhancers of CDC20 and after the disruption of the interaction of YAP and MMB through MY-COMP (Figure 23), indicating that both the enhancer activity and the interaction of YAP and MMB are relevant to induce CDK7 binding to promoters of MMB regulated genes. These findings correlate with the previous similar results for RNA-Pol II ser5 enrichment (3.8), suggesting that YAP overexpression mediates the induced initiation of transcription via RNA-Pol II ser5 phosphorylation by CDK7, where CDK7 has a dual function that promotes handoff between initiation and elongation machinery and also triggers pause release (Glover-Cutter et al., 2009; Larochelle et al., 2012). Previous publications have reported that after CDK7 inhibition genes that are controlled by BRD4 bound super-enhancers were downregulated, (Bradner et al., 2017; Wang et al., 2015). Given that BRD4 recruitment by YAP/TAZ to enhancers mediates transcriptional addiction of cancer cells, (Zanconato et al., 2018), future experiments should aim to study the CDK7-YAP axis and its role in transcription regulation by enhancers in a cancer biology context.

4.5 YAP mediates p63 inhibition to enhance oncogenic cellular migration

In contrast to the enhancer activation driven by YAP, we also identified that YAP5SA overexpression results in the closing of chromatin at p63-bound enhancers. This results in loss

of enhancer activity at a subgroup of p63 regulated enhancers; decreased p63 chromatin binding, and consequently reduced gene expression of its target genes. These findings correlate with studies that describe that p63 regulates genes through temporal- and spatial-specific active enhancers (Kouwenhoven et al., 2015). p63 is a member of p53 family of proteins, and it has been described to have redundant functions. For instance, as a tumor suppressor, reduced expression levels of ΔNp63α have been related to epithelial–mesenchymal transition (EMT) and cell motility in cancer; and as an oncogene p63 regulates epithelial cell fate and inhibits the function of p53 (Barbieri & Pietenpol, 2006; Hu et al., 2017; Lindsay et al., 2011; Tucci et al., 2012; Yoh et al., 2016). As described in (1.4.2) p63 can be expressed in two main isoforms, TAp63 and ΔNp63 (Bergholz & Xiao, 2012; Su et al., 2013) and it has previously been related to YAP/TAZ. In mammary epithelial cells, the TAp63 isoform has been associated with TAZ (YAP paralog) upregulation (Su et al., 2017). In other studies overexpression of the isoform ΔNP63, the most abundant transcript, was shown to lead to transcriptional repression of YAP in head and neck squamous cell carcinomas triggering enhanced cell proliferation, cell survival and migration (Ehsanian et al., 2010). In this thesis, I focused on ΔNp63, the most predominant isoform expressed in basal mammary epithelial cells MCF10A cells. Previously, in JHU-22 cells YAP was found to interact with ΔNp63 and regulate its stability, reducing its half-life (Chatterjee et al., 2010). Notably, in MCF10A cells YAP does not lead to proteasomal degradation of ΔNp63 but reduces the transcription of ΔNp63 mRNA. Previous reports have shown that strong repression of ΔNP63 by the PI3K and Ras or Her2 expression led to oncogenic activities as EMT and metastasis (Hu et al., 2017; Yoh et al., 2016). Similarly, in a colorectal adenocarcinoma *cell line (DLD-1*), PI3K/Akt pathway regulated YAP expression inducing cell migration (Takeda et al., 2022). The maintained downregulation of ΔNp63 triggered chromatin closing, and could reflect the sustained loss of chromatin binding of p63 in congruence with previous studies which confirmed that p63 can positively activate its own expression through its direct binding to its intronic enhancers and proximal promoter (Antonini et al., 2006; Antonini et al., 2015). However, the exact mechanism by which YAP suppresses ΔNp63 expression remains unclear and more studies are required to determine it.

Remarkably, after the integration of ChIP-seq and RNA-seq data, we could identify a subset of enhancer-associated genes regulated by ΔNp63 and YAP5SA, which are associated with cell migration and adhesion. This finding correlates with our results that confirm that repression of

ΔNp63 is decisive for YAP-induced cell migration. These results suggest a role of YAP-mediated ΔNp63 depletion and loss of activity and chromatin binding at its regulated enhancers, as positive feedback for its oncogenic induced migration, which may be explained by the downregulation of some of ΔNp63 target genes that are associated with cell adhesion and structural cell integrity. Specifically, one ΔNp63 regulated gene, interferon regulatory factor 6 (IRF6), which as downregulated after YAP5SA overexpression, was found to suppress migration and cell invasion in colorectal cancer cells in a recent study (Tan et al., 2022) Thus, downregulation of IRF6 could contribute to the observed migrating phenotype by YAP. Further investigation will be needed to identify the exact role of p63 antagonizing in YAP-induced cell migration and probably other YAP oncogenic activities in a cancer context.

4.6 Conclusion

YAP has been previously related to gene regulation through its binding to enhancers and super-enhancers (Galli et al., 2015; Pattschull et al., 2019; Zanconato et al., 2015). The results reported here substantially extend the knowledge of the importance of enhancers regulation in gene transcription, by showing that YAP overexpression induces changes in chromatin accessibility at enhancers as a means to induce cellular oncogenic activities. Specifically, the results provide a model in which YAP mediates chromatin accessibility into two states (**Figure 30**). First, YAP induces a state of increased chromatin accessibility mainly at its bound enhancers, where the acetylation of H3K27 is also induced resulting in increased enhancer activity and as established by (Pattschull et al., 2019) YAP binds to B-MYB to promote its binding to promoters, this binding in addition to the enhancer activation seems to be relevant to induce the CDK7 chromatin binding and the consequent phosphorylation of the RNA pol II at Ser5 to stimulate initiation and later the elongation of transcription of G2/M target genes to finally induce the progression of the cell cycle through G2/M phases (**Figure 30**, left). Second, YAP overexpression also leads to a state of decreased chromatin accessibility mainly at ΔNp63 binding sites, (**Figure 30**, right). ΔNp63 chromatin binding is reduced as a consequence of decreased protein and mRNA levels causing downregulation of ΔNp63 target genes. The depletion of ΔNp63 is necessary for induced YAP- cell migration, a pro-oncogenic function of YAP.

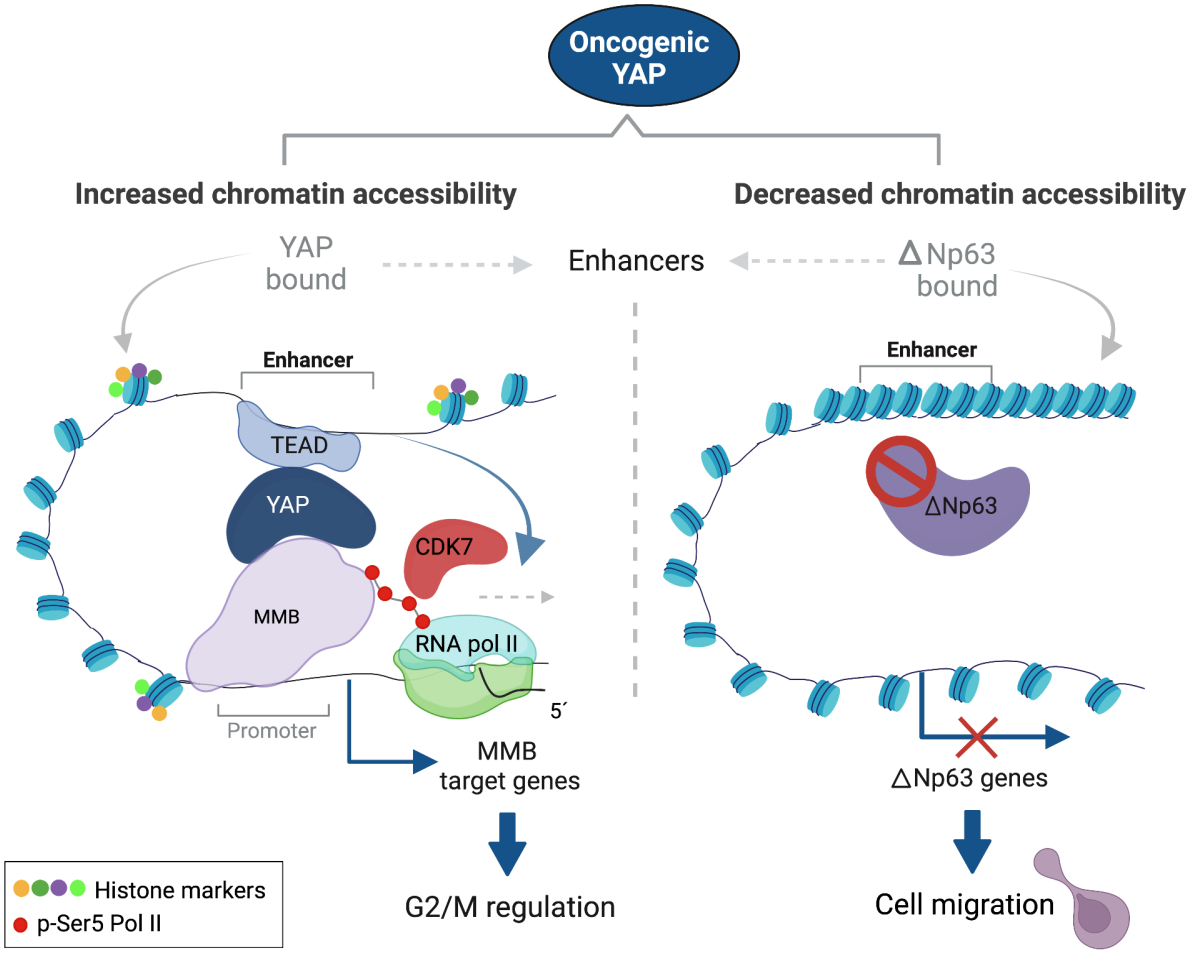

Figure 30. Model for chromatin and transcription regulation by oncogenic YAP.
This model is based on published data and on the results from this thesis. Oncogenic YAP induces changes in chromatin accessibility. Increased chromatin accessibility drives to induced expression of G2/M genes promoting the progression of cell cycle. While decreased chromatin accessibility mediates the loss of chromatin binding by ΔNp63 and consequently its depletion, as a necessary mechanism to promote cell migration. Created with BioRender.com.

The results reported in this thesis shed light on changes in chromatin accessibility and activity necessary to contribute to oncogenic activities of YAP. We demonstrate a role of YAP-bound enhancers in transcription through the stabilization of paused RNA Pol II at the promoters of YAP-MMB regulated genes which leads to hyperactive cell cycle progression. In addition, we found that YAP mediated the inactivation of tumor suppressor activities of ΔNp63 as part of the induction of cell malignant migration. Altogether, our findings point to cell oncogenic activities driven YAP that may have relevance in cancer biology.

5. References

Adelman, K., Kennedy, M. A., Nechaev, S., Gilchrist, D. A., Muse, G. W., Chinenov, Y., & Rogatsky, I. (2009). Immediate mediators of the inflammatory response are poised for gene activation through RNA polymerase II stalling. *Proceedings of the National Academy of Sciences of the United States of America*, *106*(43), 18207-18212.

Adorno, M., Cordenonsi, M., Montagner, M., Dupont, S., Wong, C., Hann, B., Solari, A., Bobisse, S., Rondina, M. B., Guzzardo, V., Parenti, A. R., Rosato, A., Bicciato, S., Balmain, A., & Piccolo, S. (2009). A Mutant-p53/Smad complex opposes p63 to empower TGFbeta-induced metastasis. *Cell*, *137*(1), 87-98.

Afgan, E., Baker, D., Batut, B., van den Beek, M., Bouvier, D., Cech, M., Chilton, J., Clements, D., Coraor, N., Grüning, B. A., Guerler, A., Hillman-Jackson, J., Hiltemann, S., Jalili, V., Rasche, H., Soranzo, N., Goecks, J., Taylor, J., Nekrutenko, A., & Blankenberg, D. (2018). The Galaxy platform for accessible, reproducible and collaborative biomedical analyses: 2018 update. *Nucleic Acids Research*, *46*(W1), W537-w544.

Alarcon, C., Zaromytidou, A. I., Xi, Q. R., Gao, S., Yu, J. Z., Fujisawa, S., Barlas, A., Miller, A. N., Manova-Todorova, K., Macias, M. J., Sapkota, G., Pan, D. J., & Massague, J. (2009). Nuclear CDKs Drive Smad Transcriptional Activation and Turnover in BMP and TGF-beta Pathways. *Cell*, *139*(4), 757-769.

Alberts, B., Johnson, A., Wilson, J., Lewis, J., Hunt, T., Roberts, K., Raff, M., & Walter, P. (2015). *Molecular Biology of the Cell*. Garland Science.

Antonini, D., Rossi, B., Han, R., Minichiello, A., Di Palma, T., Corrado, M., Banfi, S., Zannini, M., Brissette, J. L., & Missero, C. (2006). An autoregulatory loop directs the tissue-specific expression of p63 through a long-range evolutionarily conserved enhancer. *Molecular and Cellular Biology*, *26*(8), 3308-3318.

Antonini, D., Sirico, A., Aberdam, E., Ambrosio, R., Campanile, C., Fagoonee, S., Altruda, F., Aberdam, D., Brissette, J. L., & Missero, C. (2015). A composite enhancer regulates p63 gene expression in epidermal morphogenesis and in keratinocyte differentiation by multiple mechanisms. *Nucleic Acids Res*, *43*(2), 862-874.

Azzolin, L., Panciera, T., Soligo, S., Enzo, E., Bicciato, S., Dupont, S., Bresolin, S., Frasson, C., Basso, G., Guzzardo, V., Fassina, A., Cordenonsi, M., & Piccolo, S. (2014). YAP/TAZ incorporation in the β-catenin destruction complex orchestrates the Wnt response. *Cell*, *158*(1), 157-170.

Badouel, C., Garg, A., & McNeill, H. (2009). Herding Hippos: regulating growth in flies and man. *Curr Opin Cell Biol*, *21*(6), 837-843.

Bai, H. B., Gayyed, M. F., Lam-Himlin, D. M., Klein, A. P., Nayar, S. K., Xu, Y., Khan, M., Argani, P., Pan, D. J., & Anders, R. A. (2012). Expression of Yes-associated protein modulates Survivin expression in primary liver malignancies. *Human Pathology*, *43*(9), 1376-1385.

Barbieri, C. E., & Pietenpol, J. A. (2006). p63 and epithelial biology. *Experimental Cell Research*, *312*(6), 695-706.

Barger, C. J., Branick, C., Chee, L., & Karpf, A. R. (2019). Pan-Cancer Analyses Reveal Genomic Features of FOXM1 Overexpression in Cancer. *Cancers (Basel)*, *11*(2).

Bartucci, M., Svensson, S., Romania, P., Dattilo, R., Patrizii, M., Signore, M., Navarra, S., Lotti, F., Biffoni, M., Pilozzi, E., Duranti, E., Martinelli, S., Rinaldo, C., Zeuner, A., Maugeri-Saccà, M., Eramo, A., & De Maria, R. (2012). Therapeutic targeting of Chk1 in NSCLC stem cells during chemotherapy. *Cell Death Differ*, *19*(5), 768-778.

Bayarmagnai, B., Nicolay, B. N., Islam, A. B. M. M. K., Lopez-Bigas, N., & Frolov, M. V. (2012). Drosophila GAGA factor is required for full activation of the dE2f1-Yki/Sd transcriptional program. *Cell Cycle*, *11*(22), 4191-4202.

Belyi, V. A., Ak, P., Markert, E., Wang, H., Hu, W., Puzio-Kuter, A., & Levine, A. J. (2010). The origins and evolution of the p53 family of genes. *Cold Spring Harb Perspect Biol*, *2*(6), a001198.

Bergholz, J., & Xiao, Z. X. (2012). Role of p63 in Development, Tumorigenesis and Cancer Progression. *Cancer Microenviron*, *5*(3), 311-322.

Bertoli, C., Skotheim, J. M., & de Bruin, R. A. (2013). Control of cell cycle transcription during G1 and S phases. *Nat Rev Mol Cell Biol*, *14*(8), 518-528.

Beyer, T. A., Weiss, A., Khomchuk, Y., Huang, K., Ogunjimi, A. A., Varelas, X., & Wrana, J. L. (2013). Switch enhancers interpret TGF-β and Hippo signaling to control cell fate in human embryonic stem cells. *Cell Reports*, *5*(6), 1611-1624.

Bird, G., Zorio, D. A., & Bentley, D. L. (2004). RNA polymerase II carboxy-terminal domain phosphorylation is required for cotranscriptional pre-mRNA splicing and 3'-end formation. *Molecular and Cellular Biology*, *24*(20), 8963-8969.

Blakemore, D., Vilaplana-Lopera, N., Almaghrabi, R., Gonzalez, E., Moya, M., Ward, C., Murphy, G., Gambus, A., Petermann, E., Stewart, G. S., & Garcia, P. (2021). MYBL2 and ATM suppress replication stress in pluripotent stem cells. *Embo Reports*, *22*(5).

Blosser, W. D., Dempsey, J. A., McNulty, A. M., Rao, X., Ebert, P. J., Lowery, C. D., Iversen, P. W., Webster, Y. W., Donoho, G. P., Gong, X., Merzoug, F. F., Buchanan, S., Boehnke, K., Yu, C., You, X. T., Beckmann, R. P., Wu, W., McNeely, S. C., Lin, A. B., & Martinez, R. (2020). A pan-cancer transcriptome analysis identifies replication fork and innate immunity genes as modifiers of response to the CHK1 inhibitor prexasertib. *Oncotarget*, *11*(3), 216-236.

Boopathy, G. T. K., & Hong, W. J. (2019). Role of Hippo Pathway-YAP/TAZ Signaling in Angiogenesis. *Frontiers in Cell and Developmental Biology*, *7*.

Bourdon, J. C. (2007). p53 Family isoforms. *Curr Pharm Biotechnol*, *8*(6), 332-336.

Bowman, E. A., & Kelly, W. G. (2014). RNA Polymerase II transcription elongation and Pol II CTD Ser2 phosphorylation A tail of two kinases. *Nucleus*, *5*(3), 224-236.

Bracken, A. P., Ciro, M., Cocito, A., & Helin, K. (2004). E2F target genes: unraveling the biology. *Trends in Biochemical Sciences*, *29*(8), 409-417.

Bradner, J. E., Hnisz, D., & Young, R. A. (2017). Transcriptional Addiction in Cancer. *Cell*, *168*(4), 629-643.

Branigan, T. B., Kozono, D., Schade, A. E., Deraska, P., Rivas, H. G., Sambel, L., Reavis, H. D., Shapiro, G. I., D'Andrea, A. D., & DeCaprio, J. A. (2021). MMB-FOXM1-driven premature mitosis is required for CHK1 inhibitor sensitivity. *Cell Reports*, *34*(9).

Callus, B. A., Verhagen, A. M., & Vaux, D. L. (2006). Association of mammalian sterile twenty kinases, Mst1 and Mst2, with hSalvador via C-terminal coiled-coil domains, leads to its stabilization and phosphorylation. *Febs j*, *273*(18), 4264-4276.

Calvisi, D. F., Simile, M. M., Ladu, S., Frau, M., Evert, M., Tomasi, M. L., Demartis, M. I., Daino, L., Seddaiu, M. A., Brozzetti, S., Feo, F., & Pascale, R. M. (2011). Activation of v-Myb avian myeloblastosis viral oncogene homolog-like2 (MYBL2)-LIN9 complex contributes to human hepatocarcinogenesis and identifies a subset of hepatocellular carcinoma with mutant p53. *Hepatology*, *53*(4), 1226-1236.

Carroll, D. K., Carroll, J. S., Leong, C. O., Cheng, F., Brown, M., Mills, A. A., Brugge, J. S., & Ellisen, L. W. (2006). p63 regulates an adhesion programme and cell survival in epithelial cells. *Nature Cell Biology*, *8*(6), 551-561.

Cebola, I., Rodriguez-Segui, S. A., Cho, C. H. H., Bessa, J., Rovira, M., Luengo, M., Chhatriwala, M., Berry, A., Ponsa-Cobas, J., Maestro, M. A., Jennings, R. E., Pasquali, L., Moran, I., Castro, N., Hanley, N. A., Gomez-Skarmeta, J. L., Vallier, L., & Ferrer, J. (2015). TEAD and YAP regulate the enhancer network of human embryonic pancreatic progenitors. *Nature Cell Biology*, *17*(5), 615-U183.

Chatterjee, A., Sen, T., Chang, X., & Sidransky, D. (2010). Yes-associated protein 1 regulates the stability of ΔNp63α. *Cell Cycle*, *9*(1), 162-167.

Chen, J. Y., Lin, J. R., Tsai, F. C., & Meyer, T. (2013). Dosage of Dyrk1a shifts cells within a p21-cyclin D1 signaling map to control the decision to enter the cell cycle. *Molecular Cell*, *52*(1), 87-100.

Chen, L. Z., & Liu, Z. J. (2019). Multifaceted function of YAP/TEAD on chromatin: prospects of 'A non-canonical role of YAP/TEAD is required for activation of estrogen-regulated enhancers in breast cancer'. *Journal of Molecular Cell Biology*, *11*(12), 1101-1103.

Chen, X. Q., Shen, Y., Draper, W., Buenrostro, J. D., Litzenburger, U., Cho, S. W., Satpathy, A. T., Carter, A. C., Ghosh, R. P., East-Seletsky, A., Doudna, J. A., Greenleaf, W. J., Liphardt, J. T., & Changsites, H. Y. (2016). ATAC-see reveals the accessible genome by transposase-mediated imaging and sequencing. *Nature Methods*, *13*(12), 1013-+.

Cho, Y. S., Li, S., Wang, X. H., Zhu, J., Zhuo, S., Han, Y. H., Yue, T., Yang, Y. Z., & Jiang, J. (2020). CDK7 regulates organ size and tumor growth by safeguarding the Hippo pathway effector Yki/Yap/Taz in the nucleus. *Genes & Development*, *34*(1-2), 53-71.

Cicirò, Y., & Sala, A. (2021). MYB oncoproteins: emerging players and potential therapeutic targets in human cancer. *Oncogenesis*, *10*(2), 19.

Classon, M., & Dyson, N. (2001). p107 and p130: versatile proteins with interesting pockets. *Experimental Cell Research*, *264*(1), 135-147.

Compe, E., Genes, C. M., Braun, C., Coin, F., & Egly, J. M. (2019). TFIIE orchestrates the recruitment of the TFIIH kinase module at promoter before release during transcription. *Nature Communications*, *10*.

Compérat, E., Bièche, I., Dargère, D., Ferlicot, S., Laurendeau, I., Benoît, G., Vieillefond, A., Verret, C., Vidaud, M., Capron, F., Bedossa, P., & Paradis, V. (2007). p63 gene expression study and early bladder carcinogenesis. *Urology*, *70*(3), 459-462.

Core, L., & Adelman, K. (2019). Promoter-proximal pausing of RNA polymerase II: a nexus of gene regulation. *Genes & Development*, *33*(15-16), 960-982.

Croci, O., De Fazio, S., Biagioni, F., Donato, E., Caganova, M., Curti, L., Doni, M., Sberna, S., Aldeghi, D., Biancotto, C., Verrecchia, A., Olivero, D., Amati, B., & Campaner, S. (2017). Transcriptional integration of mitogenic and mechanical signals by Myc and YAP. *Genes Dev*, *31*(20), 2017-2022.

Croci, O., De Fazio, S., Biagioni, F., Donato, E., Caganova, M., Curti, L., Doni, M., Sberna, S., Aldeghi, D., Biancotto, C., Verrecchia, A., Olivero, D., Amati, B., & Campaner, S. (2017). Transcriptional integration of mitogenic and mechanical signals by Myc and YAP. *Genes & Development*, *31*(20), 2017-2022.

Crook, T., Nicholls, J. M., Brooks, L., O'Nions, J., & Allday, M. J. (2000). High level expression of deltaN-p63: a mechanism for the inactivation of p53 in undifferentiated nasopharyngeal carcinoma (NPC)? *Oncogene*, *19*(30), 3439-3444.

de Andrade, K. C., Khincha, P. P., Hatton, J. N., Frone, M. N., Wegman-Ostrosky, T., Mai, P. L., Best, A. F., & Savage, S. A. (2021). Cancer incidence, patterns, and genotype-phenotype associations in individuals with pathogenic or likely pathogenic germline TP53 variants: an observational cohort study. *Lancet Oncology*, *22*(12), 1787-1798.

Ding, L., Cao, J. Q., Lin, W., Chen, H. J., Xiong, X. H., Ao, H. S., Yu, M., Lin, J., & Cui, Q. H. (2020). The Roles of Cyclin-Dependent Kinases in Cell-Cycle Progression and Therapeutic Strategies in Human Breast Cancer. *International Journal of Molecular Sciences*, *21*(6).

Dohn, M., Zhang, S., & Chen, X. (2001). p63alpha and DeltaNp63alpha can induce cell cycle arrest and apoptosis and differentially regulate p53 target genes. *Oncogene*, *20*(25), 3193-3205.

Dong, J., Feldmann, G., Huang, J., Wu, S., Zhang, N., Comerford, S. A., Gayyed, M. F., Anders, R. A., Maitra, A., & Pan, D. (2007). Elucidation of a universal size-control mechanism in Drosophila and mammals. *Cell*, *130*(6), 1120-1133.

Donner, A. J., Ebmeier, C. C., Taatjes, D. J., & Espinosa, J. M. (2010). CDK8 is a positive regulator of transcriptional elongation within the serum response network. *Nature Structural & Molecular Biology*, *17*(2), 194-U199.

Down, C. F., Millour, J., Lam, E. W., & Watson, R. J. (2012). Binding of FoxM1 to G2/M gene promoters is dependent upon B-Myb. *Biochim Biophys Acta*, *1819*(8), 855-862.

Dukler, N., Booth, G. T., Huang, Y. F., Tippens, N., Waters, C. T., Danko, C. G., Lis, J. T., & Siepel, A. (2017). Nascent RNA sequencing reveals a dynamic global transcriptional response at genes and enhancers to the natural medicinal compound celastrol. *Genome Research*, *27*(11), 1816-1829.

Ebmeier, C. C., Erickson, B., Allen, B. L., Allen, M. A., Kim, H., Fong, N., Jacobsen, J. R., Liang, K. W., Shilatifard, A., Dowell, R. D., Old, W. M., Bentley, D. L., & Taatjes, D. J. (2017). Human TFIIH Kinase CDK7 Regulates Transcription-Associated Chromatin Modifications. *Cell Reports*, *20*(5), 1173-1186.

Eckerdt, F., Perez-Neut, M., & Colamonici, O. R. (2014). LIN-9 phosphorylation on threonine-96 is required for transcriptional activation of LIN-9 target genes and promotes cell cycle progression. *Plos One*, *9*(1), e87620.

Ehmer, U., & Sage, J. (2016). Control of Proliferation and Cancer Growth by the Hippo Signaling Pathway. *Molecular Cancer Research*, *14*(2), 127-140.

Ehsanian, R., Brown, M., Lu, H., Yang, X. P., Pattatheyil, A., Yan, B., Duggal, P., Chuang, R., Doondeea, J., Feller, S., Sudol, M., Chen, Z., & Van Waes, C. (2010). YAP dysregulation by phosphorylation or Delta Np63-mediated gene repression promotes proliferation, survival and migration in head and neck cancer subsets. *Oncogene*, *29*(46), 6160-6171.

Esterlechner, J., Reichert, N., Iltzsche, F., Krause, M., Finkernagel, F., & Gaubatz, S. (2013). LIN9, a subunit of the DREAM complex, regulates mitotic gene expression and proliferation of embryonic stem cells. *Plos One*, *8*(5), e62882.

Fagnocchi, L., Poli, V., & Zippo, A. (2018). Enhancer reprogramming in tumor progression: a new route towards cancer cell plasticity. *Cellular and Molecular Life Sciences*, *75*(14), 2537-2555.

Fan, X. Y., Wang, Y. T., Jiang, T. H., Cai, W., Jin, Y. L., Niu, Y. L., Zhu, H. F., & Bu, Y. Q. (2018). B-Myb Mediates Proliferation and Migration of Non-Small-Cell Lung Cancer via Suppressing IGFBP3. *International Journal of Molecular Sciences*, *19*(5).

Fang, G. W., Yu, H. T., & Kirschner, M. W. (1998). Direct binding of CDC20 protein family members activates the anaphase-promoting complex in mitosis and G1. *Molecular Cell*, *2*(2), 163-171.

Fant, C. B., & Taatjes, D. J. (2019). Regulatory functions of the Mediator kinases CDK8 and CDK19. *Transcription*, *10*(2), 76-90.

Feldker, N., Ferrazzi, F., Schuhwerk, H., Widholz, S. A., Guenther, K., Frisch, I., Jakob, K., Kleemann, J., Riegel, D., Bönisch, U., Lukassen, S., Eccles, R. L., Schmidl, C., Stemmler,

M. P., Brabletz, T., & Brabletz, S. (2020). Genome-wide cooperation of EMT transcription factor ZEB1 with YAP and AP-1 in breast cancer. *Embo j*, *39*(17), e103209.

Feng, J. T., Gou, J. H., Jia, J., Yi, T., Cui, T., & Li, Z. Y. (2016). Verteporfin, a suppressor of YAP-TEAD complex, presents promising antitumor properties on ovarian cancer. *Oncotargets and Therapy*, *9*, 5371-5381.

Fischer, M., Grossmann, P., Padi, M., & DeCaprio, J. A. (2016). Integration of TP53, DREAM, MMB-FOXM1 and RB-E2F target gene analyses identifies cell cycle gene regulatory networks. *Nucleic Acids Res*, *44*(13), 6070-6086.

Fischer, M., & Muller, G. A. (2017). Cell cycle transcription control: DREAM/MuvB and RB-E2F complexes. *Critical Reviews in Biochemistry and Molecular Biology*, *52*(6), 638-662.

Fisher, R. P. (2012). The CDK Network: Linking Cycles of Cell Division and Gene Expression. *Genes Cancer*, *3*(11-12), 731-738.

Fisher, R. P. (2019). Cdk7: a kinase at the core of transcription and in the crosshairs of cancer drug discovery. *Transcription*, *10*(2), 47-56.

Flores, E. R. (2007). The roles of p63 in cancer. *Cell Cycle*, *6*(3), 300-304.

Flores, E. R., Tsai, K. Y., Crowley, D., Sengupta, S., Yang, A., McKeon, F., & Jacks, T. (2002). p63 and p73 are required for p53-dependent apoptosis in response to DNA damage. *Nature*, *416*(6880), 560-564.

Frolov, M. V., & Dyson, N. J. (2004). Molecular mechanisms of E2F-dependent activation and pRB-mediated repression. *J Cell Sci*, *117*(Pt 11), 2173-2181.

Galbraith, M. D., Donner, A. J., & Espinosa, J. M. (2010). CDK8: a positive regulator of transcription. *Transcription*, *1*(1), 4-12.

Galli, G. G., Carrara, M., Yuan, W. C., Valdes-Quezada, C., Gurung, B., Pepe-Mooney, B., Zhang, T. H., Geeven, G., Gray, N. S., de Laat, W., Calogero, R. A., & Camargo, F. D. (2015). YAP Drives Growth by Controlling Transcriptional Pause Release from Dynamic Enhancers. *Molecular Cell*, *60*(2), 328-337.

Ganem, N. J., Cornils, H., Chiu, S. Y., O'Rourke, K. P., Arnaud, J., Yimlamai, D., Théry, M., Camargo, F. D., & Pellman, D. (2014). Cytokinesis failure triggers hippo tumor suppressor pathway activation. *Cell*, *158*(4), 833-848.

Gao, Y. J., Zhang, W. J., Han, X. K., Li, F. M., Wang, X. J., Wang, R., Fang, Z. Y., Tong, X. Y., Yao, S., Li, F., Feng, Y., Sun, Y. H., Hou, Y. Y., Yang, Z. Z., Guan, K. L., Chen, H. Q., Zhang, L., & Ji, H. B. (2015). YAP inhibits squamous transdifferentiation of Lkb1-deficient lung adenocarcinoma through ZEB2-dependent DNp63 repression (vol 5, 4629, 2014). *Nature Communications*, *6*.

Gartel, A. L. (2017). FOXM1 in Cancer: Interactions and Vulnerabilities. *Cancer Res*, *77*(12), 3135-3139.

Glover-Cutter, K., Larochelle, S., Erickson, B., Zhang, C., Shokat, K., Fisher, R. P., & Bentley, D. L. (2009). TFIIH-Associated Cdk7 Kinase Functions in Phosphorylation of C-Terminal Domain Ser7 Residues, Promoter-Proximal Pausing, and Termination by RNA Polymerase II. *Molecular and Cellular Biology*, *29*(20), 5455-5464.

Grundl, M., Walz, S., Hauf, L., Schwab, M., Werner, K. M., Spahr, S., Schulte, C., Maric, H. M., Ade, C. P., & Gaubatz, S. (2020). Interaction of YAP with the Myb-MuvB (MMB) complex defines a transcriptional program to promote the proliferation of cardiomyocytes. *Plos Genetics*, *16*(5).

Guiley, K. Z., Iness, A. N., Saini, S., Tripathi, S., Lipsick, J. S., Litovchick, L., & Rubin, S. M. (2018). Structural mechanism of Myb-MuvB assembly. *Proc Natl Acad Sci U S A*, *115*(40), 10016-10021.

Guiley, K. Z., Liban, T. J., Felthousen, J. G., Ramanan, P., Litovchick, L., & Rubin, S. M. (2015). Structural mechanisms of DREAM complex assembly and regulation. *Genes Dev*, *29*(9), 961-974.

Hagiwara, K., McMenamin, M. G., Miura, K., & Harris, C. C. (1999). Mutational analysis of the p63/p73L/p51/p40/CUSP/KET gene in human cancer cell lines using intronic primers. *Cancer Research*, *59*(17), 4165-4169.

Halder, G., & Camargo, F. D. (2013). The hippo tumor suppressor network: from organ size control to stem cells and cancer. *Cancer Research*, *73*(21), 6389-6392.

Hanselmann, S., Wolter, P., Malkmus, J., & Gaubatz, S. (2018). The microtubule-associated protein PRC1 is a potential therapeutic target for lung cancer. *Oncotarget*, *9*(4), 4985-4997.

Harvey, K. F., Zhang, X. M., & Thomas, D. M. (2013). The Hippo pathway and human cancer. *Nature Reviews Cancer*, *13*(4), 246-257.

Haupt, Y., Maya, R., Kazaz, A., & Oren, M. (1997). Mdm2 promotes the rapid degradation of p53. *Nature*, *387*(6630), 296-299.

He, L. Z., Pratt, H., Gao, M. S., Wei, F. X., Weng, Z. P., & Struhl, K. (2021). YAP and TAZ are transcriptional co-activators of AP-1 proteins and STAT3 during breast cellular transformation. *Elife*, *10*.

Helton, E. S., Zhu, J., & Chen, X. (2006). The unique NH2-terminally deleted (DeltaN) residues, the PXXP motif, and the PPXY motif are required for the transcriptional activity of the DeltaN variant of p63. *Journal of Biological Chemistry*, *281*(5), 2533-2542.

Hibi, K., Trink, B., Patturajan, M., Westra, W. H., Caballero, O. L., Hill, D. E., Ratovitski, E. A., Jen, J., & Sidransky, D. (2000). AIS is an oncogene amplified in squamous cell carcinoma. *Proc Natl Acad Sci U S A*, *97*(10), 5462-5467.

Hirst, M., Kobor, M. S., Kuriakose, N., Greenblatt, J., & Sadowski, I. (1999). GAL4 is regulated by the RNA polymerase II holoenzyme-associated cyclin-dependent protein kinase SRB10/CDK8. *Molecular Cell*, *3*(5), 673-678.

Hnisz, D., Abraham, B. J., Lee, T. I., Lau, A., Saint-Andre, V., Sigova, A. A., Hoke, H. A., & Young, R. A. (2013). Super-enhancers in the control of cell identity and disease. *Cell*, *155*(4), 934-947.

Honda, R., Tanaka, H., & Yasuda, H. (1997). Oncoprotein MDM2 is a ubiquitin ligase E3 for tumor suppressor p53. *FEBS Lett*, *420*(1), 25-27.

Hong, W., & Guan, K. L. (2012). The YAP and TAZ transcription co-activators: key downstream effectors of the mammalian Hippo pathway. *Semin Cell Dev Biol*, *23*(7), 785-793.

Hu, L., Liang, S., Chen, H., Lv, T., Wu, J., Chen, D., Wu, M., Sun, S., Zhang, H., You, H., Ji, H., Zhang, Y., Bergholz, J., & Xiao, Z.-X. J. (2017). ΔNp63α is a common inhibitory target in oncogenic PI3K/Ras/Her2-induced cell motility and tumor metastasis. *Proceedings of the National Academy of Sciences*, *114*(20), E3964-E3973.

Humbert, P. O., Verona, R., Trimarchi, J. M., Rogers, C., Dandapani, S., & Lees, J. A. (2000). E2f3 is critical for normal cellular proliferation. *Genes & Development*, *14*(6), 690-703.

Iltzsche, F., Simon, K., Stopp, S., Pattschull, G., Francke, S., Wolter, P., Hauser, S., Murphy, D. J., Garcia, P., Rosenwald, A., & Gaubatz, S. (2017). An important role for Myb-MuvB and its target gene KIF23 in a mouse model of lung adenocarcinoma. *Oncogene*, *36*(1), 110-121.

Iness, A. N., Felthousen, J., Ananthapadmanabhan, V., Sesay, F., Saini, S., Guiley, K. Z., Rubin, S. M., Dozmorov, M., & Litovchick, L. (2019). The cell cycle regulatory DREAM complex is disrupted by high expression of oncogenic B-Myb. *Oncogene*, *38*(7), 1080-1092.

Iness, A. N., Rubinsak, L., Meas, S. J., Chaoul, J., Sayeed, S., Pillappa, R., Temkin, S. M., Dozmorov, M. G., & Litovchick, L. (2021). Oncogenic B-Myb Is Associated With Deregulation of the DREAM-Mediated Cell Cycle Gene Expression Program in High Grade Serous Ovarian Carcinoma Clinical Tumor Samples. *Front Oncol*, *11*, 637193.

Jeronimo, C., Bataille, A. R., & Robert, F. (2013). The Writers, Readers, and Functions of the RNA Polymerase II C-Terminal Domain Code. *Chemical Reviews*, *113*(11), 8491-8522.

Jiang, Y., Saavedra, H. I., Holloway, M. P., Leone, G., & Altura, R. A. (2004). Aberrant regulation of survivin by the RB/E2F family of proteins. *Journal of Biological Chemistry*, *279*(39), 40511-40520.

Jin, Y. L., Zhu, H. F., Cai, W., Fan, X. Y., Wang, Y. T., Niu, Y. L., Song, F. Z., & Bu, Y. Q. (2017). B-Myb Is Up-Regulated and Promotes Cell Growth and Motility in Non-Small Cell Lung Cancer. *International Journal of Molecular Sciences*, *18*(6).

Johnson, T. K., Schweppe, R. E., Septer, J., & Lewis, R. E. (1999). Phosphorylation of B-Myb regulates its transactivation potential and DNA binding. *Journal of Biological Chemistry*, *274*(51), 36741-36749.

Kanai, F., Marignani, P. A., Sarbassova, D., Yagi, R., Hall, R. A., Donowitz, M., Hisaminato, A., Fujiwara, T., Ito, Y., Cantley, L. C., & Yaffe, M. B. (2000). TAZ: a novel transcriptional co-activator regulated by interactions with 14-3-3 and PDZ domain proteins. *Embo j*, *19*(24), 6778-6791.

Kanin, E. I., Kipp, R. T., Kung, C., Slattery, M., Viale, A., Hahn, S., Shokat, K. M., & Ansari, A. Z. (2007). Chemical inhibition of the TFIIH-associated kinase Cdk7/Kin28 does not impair global mRNA synthesis. *Proc Natl Acad Sci U S A*, *104*(14), 5812-5817.

Kapoor, A., Yao, W., Ying, H., Hua, S., Liewen, A., Wang, Q., Zhong, Y., Wu, C. J., Sadanandam, A., Hu, B., Chang, Q., Chu, G. C., Al-Khalil, R., Jiang, S., Xia, H., Fletcher-Sananikone, E., Lim, C., Horwitz, G. I., Viale, A., . . . DePinho, R. A. (2014). Yap1 activation enables bypass of oncogenic Kras addiction in pancreatic cancer. *Cell*, *158*(1), 185-197.

Kapoor, A., Yao, W. T., Ying, H. Q., Hua, S. J., Liewen, A., Wang, Q. Y., Zhong, Y., Wu, C. J., Sadanandam, A., Hu, B. L., Chang, Q., Chu, G., Al-Khalil, R., Jiang, S., Xia, H. G., Fletcher-Sananikone, E., Lim, C., Horwitz, G., Viale, A., . . . DePinho, R. (2014). Yap1 activation enables bypass of oncogenic Kras addiction in pancreatic cancer. *Molecular Cancer Research*, *12*.

Kent, L. N., & Leone, G. (2019). The broken cycle: E2F dysfunction in cancer. *Nature Reviews Cancer*, *19*(6), 326-338.

Keyes, W. M., Pecoraro, M., Aranda, V., Vernersson-Lindahl, E., Li, W., Vogel, H., Guo, X., Garcia, E. L., Michurina, T. V., Enikolopov, G., Muthuswamy, S. K., & Mills, A. A. (2011). ΔNp63α is an oncogene that targets chromatin remodeler Lsh to drive skin stem cell proliferation and tumorigenesis. *Cell Stem Cell*, *8*(2), 164-176.

Kim, M., Kim, T., Johnson, R. L., & Lim, D. S. (2015). Transcriptional Co-repressor Function of the Hippo Pathway Transducers YAP and TAZ. *Cell Reports*, *11*(2), 270-282.

Kim, M., Kim, T., Johnson, R. L., & Lim, D. S. (2015). Transcriptional co-repressor function of the hippo pathway transducers YAP and TAZ. *Cell Reports*, *11*(2), 270-282.

Knight, A. S., Notaridou, M., & Watson, R. J. (2009). A Lin-9 complex is recruited by B-Myb to activate transcription of G2/M genes in undifferentiated embryonal carcinoma cells. *Oncogene*, *28*(15), 1737-1747.

Knuesel, M. T., Meyer, K. D., Donner, A. J., Espinosa, J. M., & Taatjes, D. J. (2009). The Human CDK8 Subcomplex Is a Histone Kinase That Requires Med12 for Activity and Can Function Independently of Mediator. *Molecular and Cellular Biology*, *29*(3), 650-661.

Koster, M. I., Kim, S., Mills, A. A., DeMayo, F. J., & Roop, D. R. (2004). p63 is the molecular switch for initiation of an epithelial stratification program. *Genes Dev*, *18*(2), 126-131.

Kouwenhoven, E. N., Oti, M., Niehues, H., van Heeringen, S. J., Schalkwijk, J., Stunnenberg, H. G., van Bokhoven, H., & Zhou, H. Q. (2015). Transcription factor p63 bookmarks and regulates dynamic enhancers during epidermal differentiation. *Embo Reports*, *16*(7), 863-878.

Kramer, A., Mailand, N., Lukas, C., Syljuasen, R. G., Wilkinson, C. J., Nigg, E. A., Bartek, J., & Lukas, J. (2004). Centrosome-associated Chk1 prevents premature activation of cyclin-B-Cdk1 kinase. *Nature Cell Biology*, *6*(9), 884-U871.

Krupczak-Hollis, K., Wang, X., Kalinichenko, V. V., Gusarova, G. A., Wang, I. C., Dennewitz, M. B., Yoder, H. M., Kiyokawa, H., Kaestner, K. H., & Costa, R. H. (2004). The mouse Forkhead Box m1 transcription factor is essential for hepatoblast mitosis and development of intrahepatic bile ducts and vessels during liver morphogenesis. *Dev Biol*, *276*(1), 74-88.

Kubbutat, M. H., Jones, S. N., & Vousden, K. H. (1997). Regulation of p53 stability by Mdm2. *Nature*, *387*(6630), 299-303.

Lange, A. W., Sridharan, A., Xu, Y., Stripp, B. R., Perl, A. K., & Whitsett, J. A. (2015). Hippo/Yap signaling controls epithelial progenitor cell proliferation and differentiation in the embryonic and adult lung. *Journal of Molecular Cell Biology*, *7*(1), 35-47.

Langmead, B., & Salzberg, S. L. (2012). Fast gapped-read alignment with Bowtie 2. *Nature Methods*, *9*(4), 357-359.

Laoukili, J., Kooistra, M. R., Brás, A., Kauw, J., Kerkhoven, R. M., Morrison, A., Clevers, H., & Medema, R. H. (2005). FoxM1 is required for execution of the mitotic programme and chromosome stability. *Nature Cell Biology*, *7*(2), 126-136.

Larochelle, S., Amat, R., Glover-Cutter, K., Sanso, M., Zhang, C., Allen, J. J., Shokat, K. M., Bentley, D. L., & Fisher, R. P. (2012). Cyclin-dependent kinase control of the initiation-to-elongation switch of RNA polymerase II. *Nature Structural & Molecular Biology*, *19*(11), 1108-+.

Larochelle, S., Amat, R., Glover-Cutter, K., Sansó, M., Zhang, C., Allen, J. J., Shokat, K. M., Bentley, D. L., & Fisher, R. P. (2012). Cyclin-dependent kinase control of the initiation-to-elongation switch of RNA polymerase II. *Nature Structural & Molecular Biology*, *19*(11), 1108-1115.

Lehmann, W., Mossmann, D., Kleemann, J., Mock, K., Meisinger, C., Brummer, T., Herr, R., Brabletz, S., Stemmler, M. P., & Brabletz, T. (2016). ZEB1 turns into a transcriptional activator by interacting with YAP1 in aggressive cancer types. *Nature Communications*, *7*, 10498.

Leong, C. O., Vidnovic, N., DeYoung, M. P., Sgroi, D., & Ellisen, L. W. (2007). The p63/p73 network mediates chemosensitivity to cisplatin in a biologically defined subset of primary breast cancers. *J Clin Invest*, *117*(5), 1370-1380.

Li, L., Ugalde, A. P., Scheele, C. L. G. J., Dieter, S. M., Nagel, R., Ma, J., Pataskar, A., Korkmaz, G., Elkon, R., Chien, M. P., You, L., Su, P. R., Bleijerveld, O. B., Altelaar, M., Momchev, L., Manber, Z., Han, R. Q., van Breugel, P. C., Lopes, R., . . . Agami, R. (2021). A comprehensive enhancer screen identifies TRAM2 as a key and novel mediator of YAP oncogenesis. *Genome Biology*, *22*(1).

Lian, I., Kim, J., Okazawa, H., Zhao, J., Zhao, B., Yu, J., Chinnaiyan, A., Israel, M. A., Goldstein, L. S., Abujarour, R., Ding, S., & Guan, K. L. (2010). The role of YAP transcription coactivator in regulating stem cell self-renewal and differentiation. *Genes Dev*, *24*(11), 1106-1118.

Lim, S., & Kaldis, P. (2013). Cdks, cyclins and CKIs: roles beyond cell cycle regulation. *Development*, *140*(15), 3079-3093.

Lindsay, J., McDade, S. S., Pickard, A., McCloskey, K. D., & McCance, D. J. (2011). Role of DeltaNp63gamma in epithelial to mesenchymal transition. *Journal of Biological Chemistry*, *286*(5), 3915-3924.

Litovchick, L., Florens, L. A., Swanson, S. K., Washburn, M. P., & DeCaprio, J. A. (2011). DYRK1A protein kinase promotes quiescence and senescence through DREAM complex assembly. *Genes Dev*, *25*(8), 801-813.

Litovchick, L., Sadasivam, S., Florens, L., Zhu, X., Swanson, S. K., Velmurugan, S., Chen, R., Washburn, M. P., Liu, X. S., & DeCaprio, J. A. (2007). Evolutionarily conserved multisubunit RBL2/p130 and E2F4 protein complex represses human cell cycle-dependent genes in quiescence. *Molecular Cell*, *26*(4), 539-551.

Liu, R., Holik, A. Z., Su, S., Jansz, N., Chen, K., Leong, H. S., Blewitt, M. E., Asselin-Labat, M. L., Smyth, G. K., & Ritchie, M. E. (2015). Why weight? Modelling sample and observational level variability improves power in RNA-seq analyses. *Nucleic Acids Res*, *43*(15), e97.

Liu, X. F., Li, H. P., Rajurkar, M., Li, Q., Cotton, J. L., Ou, J. H., Zhu, L. H. J., Goel, H. L., Mercurio, A. M., Park, J. S., Davis, R. J., & Mao, J. H. (2016). Tead and AP1 Coordinate Transcription and Motility. *Cell Reports*, *14*(5), 1169-1180.

Liu, Y., Wang, G., Yang, Y., Mei, Z., Liang, Z., Cui, A., Wu, T., Liu, C. Y., & Cui, L. (2016). Increased TEAD4 expression and nuclear localization in colorectal cancer promote epithelial-mesenchymal transition and metastasis in a YAP-independent manner. *Oncogene*, *35*(21), 2789-2800.

Lolli, G., & Johnson, L. N. (2005). CAK-Cyclin-dependent Activating Kinase: a key kinase in cell cycle control and a target for drugs? *Cell Cycle*, *4*(4), 572-577.

Lopez-Hernandez, A., Sberna, S., & Campaner, S. (2021). Emerging Principles in the Transcriptional Control by YAP and TAZ. *Cancers*, *13*(16).

Lopez-Hernandez, A., Sberna, S., & Campaner, S. (2021). Emerging Principles in the Transcriptional Control by YAP and TAZ. *Cancers (Basel)*, *13*(16).

Lorvellec, M., Dumon, S., Maya-Mendoza, A., Jackson, D., Frampton, J., & Garcia, P. (2010). B-Myb is Critical for Proper DNA Duplication During an Unperturbed S Phase in Mouse Embryonic Stem Cells. *Stem Cells*, *28*(10), 1751-1759.

Low, B. C., Pan, C. Q., Shivashankar, G. V., Bershadsky, A., Sudol, M., & Sheetz, M. (2014). YAP/TAZ as mechanosensors and mechanotransducers in regulating organ size and tumor growth. *Febs Letters*, *588*(16), 2663-2670.

Malumbres, M. (2014). Cyclin-dependent kinases. *Genome Biology*, *15*(6), 122.

Malumbres, M., & Barbacid, M. (2001). To cycle or not to cycle: a critical decision in cancer. *Nature Reviews Cancer*, *1*(3), 222-231.

Marceau, A. H., Felthousen, J. G., Goetsch, P. D., Iness, A. N., Lee, H. W., Tripathi, S. M., Strome, S., Litovchick, L., & Rubin, S. M. (2016). Structural basis for LIN54 recognition of CHR elements in cell cycle-regulated promoters. *Nature Communications*, *7*.

Marchini, S., Marabese, M., Marrazzo, E., Mariani, P., Cattaneo, D., Fossati, R., Compagnoni, A., Fruscio, R., Lissoni, A. A., & Broggini, M. (2008). DeltaNp63 expression is associated with poor survival in ovarian cancer. *Ann Oncol*, *19*(3), 501-507.

Massion, P. P., Taflan, P. M., Jamshedur Rahman, S. M., Yildiz, P., Shyr, Y., Edgerton, M. E., Westfall, M. D., Roberts, J. R., Pietenpol, J. A., Carbone, D. P., & Gonzalez, A. L. (2003). Significance of p63 amplification and overexpression in lung cancer development and prognosis. *Cancer Research*, *63*(21), 7113-7121.

Matsuo, T., Kuramoto, H., Kumazaki, T., Mitsui, Y., & Takahashi, T. (2012). LIN54 harboring a mutation in CHC domain is localized to the cytoplasm and inhibits cell cycle progression. *Cell Cycle*, *11*(17), 3227-3236.

Matsuoka, S., Rotman, G., Ogawa, A., Shiloh, Y., Tamai, K., & Elledge, S. J. (2000). Ataxia telangiectasia-mutated phosphorylates Chk2 in vivo and in vitro. *Proceedings of the National Academy of Sciences of the United States of America*, *97*(19), 10389-10394.

Melino, G., Lu, X., Gasco, M., Crook, T., & Knight, R. A. (2003). Functional regulation of p73 and p63: development and cancer. *Trends in Biochemical Sciences*, *28*(12), 663-670.

Meng, Z., Moroishi, T., & Guan, K. L. (2016). Mechanisms of Hippo pathway regulation. *Genes Dev*, *30*(1), 1-17.

Monroe, T. O., Hill, M. C., Morikawa, Y., Leach, J. P., Heallen, T., Cao, S., Krijger, P. H. L., de Laat, W., Wehrens, X. H. T., Rodney, G. G., & Martin, J. F. (2019). YAP Partially Reprograms Chromatin Accessibility to Directly Induce Adult Cardiogenesis In Vivo. *Developmental Cell*, *48*(6), 765-779.e767.

Monroe, T. O., Hill, M. C., Morikawa, Y., Leach, J. P., Heallen, T., Cao, S. Y., Krijger, P. H. L., de Laat, W., Wehrens, X. H. T., Rodney, G. G., & Martin, J. F. (2019). YAP Partially Reprograms Chromatin Accessibility to Directly Induce Adult Cardiogenesis In Vivo. *Developmental Cell*, *48*(6), 765-+.

Morgan, D. O. (2016). The cell cycle principles of control. *Primers in Biology*.

Moroishi, T., Hansen, C. G., & Guan, K. L. (2015). The emerging roles of YAP and TAZ in cancer. *Nature Reviews Cancer*, *15*(2), 73-79.

Murzina, N. V., Pei, X. Y., Zhang, W., Sparkes, M., Vicente-Garcia, J., Pratap, J. V., McLaughlin, S. H., Ben-Shahar, T. R., Verreault, A., Luisi, B. F., & Laue, E. D. (2008). Structural basis for the recognition of histone H4 by the histone-chaperone RbAp46. *Structure*, *16*(7), 1077-1085.

Musa, J., Aynaud, M. M., Mirabeau, O., Delattre, O., & Grünewald, T. G. (2017). MYBL2 (B-Myb): a central regulator of cell proliferation, cell survival and differentiation involved in tumorigenesis. *Cell Death Dis*, *8*(6), e2895.

Nabet, B., Roberts, J. M., Buckley, D. L., Paulk, J., Dastjerdi, S., Yang, A., Leggett, A. L., Erb, M. A., Lawlor, M. A., Souza, A., Scott, T. G., Vittori, S., Perry, J. A., Qi, J., Winter, G. E., Wong, K. K., Gray, N. S., & Bradner, J. E. (2018). The dTAG system for immediate and target-specific protein degradation. *Nature Chemical Biology*, *14*(5), 431-+.

Neizer-Ashun, F., & Bhattacharya, R. (2021). Reality CHEK: Understanding the biology and clinical potential of CHK1. *Cancer Letters*, *497*, 202-211.

Neto-Silva, R. M., de Beco, S., & Johnston, L. A. (2010). Evidence for a growth-stabilizing regulatory feedback mechanism between Myc and Yorkie, the Drosophila homolog of Yap. *Developmental Cell*, *19*(4), 507-520.

Nicolas, E., Ait-Si-Ali, S., & Trouche, D. (2001). The histone deacetylase HDAC3 targets RbAp48 to the retinoblastoma protein. *Nucleic Acids Research*, *29*(15), 3131-3136.

O'Connell, M. J., Lavery, I., Yothers, G., Paik, S., Clark-Langone, K. M., Lopatin, M., Watson, D., Baehner, F. L., Shak, S., Baker, J., Cowens, J. W., & Wolmark, N. (2010). Relationship between tumor gene expression and recurrence in four independent studies of patients with stage II/III colon cancer treated with surgery alone or surgery plus adjuvant fluorouracil plus leucovorin. *J Clin Oncol*, *28*(25), 3937-3944.

Osterloh, L., von Eyss, B., Schmit, F., Rein, L., Hübner, D., Samans, B., Hauser, S., & Gaubatz, S. (2007). The human synMuv-like protein LIN-9 is required for transcription of G2/M genes and for entry into mitosis. *Embo j*, *26*(1), 144-157.

Otto, T., & Sicinski, P. (2017). Cell cycle proteins as promising targets in cancer therapy. *Nature Reviews Cancer*, *17*(2), 93-115.

Paik, S., Shak, S., Tang, G., Kim, C., Baker, J., Cronin, M., Baehner, F. L., Walker, M. G., Watson, D., Park, T., Hiller, W., Fisher, E. R., Wickerham, D. L., Bryant, J., & Wolmark, N. (2004).

A multigene assay to predict recurrence of tamoxifen-treated, node-negative breast cancer. *N Engl J Med*, *351*(27), 2817-2826.

Pan, D. (2010). The hippo signaling pathway in development and cancer. *Developmental Cell*, *19*(4), 491-505.

Park, B. J., Lee, S. J., Kim, J. I., Lee, S. J., Lee, C. H., Chang, S. G., Park, J. H., & Chi, S. G. (2000). Frequent alteration of p63 expression in human primary bladder carcinomas. *Cancer Research*, *60*(13), 3370-3374.

Park, H. J., Costa, R. H., Lau, L. F., Tyner, A. L., & Raychaudhuri, P. (2008). Anaphase-promoting complex/cyclosome-CDH1-mediated proteolysis of the forkhead box M1 transcription factor is critical for regulated entry into S phase. *Molecular and Cellular Biology*, *28*(17), 5162-5171.

Parua, P. K., & Fisher, R. P. (2020). Dissecting the Pol II transcription cycle and derailing cancer with CDK inhibitors. *Nature Chemical Biology*, *16*(7), 716-724.

Pattschull, G., Walz, S., Gründl, M., Schwab, M., Rühl, E., Baluapuri, A., Cindric-Vranesic, A., Kneitz, S., Wolf, E., Ade, C. P., Rosenwald, A., von Eyss, B., & Gaubatz, S. (2019). The Myb-MuvB Complex Is Required for YAP-Dependent Transcription of Mitotic Genes. *Cell Reports*, *27*(12), 3533-3546.e3537.

Peng, C. Y., Graves, P. R., Thoma, R. S., Wu, Z., Shaw, A. S., & Piwnica-Worms, H. (1997). Mitotic and G2 checkpoint control: regulation of 14-3-3 protein binding by phosphorylation of Cdc25C on serine-216. *Science*, *277*(5331), 1501-1505.

Peterlin, B. M., & Price, D. H. (2006). Controlling the elongation phase of transcription with P-TEFb. *Molecular Cell*, *23*(3), 297-305.

Pilkinton, M., Sandoval, R., & Colamonici, O. R. (2007). Mammalian Mip/LIN-9 interacts with either the p107, p130/E2F4 repressor complex or B-Myb in a cell cycle-phase-dependent context distinct from the Drosophila dREAM complex. *Oncogene*, *26*(54), 7535-7543.

Qing, Y., Yin, F., Wang, W., Zheng, Y. G., Guo, P. F., Schozer, F., Deng, H., & Pan, D. J. (2014). The Hippo effector Yorkie activates transcription by interacting with a histone methyltransferase complex through Ncoa6. *Elife*, *3*.

Raj, N., & Bam, R. (2019). Reciprocal Crosstalk Between YAP1/Hippo Pathway and the p53 Family Proteins: Mechanisms and Outcomes in Cancer. *Frontiers in Cell and Developmental Biology*, *7*.

Ramírez, F., Ryan, D. P., Grüning, B., Bhardwaj, V., Kilpert, F., Richter, A. S., Heyne, S., Dündar, F., & Manke, T. (2016). deepTools2: a next generation web server for deep-sequencing data analysis. *Nucleic Acids Res*, *44*(W1), W160-165.

Reichert, N., Wurster, S., Ulrich, T., Schmitt, K., Hauser, S., Probst, L., Götz, R., Ceteci, F., Moll, R., Rapp, U., & Gaubatz, S. (2010). Lin9, a subunit of the mammalian DREAM complex, is essential for embryonic development, for survival of adult mice, and for tumor suppression. *Molecular and Cellular Biology*, *30*(12), 2896-2908.

Rimel, J. K., & Taatjes, D. J. (2018). The essential and multifunctional TFIIH complex. *Protein Science*, *27*(6), 1018-1037.

Roberts, M. S., Sahni, J. M., Schrock, M. S., Piemonte, K. M., Weber-Bonk, K. L., Seachrist, D. D., Avril, S., Anstine, L. J., Singh, S., Sizemore, S. T., Varadan, V., Summers, M. K., & Keri, R. A. (2020). LIN9 and NEK2 Are Core Regulators of Mitotic Fidelity That Can Be Therapeutically Targeted to Overcome Taxane Resistance. *Cancer Res*, *80*(8), 1693-1706.

Robinson, J. T., Thorvaldsdóttir, H., Winckler, W., Guttman, M., Lander, E. S., Getz, G., & Mesirov, J. P. (2011). Integrative genomics viewer. *Nat Biotechnol*, *29*(1), 24-26.

Rocco, J. W., Leong, C. O., Kuperwasser, N., DeYoung, M. P., & Ellisen, L. W. (2006). p63 mediates survival in squamous cell carcinoma by suppression of p73-dependent apoptosis. *Cancer Cell*, *9*(1), 45-56.

Romano, R. A., Ortt, K., Birkaya, B., Smalley, K., & Sinha, S. (2009). An active role of the DeltaN isoform of p63 in regulating basal keratin genes K5 and K14 and directing epidermal cell fate. *Plos One*, *4*(5), e5623.

Saade, E., Mechold, U., Kulyyassov, A., Vertut, D., Lipinski, M., & Ogryzko, V. (2009). Analysis of interaction partners of H4 histone by a new proteomics approach. *Proteomics*, *9*(21), 4934-4943.

Sadasivam, S., & DeCaprio, J. A. (2013). The DREAM complex: master coordinator of cell cycle-dependent gene expression. *Nature Reviews Cancer*, *13*(8), 585-595.

Sadasivam, S., Duan, S., & DeCaprio, J. A. (2012). The MuvB complex sequentially recruits B-Myb and FoxM1 to promote mitotic gene expression. *Genes Dev*, *26*(5), 474-489.

Sahni, J. M., Gayle, S. S., Webb, B. M., Weber-Bonk, K. L., Seachrist, D. D., Singh, S., Sizemore, S. T., Restrepo, N. A., Bebek, G., Scacheri, P. C., Varadan, V., Summers, M. K., & Keri, R. A. (2017). Mitotic Vulnerability in Triple-Negative Breast Cancer Associated with LIN9 Is Targetable with BET Inhibitors. *Cancer Res*, *77*(19), 5395-5408.

Sakuma, T., Nakade, S., Sakane, Y., Suzuki, K. T., & Yamamoto, T. (2016). MMEJ-assisted gene knock-in using TALENs and CRISPR-Cas9 with the PITCh systems. *Nature Protocols*, *11*(1), 118-133.

Sala, A. (2005). B-MYB, a transcription factor implicated in regulating cell cycle, apoptosis and cancer. *Eur J Cancer*, *41*(16), 2479-2484.

Saladi, S. V., Ross, K., Karaayvaz, M., Tata, P. R., Mou, H. M., Rajagopal, J., Ramaswamy, S., & Ellisen, L. W. (2017). ACTL6A Is Co-Amplified with p63 in Squamous Cell Carcinoma to Drive YAP Activation, Regenerative Proliferation, and Poor Prognosis. *Cancer Cell*, *31*(1), 35-49.

Saldivar, J. C., Cortez, D., & Cimprich, K. A. (2017). The essential kinase ATR: ensuring faithful duplication of a challenging genome. *Nature Reviews Molecular Cell Biology*, *18*(12), 783-783.

Saldivar, J. C., Hamperl, S., Bocek, M. J., Chung, M., Bass, T. E., Cisneros-Soberanis, F., Samejima, K., Xie, L., Paulson, J. R., Earnshaw, W. C., Cortez, D., Meyer, T., & Cimprich, K. A. (2018). An intrinsic S/G(2) checkpoint enforced by ATR. *Science*, *361*(6404), 806-810.

Santamaria, D., Barriere, C., Cerqueira, A., Hunt, S., Tardy, C., Newton, K., Caceres, J. F., Dubus, P., Malumbres, M., & Barbacid, M. (2007). Cdk1 is sufficient to drive the mammalian cell cycle. *Nature*, *448*(7155), 811-U818.

Schep, A. N., Buenrostro, J. D., Denny, S. K., Schwartz, K., Sherlock, G., & Greenleaf, W. J. (2015). Structured nucleosome fingerprints enable high-resolution mapping of chromatin architecture within regulatory regions. *Genome Research*, *25*(11), 1757-1770.

Schep, A. N., Wu, B., Buenrostro, J. D., & Greenleaf, W. J. (2017). chromVAR: inferring transcription-factor-associated accessibility from single-cell epigenomic data. *Nature Methods*, *14*(10), 975-978.

Schep, A. N., Wu, B. J., Buenrostro, J. D., & Greenleaf, W. J. (2017). chromVAR : inferring transcription-factor-associated accessibility from single-cell epigenomic data. *Nature Methods*, *14*(10), 975-+.

Schmit, F., Cremer, S., & Gaubatz, S. (2009). LIN54 is an essential core subunit of the DREAM/LINC complex that binds to the cdc2 promoter in a sequence-specific manner. *Febs j*, *276*(19), 5703-5716.

Schmit, F., Korenjak, M., Mannefeld, M., Schmitt, K., Franke, C., von Eyss, B., Gagrica, S., Hanel, F., Brehm, A., & Gaubatz, S. (2007). LINC, a Human Complex That is Related to pRB-Containing Complexes in Invertebrates Regulates the Expression of G2/M Genes. *Cell Cycle*, *6*(15), 1903-1913.

Schmitt, E., Boutros, R., Froment, C., Monsarrat, B., Ducommun, B., & Dozier, C. (2006). CHK1 phosphorylates CDC25B during the cell cycle in the absence of DNA damage. *Journal of Cell Science*, *119*(20), 4269-4275.

Shen, Z. W., & Stanger, B. Z. (2015). YAP Regulates S-Phase Entry in Endothelial Cells. *Plos One*, *10*(1).

Shlyueva, D., Stampfel, G., & Stark, A. (2014). Transcriptional enhancers: from properties to genome-wide predictions. *Nature Reviews Genetics*, *15*(4), 272-286.

Skibinski, A., Breindel, J. L., Prat, A., Galván, P., Smith, E., Rolfs, A., Gupta, P. B., LaBaer, J., & Kuperwasser, C. (2014). The Hippo transducer TAZ interacts with the SWI/SNF complex to regulate breast epithelial lineage commitment. *Cell Reports*, *6*(6), 1059-1072.

Smith, J., Tho, L. M., Xu, N., & Gillespie, D. A. (2010). The ATM-Chk2 and ATR-Chk1 pathways in DNA damage signaling and cancer. *Adv Cancer Res*, *108*, 73-112.

Stein, C., Bardet, A. F., Roma, G., Bergling, S., Clay, I., Ruchti, A., Agarinis, C., Schmelzle, T., Bouwmeester, T., Schübeler, D., & Bauer, A. (2015). YAP1 Exerts Its Transcriptional Control via TEAD-Mediated Activation of Enhancers. *Plos Genetics*, *11*(8), e1005465.

Su, X., Napoli, M., Abbas, H. A., Venkatanarayan, A., Bui, N. H. B., Coarfa, C., Gi, Y. J., Kittrell, F., Gunaratne, P. H., Medina, D., Rosen, J. M., Behbod, F., & Flores, E. R. (2017). TAp63 suppresses mammary tumorigenesis through regulation of the Hippo pathway. *Oncogene*, *36*(17), 2377-2393.

Su, X. H., Chakravarti, D., & Flores, E. R. (2013). p63 steps into the limelight: crucial roles in the suppression of tumorigenesis and metastasis. *Nature Reviews Cancer*, *13*(2), 136-143.

Suh, H., Hazelbaker, D. Z., Soares, L. M., & Buratowski, S. (2013). The C-Terminal Domain of Rpb1 Functions on Other RNA Polymerase II Subunits. *Molecular Cell*, *51*(6), 850-858.

Sunahara, M., Shishikura, T., Takahashi, M., Todo, S., Yamamoto, N., Kimura, H., Kato, S., Ishioka, C., Ikawa, S., Ikawa, Y., & Nakagawara, A. (1999). Mutational analysis of p51A/TAp63gamma, a p53 homolog, in non-small cell lung cancer and breast cancer. *Oncogene*, *18*(25), 3761-3765.

Takeda, T., Yamamoto, Y., Tsubaki, M., Matsuda, T., Kimura, A., Shimo, N., & Nishida, S. (2022). PI3K/Akt/YAP signaling promotes migration and invasion of DLD-1 colorectal cancer cells. *Oncology Letters*, *23*(4).

Tan, L., Qu, W. M., Wu, D. J., Liu, M. J., Ai, Q. J., Hu, H. S., Wang, Q., Chen, W. S., & Zhou, H. B. (2022). The interferon regulatory factor 6 promotes cisplatin sensitivity in colorectal cancer. *Bioengineered*, *13*(4), 10504-10517.

Tanaka, Y., Patestos, N. P., Maekawa, T., & Ishii, S. (1999). B-myb is required for inner cell mass formation at an early stage of development. *Journal of Biological Chemistry*, *274*(40), 28067-28070.

Tanner, M. M., Grenman, S., Koul, A., Johannsson, O., Meltzer, P., Pejovic, T., Borg, A., & Isola, J. J. (2000). Frequent amplification of chromosomal region 20q12-q13 in ovarian cancer. *Clin Cancer Res*, *6*(5), 1833-1839.

Tao, W., Zhang, S., Turenchalk, G. S., Stewart, R. A., St John, M. A., Chen, W., & Xu, T. (1999). Human homologue of the Drosophila melanogaster lats tumour suppressor modulates CDC2 activity. *Nature Genetics*, *21*(2), 177-181.

Tapon, N., Harvey, K. F., Bell, D. W., Wahrer, D. C., Schiripo, T. A., Haber, D., & Hariharan, I. K. (2002). salvador Promotes both cell cycle exit and apoptosis in Drosophila and is mutated in human cancer cell lines. *Cell*, *110*(4), 467-478.

Tarasov, K. V., Tarasova, Y. S., Tam, W. L., Riordon, D. R., Elliott, S. T., Kania, G., Li, J., Yamanaka, S., Crider, D. G., Testa, G., Li, R. A., Lim, B., Stewart, C. L., Liu, Y., Van Eyk, J. E., Wersto, R. P., Wobus, A. M., & Boheler, K. R. (2008). B-MYB is essential for normal cell cycle progression and chromosomal stability of embryonic stem cells. *Plos One*, *3*(6), e2478.

Tarasov, K. V., Tarasova, Y. S., Tam, W. L., Riordon, D. R., Elliott, S. T., Kania, G., Li, J. L., Yamanaka, S., Crider, D. G., Testa, G., Li, R. A., Lim, B., Stewart, C. L., Liu, Y., Van Eyk, J. E., Wersto, R. P., Wobus, A. M., & Boheler, K. R. (2008). B-MYB Is Essential for Normal Cell Cycle Progression and Chromosomal Stability of Embryonic Stem Cells. *Plos One*, *3*(6).

Thalmeier, K., Synovzik, H., Mertz, R., Winnacker, E. L., & Lipp, M. (1989). Nuclear factor E2F mediates basic transcription and trans-activation by E1a of the human MYC promoter. *Genes Dev*, *3*(4), 527-536.

Thorner, A. R., Hoadley, K. A., Parker, J. S., Winkel, S., Millikan, R. C., & Perou, C. M. (2009). In vitro and in vivo analysis of B-Myb in basal-like breast cancer. *Oncogene*, *28*(5), 742-751.

Tian, S., Roepman, P., Van't Veer, L. J., Bernards, R., de Snoo, F., & Glas, A. M. (2010). Biological functions of the genes in the mammaprint breast cancer profile reflect the hallmarks of cancer. *Biomark Insights*, *5*, 129-138.

Tremblay, A. M., Missiaglia, E., Galli, G. G., Hettmer, S., Urcia, R., Carrara, M., Judson, R. N., Thway, K., Nadal, G., Selfe, J. L., Murray, G., Calogero, R. A., De Bari, C., Zammit, P. S., Delorenzi, M., Wagers, A. J., Shipley, J., Wackerhage, H., & Camargo, F. D. (2014). The Hippo Transducer YAP1 Transforms Activated Satellite Cells and Is a Potent Effector of Embryonal Rhabdomyosarcoma Formation. *Cancer Cell*, *26*(2), 273-287.

Truong, A. B., Kretz, M., Ridky, T. W., Kimmel, R., & Khavari, P. A. (2006). p63 regulates proliferation and differentiation of developmentally mature keratinocytes. *Genes Dev*, *20*(22), 3185-3197.

Tschop, K., Conery, A. R., Litovchick, L., DeCaprio, J. A., Settleman, J., Harlow, E., & Dyson, N. (2011). A kinase shRNA screen links LATS2 and the pRB tumor suppressor. *Genes & Development*, *25*(8), 814-830.

Tucci, P., Agostini, M., Grespi, F., Markert, E. K., Terrinoni, A., Vousden, K. H., Muller, P. A., Dötsch, V., Kehrloesser, S., Sayan, B. S., Giaccone, G., Lowe, S. W., Takahashi, N., Vandenabeele, P., Knight, R. A., Levine, A. J., & Melino, G. (2012). Loss of p63 and its microRNA-205 target results in enhanced cell migration and metastasis in prostate cancer. *Proc Natl Acad Sci U S A*, *109*(38), 15312-15317.

Uzunbas, G. K., Ahmed, F., & Sammons, M. A. (2019). Control of p53-dependent transcription and enhancer activity by the p53 family member p63. *Journal of Biological Chemistry*, *294*(27), 10720-10736.

Valencia-Sama, I., Zhao, Y., Lai, D., Janse van Rensburg, H. J., Hao, Y., & Yang, X. (2015). Hippo Component TAZ Functions as a Co-repressor and Negatively Regulates ΔNp63 Transcription through TEA Domain (TEAD) Transcription Factor. *Journal of Biological Chemistry*, *290*(27), 16906-16917.

Varelas, X., Samavarchi-Tehrani, P., Narimatsu, M., Weiss, A., Cockburn, K., Larsen, B. G., Rossant, J., & Wrana, J. L. (2010). The Crumbs complex couples cell density sensing to Hippo-dependent control of the TGF-β-SMAD pathway. *Developmental Cell*, *19*(6), 831-844.

Verfaillie, A., Imrichova, H., Atak, Z. K., Dewaele, M., Rambow, F., Hulselmans, G., Christiaens, V., Svetlichnyy, D., Luciani, F., Van den Mooter, L., Claerhout, S., Fiers, M., Journe, F., Ghanem, G. E., Herrmann, C., Halder, G., Marine, J. C., & Aerts, S. (2015). Decoding the regulatory landscape of melanoma reveals TEADS as regulators of the invasive cell state. *Nat Commun*, *6*, 6683.

Vierbuchen, T., Ling, E., Cowley, C. J., Couch, C. H., Wang, X., Harmin, D. A., Roberts, C. W. M., & Greenberg, M. E. (2017). AP-1 Transcription Factors and the BAF Complex Mediate Signal-Dependent Enhancer Selection. *Molecular Cell*, *68*(6), 1067-1082.e1012.

Viladevall, L., St Amour, C. V., Rosebrock, A., Schneider, S., Zhang, C., Allen, J. J., Shokat, K. M., Schwer, B., Leatherwood, J. K., & Fisher, R. P. (2009). TFIIH and P-TEFb coordinate transcription with capping enzyme recruitment at specific genes in fission yeast. *Molecular Cell*, *33*(6), 738-751.

Vilgelm, A. E., Washington, M. K., Wei, J. X., Chen, H. D., Prassolov, V. S., & Zaika, A. I. (2010). Interactions of the p53 Protein Family in Cellular Stress Response in Gastrointestinal Tumors. *Molecular Cancer Therapeutics*, *9*(3), 693-705.

von Eyss, B., Jaenicke, L. A., Kortlever, R. M., Royla, N., Wiese, K. E., Letschert, S., McDuffus, L. A., Sauer, M., Rosenwald, A., Evan, G. I., Kempa, S., & Eilers, M. (2015). A MYC-Driven Change in Mitochondrial Dynamics Limits YAP/TAZ Function in Mammary Epithelial Cells and Breast Cancer. *Cancer Cell*, *28*(6), 743-757.

Wang, I. C., Chen, Y. J., Hughes, D., Petrovic, V., Major, M. L., Park, H. J., Tan, Y., Ackerson, T., & Costa, R. H. (2005). Forkhead box M1 regulates the transcriptional network of genes essential for mitotic progression and genes encoding the SCF (Skp2-Cks1) ubiquitin ligase. *Molecular and Cellular Biology*, *25*(24), 10875-10894.

Wang, J. L., Wang, X., Wang, H., Iliakis, G., & Wang, Y. (2002). CHK1-regulated S-phase checkpoint response reduces camptothecin cytotoxicity. *Cell Cycle*, *1*(4), 267-272.

Wang, Y. B., Zhang, T. H., Kwiatkowski, N., Abraham, B. J., Lee, T. I., Xie, S. Z., Yuzugullu, H., Von, T., Li, H. Y., Lin, Z., Stover, D. G., Lim, E., Wang, Z. G. C., Iglehart, J. D., Young, R. A., Gray, N. S., & Zhao, J. J. (2015). CDK7-Dependent Transcriptional Addiction in Triple-Negative Breast Cancer. *Cell*, *163*(1), 174-186.

Watanabe, N., Broome, M., & Hunter, T. (1995). Regulation of the human WEE1Hu CDK tyrosine 15-kinase during the cell cycle. *Embo j*, *14*(9), 1878-1891.

Wei, J., Zaika, E., & Zaika, A. (2012). p53 Family: Role of Protein Isoforms in Human Cancer. *Journal of Nucleic Acids*, *2012*, 687359.

Wei, T., Weiler, S. M. E., Tóth, M., Sticht, C., Lutz, T., Thomann, S., De La Torre, C., Straub, B., Merker, S., Ruppert, T., Marquardt, J., Singer, S., Gretz, N., Schirmacher, P., & Breuhahn, K. (2019). YAP-dependent induction of UHMK1 supports nuclear enrichment of the oncogene MYBL2 and proliferation in liver cancer cells. *Oncogene*, *38*(27), 5541-5550.

Wei, Y., Jiang, S. J., Si, M. T., Zhang, X. H., Liu, J. Y., Wang, Z., Cao, C., Huang, J. Y., Huang, H. B., Chen, L. L., Wang, S. T., Feng, C. L., Deng, X. L., & Jiang, L. (2019). Chirality Controls Mesenchymal Stem Cell Lineage Diversification through Mechanoresponses. *Advanced Materials*, *31*(16).

Weinberg, R. A. (2014). *The Biology of Cancer*. W.W. Norton.

Whittaker, S. R., Mallinger, A., Workman, P., & Clarke, P. A. (2017). Inhibitors of cyclin-dependent kinases as cancer therapeutics. *Pharmacology & Therapeutics*, *173*, 83-105.

Wiseman, E. F., Chen, X., Han, N., Webber, A., Ji, Z., Sharrocks, A. D., & Ang, Y. S. (2015). Deregulation of the FOXM1 target gene network and its coregulatory partners in oesophageal adenocarcinoma. *Mol Cancer*, *14*, 69.

Wolter, P., Hanselmann, S., Pattschull, G., Schruf, E., & Gaubatz, S. (2017). Central spindle proteins and mitotic kinesins are direct transcriptional targets of MuvB, B-MYB and FOXM1 in breast cancer cell lines and are potential targets for therapy. *Oncotarget*, *8*(7), 11160-11172.

Wu, B. K., Mei, S. C., Chen, E. H., Zheng, Y. G., & Pan, D. J. (2022). YAP induces an oncogenic transcriptional program through TET1-mediated epigenetic remodeling in liver growth and tumorigenesis. *Nature Genetics*, *54*(8), 1202-+.

Yamaguchi, K., Wu, L., Caballero, O. L., Hibi, K., Trink, B., Resto, V., Cairns, P., Okami, K., Koch, W. M., Sidransky, D., & Jen, J. (2000). Frequent gain of the p40/p51/p63 gene locus in primary head and neck squamous cell carcinoma. *International Journal of Cancer*, *86*(5), 684-689.

Yang, A., & McKeon, F. (2000). P63 and P73: P53 mimics, menaces and more. *Nat Rev Mol Cell Biol*, *1*(3), 199-207.

Yang, S., Zhang, L., Purohit, V., Shukla, S. K., Chen, X., Yu, F., Fu, K., Chen, Y., Solheim, J., Singh, P. K., Song, W., & Dong, J. (2015). Active YAP promotes pancreatic cancer cell motility, invasion and tumorigenesis in a mitotic phosphorylation-dependent manner through LPAR3. *Oncotarget*, *6*(34), 36019-36031.

Yoh, K. E., Regunath, K., Guzman, A., Lee, S. M., Pfister, N. T., Akanni, O., Kaufman, L. J., Prives, C., & Prywes, R. (2016). Repression of p63 and induction of EMT by mutant Ras in mammary epithelial cells. *Proceedings of the National Academy of Sciences of the United States of America*, *113*(41), E6107-E6116.

Yu, F. X., & Guan, K. L. (2013). The Hippo pathway: regulators and regulations. *Genes Dev*, *27*(4), 355-371.

Yu, F. X., Zhao, B., & Guan, K. L. (2015). Hippo Pathway in Organ Size Control, Tissue Homeostasis, and Cancer. *Cell*, *163*(4), 811-828.

Yu, F. X., Zhao, B., & Guan, K. L. (2015). Hippo Pathway in Organ Size Control, Tissue Homeostasis, and Cancer. *Cell*, *163*(4), 811-828.

Zanconato, F., Battilana, G., Forcato, M., Filippi, L., Azzolin, L., Manfrin, A., Quaranta, E., Di Biagio, D., Sigismondo, G., Guzzardo, V., Lejeune, P., Haendler, B., Krijgsveld, J., Fassan, M., Bicciato, S., Cordenonsi, M., & Piccolo, S. (2018). Transcriptional addiction in cancer cells is mediated by YAP/TAZ through BRD4. *Nature Medicine*, *24*(10), 1599-+.

Zanconato, F., Cordenonsi, M., & Piccolo, S. (2016). YAP/TAZ at the Roots of Cancer. *Cancer Cell*, *29*(6), 783-803.

Zanconato, F., Forcato, M., Battilana, G., Azzolin, L., Quaranta, E., Bodega, B., Rosato, A., Bicciato, S., Cordenonsi, M., & Piccolo, S. (2015). Genome-wide association between YAP/TAZ/TEAD and AP-1 at enhancers drives oncogenic growth. *Nature Cell Biology*, *17*(9), 1218-+.

Zawacka-Pankau, J. E. (2022). The Role of p53 Family in Cancer. *Cancers (Basel)*, *14*(3).

Zhang, W., Tyl, M., Ward, R., Sobott, F., Maman, J., Murthy, A. S., Watson, A. A., Fedorov, O., Bowman, A., Owen-Hughes, T., El Mkami, H., Murzina, N. V., Norman, D. G., & Laue, E. D. (2013). Structural plasticity of histones H3-H4 facilitates their allosteric exchange between RbAp48 and ASF1. *Nature Structural & Molecular Biology*, *20*(1), 29-U43.

Zhang, X., Yang, L., Szeto, P., Abali, G. K., Zhang, Y., Kulkarni, A., Amarasinghe, K., Li, J., Vergara, I. A., Molania, R., Papenfuss, A. T., McLean, C., Shackleton, M., & Harvey, K. F. (2020). The Hippo pathway oncoprotein YAP promotes melanoma cell invasion and spontaneous metastasis. *Oncogene*, *39*(30), 5267-5281.

Zhao, B., Li, L., Tumaneng, K., Wang, C. Y., & Guan, K. L. (2010). A coordinated phosphorylation by Lats and CK1 regulates YAP stability through SCF(beta-TRCP). *Genes Dev*, *24*(1), 72-85.

Zhao, B., Wei, X., Li, W., Udan, R. S., Yang, Q., Kim, J., Xie, J., Ikenoue, T., Yu, J., Li, L., Zheng, P., Ye, K., Chinnaiyan, A., Halder, G., Lai, Z. C., & Guan, K. L. (2007). Inactivation of YAP oncoprotein by the Hippo pathway is involved in cell contact inhibition and tissue growth control. *Genes & Development*, *21*(21), 2747-2761.

Zhao, B., Wei, X., Li, W., Udan, R. S., Yang, Q., Kim, J., Xie, J., Ikenoue, T., Yu, J., Li, L., Zheng, P., Ye, K., Chinnaiyan, A., Halder, G., Lai, Z. C., & Guan, K. L. (2007). Inactivation of YAP oncoprotein by the Hippo pathway is involved in cell contact inhibition and tissue growth control. *Genes Dev*, *21*(21), 2747-2761.

Zhao, B., Ye, X., Yu, J., Li, L., Li, W., Li, S., Yu, J., Lin, J. D., Wang, C. Y., Chinnaiyan, A. M., Lai, Z. C., & Guan, K. L. (2008). TEAD mediates YAP-dependent gene induction and growth control. *Genes Dev*, *22*(14), 1962-1971.

Zhao, H., Watkins, J. L., & Piwnica-Worms, H. (2002). Disruption of the checkpoint kinase 1/cell division cycle 25A pathway abrogates ionizing radiation-induced S and G2 checkpoints. *Proc Natl Acad Sci U S A*, *99*(23), 14795-14800.

Zhao, R., Fallon, T. R., Saladi, S. V., Pardo-Saganta, A., Villoria, J., Mou, H. M., Vinarsky, V., Gonzalez-Celeiro, M., Nunna, N., Hariri, L. P., Camargo, F., Ellisen, L. W., & Rajagopal, J. (2014). Yap Tunes Airway Epithelial Size and Architecture by Regulating the Identity, Maintenance, and Self-Renewal of Stem Cells. *Developmental Cell*, *30*(2), 151-165.

Zheng, Y. G., & Pan, D. J. (2019). The Hippo Signaling Pathway in Development and Disease. *Developmental Cell*, *50*(3), 264-282.

Zhu, W., Giangrande, P. H., & Nevins, J. R. (2004). E2Fs link the control of G1/S and G2/M transcription. *Embo j*, *23*(23), 4615-4626.

6. Appendix

6.1 List of Figures

6.2 List of Tables

6.3 Abbreviations

4-OHT	4-Hydroxytamoxifen
APS	Ammonium persulfate
ATAC-seq	Transposase-Accessible Chromatin using sequencing
ATACsee	Transposase-accessible chromatin with visualization
ATM	Ataxia-telangiectasia-mutated
ATR	Ataxia telangiectasia and Rad-related
AURKA	Aurora kinase A
bp	Base pairs
BPE	Bovine Pituitary Extract
BrdU	Bromdesoxyuridin
BRDU	Bromodomain-containing protein
BSA	Bovine serum albumin
BSD	Blasticidin
C2H3NaO2	Sodium acetate
CAK complex	Cyclin-dependent kinase (CDK) Activating Kinase
Cas9	CRISPR associated protein 9
CDC25A	cell division cyclin 25A
CDK	Cyclin dependent kinase
cDNA	Complementary deoxyribonucleic acid
ChIP	Chromatin immunoprecipitation
ChIP-seq	Chromatin immunoprecipitation followed by high-throughput sequencing
CHK1i	CHK1 inhibitor (prexasertib)
CKIs	Cyclin-dependent kinase inhibitors
Co-IP	Co-immunoprecipitation
CRISPRi	CRISPR interference
CTD	C-terminal domain
Ctrl	Control
CUT&RUN	Cleavage Under Targets and Release Using Nuclease
cyclin A	CCNA

Cyclin B	CCNB
cyclin E	CCNE
ddH2O	Double-distilled/purified water
DEPC	Diethyl pyrocarbonate
DMEM	Dulbecco's modified eagle medium
DMSO	Dimethyl sulfoxide
DNA	Deoxyribonucleic acid
dNTP	Deoxyribonucleotide triphosphate
Dox	Doxycycline
DP1	dimerization partner 1
DP2	dimerization partner 2
DRB	5,6-dichloro-1-beta-D-ribofuranosyl-1H-benzimidazole
DREAM	DP, RB-like, E2F and multi-vulval class B complex
DSBs	Double strand breaks
dTAG	Degradation TAG
DTT	Dithiothreitol
EB	Elution buffer
EDTA	Ethylenediaminetetraacetic acid
EGF	Epidermal growth factor
EGF	Human Epidermal growth factor
EMT	Epithelial–mesenchymal transition
ER	Estrogen receptor
eRNAs	Enhancer RNAs
ESB	Electrophoresis sample buffer
FBS	Fetal bovine serum
FCA	Flow cytometry analysis
gDNA	Genomic deoxyribonucleic acid
GFP	Green fluorescent protein
gRNA	Guide RNA
h	Hours
H2O	Water
HBS	HEPES buffered saline

HCl	Hydrochloric acid
HDAC	Histone deacetylases
HEPES	Hydroxyethyl-piperazineethane-sulfonic acid
HRP	Horseradish peroxidase
IF	Immunofluorescence
IGFBP3	Insulin-like growth factor binding protein 3
IRF6	Interferon regulatory factor 6
kb	Kilobase/kilo base pairs
KRAB	Krüppel associated box domain
LB	Luria Bertani
M	Mitosis
MMB	Myb-MuvB complex
MMEJ	microhomology-mediated end joining
MuvB	Multi-vulval class B
MY-COMP	MYB-YAP competition
N-Ter	N-terminus
NaCl	Sodium Chloride
NEB	New England Biolabs
NELF	Negative elongation factor
NGS	Next-generation sequencing
NuRD	Nucleosome remodeling and histone deacetylase
OE	Overexpression
Opti-MEM	Opti-Minimum essential media (reduced serum media)
PBS	Phosphate buffered saline
PBS-T	Phosphate buffered saline-tween
PCR	Polymerase chain reaction
PDAC	prostate-ductal adenocarcinomas
PEI	Polyethylenimine
Pen-Strep	Penicillin-Streptomycin
PFA	Paraformaldehyde
PI	Propidium idodide
PIC	Protease inhibitor cocktail

PITCh	Precise Integration into Target chromosome
PLA	Proximity ligation assay
PMSF	Phenylmethylsulfonyl fluoride
pRB	Retinoblastoma protein
PRO-sequencing	Precision nuclear run-on sequencing
PSP	3% paraformaldehyde, 2% sucrose in phosphate buffered saline
PVDF	Polyvinylidene fluoride
qPCR	Quantitative polymerase chain reaction
RIPA	Radioimmunoprecipitation assay buffer
RNA	Ribonucleic acid
RNA Pol II	RNA polymerase II
RNAi	Ribonucleic acid interference
rpm	Rounds per minute
RT	Room temperature
RT-qPCR	Reverse transcription quantitative real-time PCR
SAC	Spindle assembly checkpoint
SDS	Sodium dodecyl sulfate
SDS-PAGE	Sodium dodecyl sulfate-polyacrylamide gel electrophoresis
siRNA	Small interfering ribonucleic acid
TAD	Transactivation domain
TAE	Tris-acetate-ethylenediaminetetraacetic acid buffer
TAE	Tris-acetate-ethylenediaminetetraacetic acid buffer
TAZ	Transcriptional co-activator with PDZ-binding motif
TBS	Tris-buffered saline
TBS-T	Tris-buffered saline with-Tween
TE	Tris- Ethylenediaminetetraacetic acid (EDTA)
TEMED	Tetramethylethylenediamine
TES	Transcription End Site
TOP2A	DNA topoisomerase 2a
Tris	Tris (hydroxymethyl) aminomethane
TSS	Transcription Start Sites

UV	Ultraviolet
VP	Verteporfin
WB	Western Blot
WT	Wild-type
YAP	yes-associated protein 1

6.4 Curriculum Vitae

6.5 Publications and conference contributions

6.5.1 Publications

Fetiva MC., Liss F., Gertzmann D., Thomas Julius., Gantert B., Vogl M., Sira N, Weinstock G., Kneitz S., Ade CP, Gaubatz S. (2022). **Oncogenic YAP mediates changes in chromatin accessibility and activity that drive cell cycle gene expression and cell migration.** BioRxiv. [**Preprint**]. September 08, 2022. Available from: https://doi.org/10.1101/2022.09.08.507127 (In revision in Nucleic Acids Research, 2022).

6.5.2 Conference contributions

09/2022 **Poster presentation at Epigenetics & Chromatin meeting,** at the Cold Spring Harbor Laboratory Conference; NY, USA.
Poster: "Oncogenic YAP mediates changes in chromatin accessibility and activity that drive cell cycle gene expression and cell migration". By Camila Fetiva, Franziska Liss, Julius Thomas, Benedikt Gantert, Susanne Kneitz, Carsten P. Ade, Stefan Gaubatz.

09/2021 **Talk at the 16th International GSLS Students' Symposium Eureka!** Würzburg, Germany.
Talk: "Crosstalk between MMB complex and YAP in transcriptional regulation of cell cycle". By Camila Fetiva, Annika Eggestein, Benedikt Gantert, Carsten P.Ade, Stefan Gaubatz.

08/2020 **Poster presentation at the online Transcription and Chromatin meeting**, at EMBL Heidelberg, Germany. By Camila Fetiva, Annika Eggestein, Benedikt Gantert, Carsten P.Ade, Stefan Gaubatz.
Poster: Crosstalk between the MMB complex and YAP in transcriptional regulation of the cell cycle. By Camila Fetiva, Annika Eggestein, Benedikt Gantert, Carsten P.Ade, Stefan Gaubatz.

10/2019 **Poster presentation at the 14th International GSLS Students' Symposium Eureka!** Würzburg, Germany.
Poster: "Crosstalk between MMB complex and YAP in transcriptional regulation of cell cycle". Camila Fetiva, Grit Pattschull, Carsten P.Ade, Stefan Gaubatz.

6.6 Supervised theses

Annika Eggestein. Master thesis: *Investigating the function of YAP-bound enhancers using a CRISPR interference system (CRISPRi);* 2020.

Nataliia Sira. Bachelor thesis: *Activation mechanisms of mitotic genes after the inhibition of S/G2 checkpoint;* 2021.

Julius Thomas. Research internship: Biomedicine. 2021

Julius Thomas. Master thesis: *Transcriptional regulation of cell cycle genes in S-phase and effects of YAP-ΔNp63 interaction;* 2022.

6.7 Acknowledgements

I would like to express my deepest gratitude to Prof. Dr. Stefan Gaubatz first of all for the incredible opportunity of doing my Ph.D. at his Lab and secondly for his invaluable patience, feedback, and positive mind. This endeavor would not have been possible without the scientific discussions, his answers to my many questions, and all the time he invested in my project and in my supervision, it was a completely enriching experience working in his Lab.

I also could not have undertaken this journey without my thesis committee. I thank Prof. Dr. Svenja Meierjohann and Prof Dr. Elmar Wolf for their scientific input and generosity in kindly providing knowledge and expertise. I am also grateful to Dr. Carsten Ade, Dr Susanne Kneitz, Doerthe Gertzmann, Franziska Liss, Julius Thomas, Natalie Sira, Annika Eggestein, Benedikt Gantert, Magdalena Vogl and Susanne Spahr for their contribution and work in this project.

Thanks should also go to the AG-Gaubatz for the nice environment, enthusiasm for the topic, fun, and personal and scientific support. To the former members, Grit Pattschull, Marco Gründl and Steffen Hanselmann thanks for helping me at the beginning of my Ph.D stages. Big thanks should also go to my current colleagues Franziska Liss, Doerthe Gertzman and Susi Spahr for all their kind help and their treasured support which was really influential in shaping my experiments; I also thank the medicine and master students: Julius Thomas, Cornelius Presek, Anna Lena Mattes, and Marco Sänger, for bringing new and kind energy to the Lab. Special thanks to Doerthe Gertzmann for all her encouragement in Lab and life matters, particularly for answering my many repetitive questions, for her generous help, and for teaching me nice and important words in German.

Getting through my dissertation required more than academic support. My biggest thanks to my family in Colombia, especially to my mom, who inspired me to pursue my dreams, and to fight hard to achieve my goals even when they drove me far away from her, infinite thanks to her for being there and teaching me about persistence “Gracias mami”. I also would like to express my sincere gratitude to Hannes, for his incredible care, his great dinners all made with love, and his comforting words in the hard times, without which I would have not reached to this stage, sorry for being grumpier and stressed in the last days., you have been amazing.

Finally, I express my sincere thanks to my other family my old and new friends especially to Juanpa, Jhonatan and Gemma for listening to me when I needed them and for being there to support and motivate me to accomplish this stage of my life and career, thanks for many memorable conversations and time together.

6.8 Affidavit

6.8.1 Affidavit

I hereby confirm that my thesis entitled “Changes in chromatin accessibility by oncogenic YAP and its relevance for regulation of cell cycle gene expression and cell migration” is the result of my own work. I did not receive any help pr support from commercial consultants. All sources and/or materials applied are listed and specified in the thesis.

Furthermore, I confirm that this thesis has not yet been submitted as part of another examination process neither in identical nor in similar form.

Place, Date Signature

6.8.2 Eidesstattliche Erklärung

Hiermit erkläre ich an Eides statt, die Dissertation „Änderungen der Chromatinzugänglichkeit durch onkogenes YAP und seine Relevanz für die Genexpression während des Zellzyklus und für die Zellmigration“ eigenständig, d.h. insbesondere selbstständig und ohne Hilfe eines kommerziellen Promotionsberaters, angefertigt und keine anderen als die von mir angegebenen Quellen und Hilfsmittel verwendet zu haben.

Ich erkläre außerdem, dass die Dissertation weder in gleicher noch in ähnlicher Form bereits in einem anderen Prüfungsverfahren vorgelegen hat.

Place, Date Signature